Installation of a Large Diameter Cold Water Pipeline for a 3MW Onshore Based OTEC Plant

R.L. van Kooten

Technische Universiteit Delft

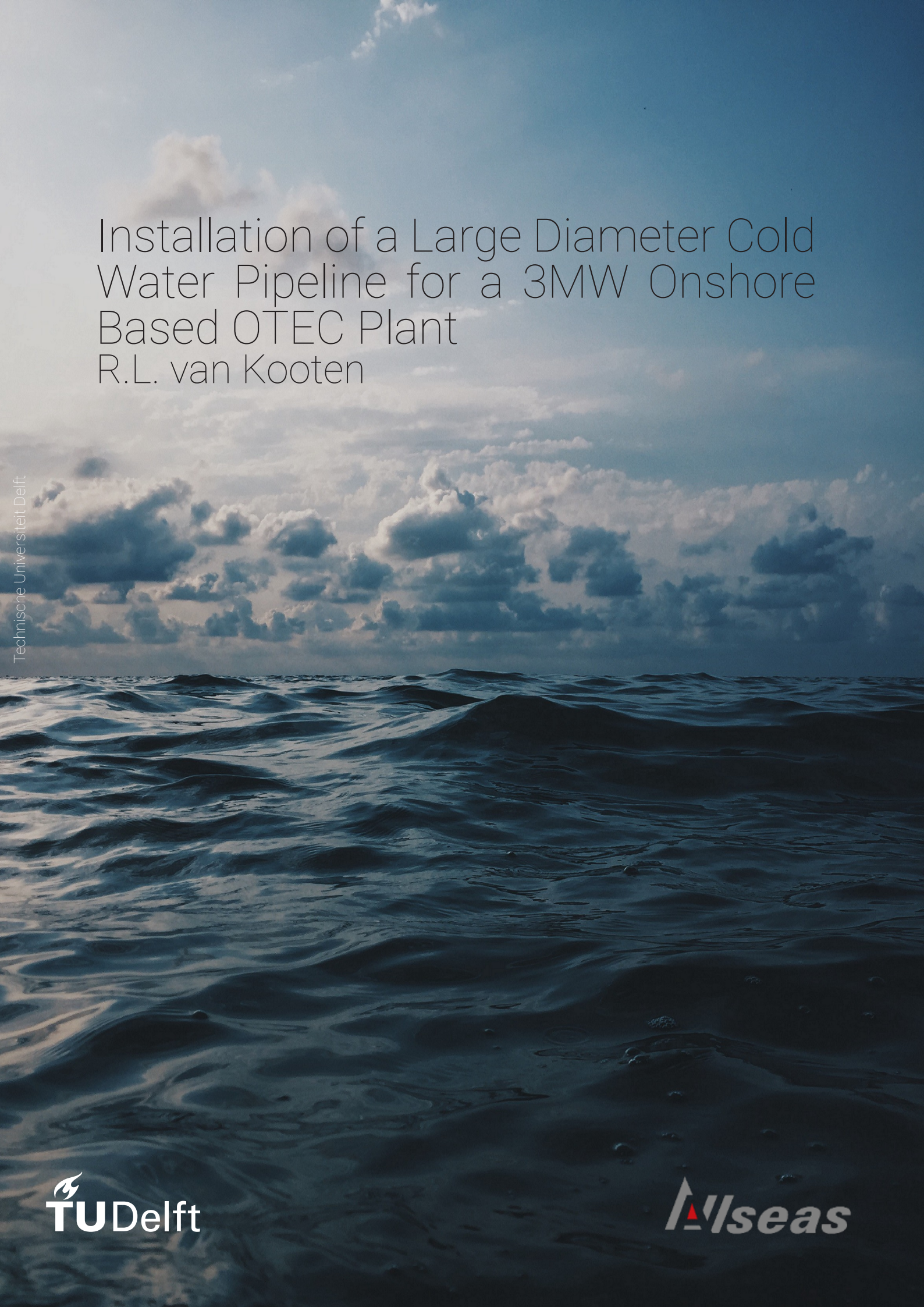

TU Delft

Allseas

Installation of a Large Diameter Cold Water Pipeline for a 3MW Onshore Based OTEC Plant

by

R.L. van Kooten

to obtain the degree of Master of Science
at the Delft University of Technology

Student number:	4219120	
Project duration:	November, 2019 – August, 2020	
Thesis committee:	Prof. dr. A. Metrikine,	TU Delft, chairman
	Ir. J. S. Hoving,	TU Delft, supervisor
	Dr. Ir. K. N. van Dalen,	TU Delft
	Ir. B.J. Kleute,	Allseas Engineering, supervisor

An electronic version of this thesis is available at `http://repository.tudelft.nl/`.

TU Delft

Abstract

Ocean thermal energy conversion (OTEC) is a renewable energy resource that uses the thermal gradient of the ocean to generate electricity. Warm surface water and cold deep sea water, which can be found at depths of approximately 1000 [m], are used to generate electricity in a thermodynamic Rankine cycle. Due to its dimensions, the installation of the cold water pipeline is one of the most challenging aspects of an OTEC plant. Allseas Engineering B.V. is planning to install a 3 [MW] onshore based OTEC plant on Bonaire. For this OTEC plant, a cold water pipeline with an outer diameter of 2.25 [m] is required that pumps up water from 950 [m] water depth. High density polyethylene (HDPE) is used as the material for the pipeline. HDPE is buoyant and therefore requires additional downwards force to be installed below the sea surface. Two installation methods are considered for this cold water pipeline: the 'hold and sink installation method' and the 'pull down installation method'. A numerical non-linear Euler Bernoulli beam model is used to optimize both installation methods. The Von Mises equivalent stress criterion is used to assess whether structural integrity is maintained during the installation.
The hold and sink installation pipeline is ballasted using concrete weights to provide the necessary downwards force. The seabed stability criterion is used to determine the required amount of ballast. Hold points are attached along the length of the pipeline that provide a vertical upwards force to control the sinking velocity. A pull force is applied at the offshore end to reduce pipeline bending stress and to reduce the lateral deflection that results from the sea current. Using the hold and sink installation method, the pipeline can be successfully installed without exceeding the design stress.
The pull down installation pipeline is divided into two sections: a ballasted section of 450 [m] and the remainder of the pipeline that is not ballasted and remains afloat. A concrete ballast weight is installed at the seabed, at the final position of the offshore end of the pipeline. The ballasted section is installed using an installation method that is frequently used for HDPE pipelines called the float and sink method. A chain is connected to the offshore end of the pipeline. The chain is connected to a pull cable that runs through the anchorbox at the seabed to a crane vessel at the sea surface. The unballasted section is then pulled down to the anchorbox, where the chain is secured in the anchorbox and the pipeline remains in a reversed catenary shape during its operational life. In the transition zone where the transition between the ballasted section and the floating section of the pipeline occurs, the Von Mises stress exceeds the design stress. The Von Mises stress results primarily from pipeline bending, therefore additional bending stiffness is applied in the transition zone. The maximum pull force is limited to the weight of the anchorbox. The required pull force to install the pipeline exceeds the allowed pull force. Additional ballast weights are attached to the free span of the pipeline to reduce the required pull force. The pipeline can be installed without exceeding the design stress when the bending stiffness in the transition zone is increased and the required pull force is reduced.

A preliminary multi-criteria analysis is conducted as an initial comparison between the two installation methods. From this analysis no obvious preferred installation method can be selected. A recommendation is made to expand this preliminary multi-criteria analysis and include a detailed cost estimation of the installation methods. Furthermore, it is recommended to include a detailed operational lifetime analysis on the structural integrity of the pipeline for both installation methods.

Preface

This thesis work concludes my time at the TU Delft. This would not have been possible without several people, whom I would like to thank. First of all, special thanks go out to my family and girlfriend for their support during my time in Delft and especially during this thesis.
Furthermore, I would like to thank the members of my committee: Berend Jan Kleute for giving me the opportunity to do my thesis research on a challenging and interesting subject and providing guidance throughout these 9 months, Jeroen Hoving for giving his opinion and advice when it was needed and Andrei Mertrikine for being the chairman of this thesis committee and sharing his thoughts on the progress during this thesis work.
Lastly, I want to say thanks to the people at Allseas for providing a great work and social environment to conduct this thesis research in.

R.L. van Kooten
Delft, 2020

Contents

List of Figures

List of Tables

Nomenclature

α	Thermal Expansion Coefficient
$\dot{u}_f$	Flow Acceleration
$\dot{v}_f$	Pipeline Acceleration
μ	Friction Coefficient
ρ_c	Concrete Density
ρ_p	HDPE Density
ρ_w	Seawater Density
σ_D	Design Stress
σ_H	Hoop Stress
σ_L	Longitudinal Stress
σ_R	Radial Stress
σ_{VM}	Von Mises Stress
A_c	Concrete Surface Area
A_e	External Surface Area
A_i	Inner Surface Area
A_p	Pipeline Surface Area
C_A	Added Mass Coefficient
C_D	Drag Coefficient
C_I	Inertia Coefficient
C_L	Lift Coefficient
CWP	Cold Water Pipe
D_i	Inner Diameter
D_o	Outer Diameter
DNV	Det Norske Veritas
$F\&S$	Float & Sink
$F_{B,c}$	Buoyancy Force of Concrete Ballast
$F_{B,p}$	Buoyancy Force of Pipeline
F_D	Drag Force
F_I	Inertia Force
F_L	Lift Force
g	Gravitational Acceleration
$H\&S$	Hold & Sink
$HDPE$	High Density Polyethylene
kN	Kilo Newton
mT	Metric Ton (1 [mT] = 9.8 [kN])
MW	Megawatt
$OTEC$	Ocean Thermal Energy Conversion
p_e	External Pressure
p_i	Internal Pressure
R_i	Inner Radius
R_o	Outer Radius
SDR	Standard Dimension Ratio
SG	Specific Gravity
$SWAC$	Seawater Airconditioning
TW	Terawatt
u_f	Flow Velocity
v_p	Pipeline Velocity
W_c	Weight Of Concrete In Air
W_p	Weight Of Pipeline In Air
W_{sub}	Submerged Weight of the Pipeline

1 Introduction

1.1. Ocean Thermal Energy Conversion

As the global population keeps growing with increasing living standards, the global demand for energy increases simultaneously. It is projected that the energy consumption will grow by nearly 50% in 2050 [46]. Currently, the main sources of energy are fossil fuels, such as oil and gas. The fact that these fossil fuels will eventually run out and have a negative impact on the environment has resulted in an increase in interest and need for renewable energy resources.

One of these renewable energy resources is Ocean Thermal Energy Conversion, or OTEC in short. OTEC makes use of the temperature difference between warm surface water that is heated by the sun and cold deep seawater that can be found at depths of approximately 1000 [m] to generate electricity.
The working principle is based on a thermodynamic Rankine cycle [35]. A working fluid with a low boiling point, such as ammonia, is evaporated by the warm surface water. The vapor drives a turbine to generate the electricity. The cold seawater then condenses the vapor so that it can be used again, creating a closed thermodynamic cycle. A schematic of the thermodynamic cycle can be seen in Figure 1.1.The estimated global amount of electricity that can be generated by OTEC is 5 [TW] [38].

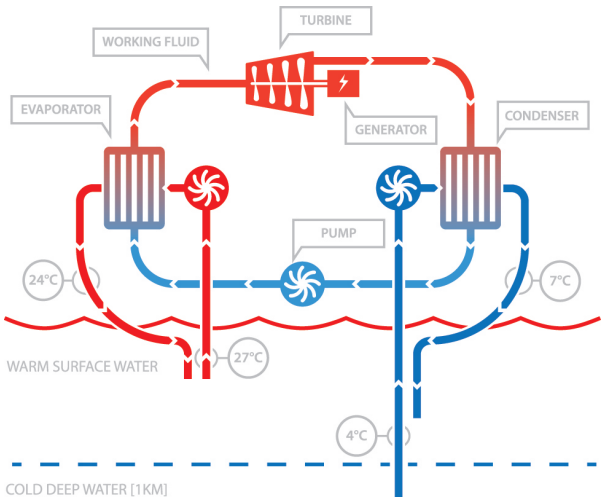

Figure 1.1: OTEC working principle

The temperature difference between the cold water and warm water to make OTEC viable lies in the range of 20-22 °C [40]. The areas that meet this requirement are located around the equator illustrated in Figure 1.2. Especially for small islands around the equator, OTEC can provide a sustainable and economically attractive alternative energy resource.

At the moment, these island are heavily dependent on the import of expensive fossil fuels from other countries. OTEC will provide these islands with more independence from other countries as well [50]. The OTEC plants can be located on land, in shallow water on a bottom founded platform or offshore in deeper waters on a floating platform. For land based OTEC plants, the technology and equipment that is used can be combined with seawater airconditioning (SWAC) and desalination plants. The seawater airconditioning uses the cold water to cool the air and in desalination plants the thermal gradient is used to make potable water. By combining these sustainable projects, the high investment costs can be spread among multiple developments.

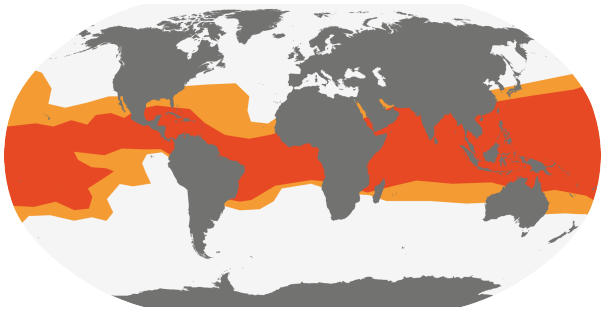

Figure 1.2: OTEC Ocean Resource

As the efficiency of the OTEC thermodynamic cycle is low, with an efficiency of up to 8% on an annual basis, large quantities of seawater are required to generate the required power [11]. To provide these amounts of seawater, large seawater intake pipelines are required. A 10 [MW] OTEC plant requires a cold water pipeline with a diameter of 4 [m] for example. The design and installation of the cold water pipeline in deep water is one of the main challenges in the development of OTEC as an energy resource.

1.2. Thesis Scope

Allseas Engineering B.V [1], in this thesis referred to as Allseas, is investigating the possibility to install a 3MW OTEC plant on Bonaire. For this OTEC plant, a cold water pipeline is required with an outer diameter of 2.25 [m] and a target installation depth of 950 [m]. The layout of the OTEC plant is illustrated in Figure 1.3. The aim of this thesis is to define an optimal installation configuration for the cold water pipeline. Two promising installation methods with two different working principles are considered, the 'hold and sink installation method' and the 'pull down installation method'. Both installation methods are implemented in a numerical non-linear Euler Bernoulli beam model, which was derived by van der Veer [47]. The numerical model is programmed in MATLAB [7] and an overview of the working principle of the numerical model is given in Appendix C. A preliminary multi-criteria analysis is used as an initial comparison between both installation methods, based on relevant installation criteria [18]. The main research question of this thesis is:
What is the optimal installation configuration of the cold water pipeline for the 3MW OTEC plant on Bonaire?
Sub questions accompanying the main research question include:

- What are potential critical risks during the installation and how do they affect the installation?
- What is the influence of the environmental conditions during the installation?

After a successful installation of the cold water pipeline, it will be the largest of its kind that has been installed yet. It will be a milestone in the OTEC development and will help increase the possibilities of harvesting the ocean thermal gradient.

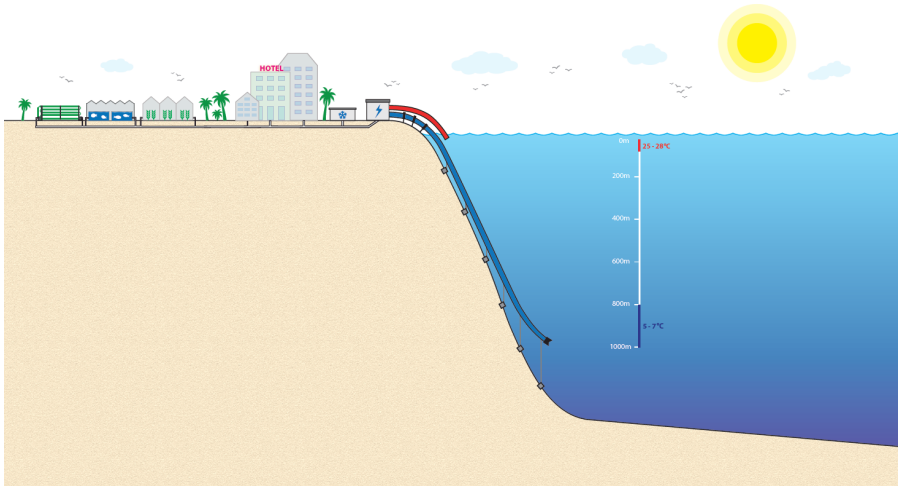

Figure 1.3: Onshore OTEC Plant Layout

1.3. Thesis Outline

The thesis structure is shown in Figure 1.4. Developments in cold water pipelines will be considered first, including cold water pipelines that have been installed in the past, the material of the cold water pipeline and an overview of installation methods. Relevant installation parameters and boundary conditions will be defined in Chapter 3. Both installation methods are implemented in the numerical model and optimized. A preliminary multi-criteria analysis is conducted as an initial comparison between the two installation methods, followed by the conclusions and recommendations.

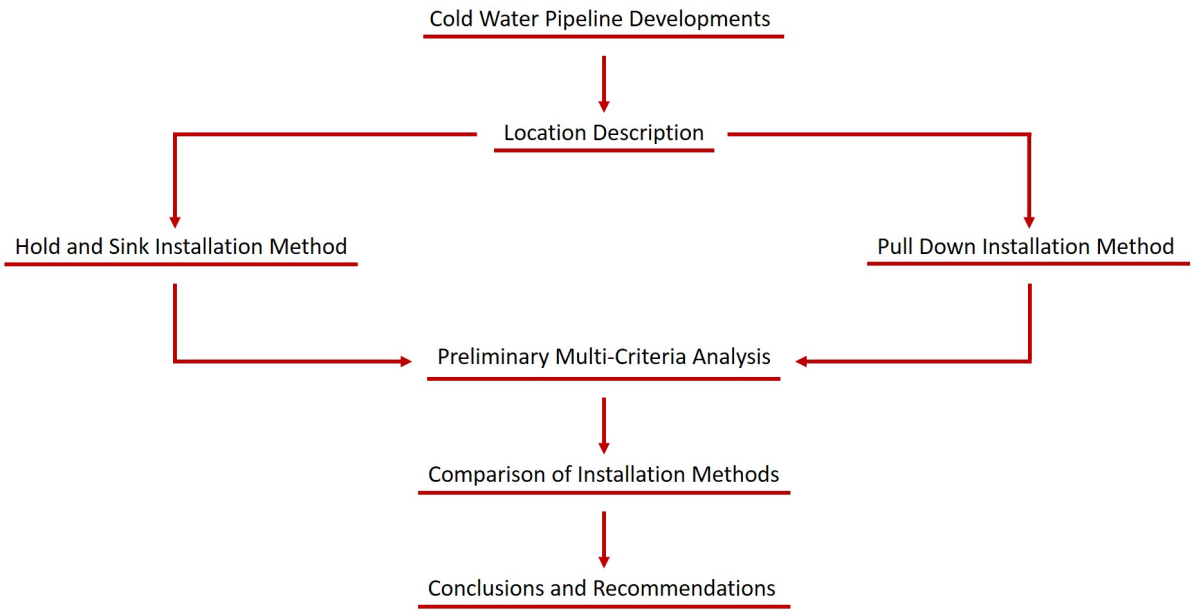

Figure 1.4: Thesis Structure

1.4. Previous Work

The installation of the cold water pipeline for OTEC plants is one of the most challenging aspects of OTEC. This challenge is mainly caused by the large diameter and long length of the cold water pipeline in the harsh offshore environment. Multiple thesis works have already been conducted on this subject:
In 2015, Keesmaat [29] concluded that high density polyethylene (HDPE), is the most suitable material for a cold water pipeline. This conclusion was made based on the developments in the industry and the material properties of HDPE. The traditional 'float and sink installation method', which is mostly used for the installation of large diameter HDPE pipelines in the marine environment, was evaluated to see whether this installation method can be used for the OTEC cold water pipeline as well. Based on a derived numerical natural catenary model, Keesmaat concluded that the theoretical limit of the float and sink installation method is a HDPE pipeline with an outer diameter of 2.3 [m] in combination with an applied pull force of 350 [mT]. Recommendations for improving the float and sink installation method, as well as analysing other installation methods and different pipeline materials, were proposed.
Based on these recommendations, van Nauta Lemke [48] conducted his research in finding the preferred installation method for a large diameter cold water pipeline. A multi-criteria analysis was conducted to compare available materials that can be used for a cold water pipeline. He concluded that HDPE is still the most suitable material for a cold water pipeline. Based on the material selection, multiple installation methods were considered. The most promising installation method was numerically modelled as a Euler Bernoulli beam [39]. Scale model tests were conducted in MARIN to validate the numerical model.
A recommendation made by van Nauta Lemke was to expand the Euler Bernoulli beam model, as some properties of the pipeline may not be captured to full extend by the model. Van der Veer [47] picked up this recommendation and derived a non-linear three-dimensional Euler Bernoulli beam model, to analyse the proposed installation method with greater detail. The non-linear three-dimensional Euler Bernoulli beam model was validated with the model tests performed by van Nauta Lemke. It was concluded that the model is able to capture bending of the pipeline with satisfactory accuracy.

2

Cold Water Pipeline

In this chapter, the general aspects regarding the cold water pipeline are discussed, such as the material and stresses during the installation.

2.1. Cold Water Pipeline Developments

The first attempt to install a large diameter cold water pipeline dates back to 1930, when the first land based OTEC plant was installed in Cuba. A 1.5 [m] pipeline made out of corrugated steel was installed by George Claude [16]. A successful installation was followed by 11 days of operation of the OTEC plant. After 11 days, the pipeline was eventually destroyed by a storm. The destruction was mainly caused by a lack of experience in ocean engineering [21].

Since the first OTEC plant, multiple studies have been conducted on the cold water pipeline. In 1979, Brewer et al. [15] performed a study on the cold water pipeline for an onshore based OTEC plant. Two installation sites were studied, Hawaii and Puerto Rico, with two potential OTEC plant sizes: 10 [MW] and 40 [MW]. From the study it followed that the diameter of the cold water pipeline would be in the range of 7 - 10 [m] for onshore OTEC plants of that size. It was stated that the material selection depends on the seabed bathymetry and the availability of materials that can be used to manufacture pipelines of the required dimensions. The optimal materials were found to be concrete and fiber reinforced plastic and the optimal installation method depends on the chosen material.

In 1987, one of the largest cold water pipelines was installed in Hawaii. The cold water pipeline has an outer diameter of 1 [m] and reaches a depth of 675 [m]. This cold water pipeline is made out of HDPE and is currently still in use. In 2002, a second, larger, cold water pipeline was installed at the same location in Hawaii. This pipeline has an outer diameter of 1.4 [m], reaches a water depth of 900 [m] and is made out of HDPE as well. The second pipeline is currently still the largest cold water pipeline that is still operational. Both cold water pipelines on Hawaii are operated by the Natural Energy Laboratory of Hawaii Authority and are used for ocean energy research purposes, as well as sea water air conditioning [36].

A more recently installed cold water pipeline can be found in India, where a cold water pipeline was installed for a desalination plant. The cold water pipeline has an outer diameter of 0.63 [m] and reaches a depth of 400 [m] and is made out of HDPE as well [4].

2.2. Material Selection

A marine pipeline can be categorized into two categories: A heavy pipeline that sinks, or a light pipeline that floats due to its buoyancy. Choosing the right material for the cold water pipeline is an important factor for both economical and technical reasons. As was also concluded by Brewer et al., the material selection greatly influences the installation method. Materials that are readily available and can be produced in the required dimensions include steel, concrete and polyethylene [21]. Both Keesmaat [29] and Van Nauta Lemke [48] performed an extensive study on the material selection for a cold water pipeline. Van Nauta Lemke studied materials that are readily available in the required cold water pipeline dimensions. He concluded via a multi-criteria analysis that high density polyethylene is currently the most suitable material for a cold water pipeline, similar to the cold water pipelines that are already installed and operational. Based on this conclusion, high density polyethylene is selected for the Bonaire cold water pipeline as well.

A summary of his material selection is provided in table 2.1 with the main advantages and disadvantages of the considered materials.

Material	**Key Advantage**	**Key Disadvantage**
High density polyethylene	Long Length Segments	Additional Ballast required
Steel	Engineering Experience	Subjective to Corrosion
Fiber reinforce plastic	Not Subjective to Corrosion	Expensive
Concrete	Inexpensive	Short segments

Table 2.1: Key Advantages and Disadvantages as by Van Nauta Lemke [48]

2.3. High Density Polyethylene

High density polyethylene is widely used for the construction of large diameter sea outfall and intake pipelines [41]. These outfall and intake pipelines can have diameters that exceed the diameter of the OTEC cold water pipeline for Bonaire. One of the largest marine pipelines made out of HDPE is the marine outfall pipeline for the Taboada wastewater treatment plant in Lima, Peru with an outer diameter of 3 [m] [31]. The main difference between a cold water pipeline and an intake or outfall pipeline is the water depth in which they are installed. Cold water pipelines have a target depth of approximately a 1000 [m], whereas the intake and outfall pipelines are not installed in deep waters. The pipeline in Peru has a maximum water depth of only 20 [m] for example

Polyethylene is categorized based on the polymer resins that are used in the manufacturing process, for pipelines extrusion is the main manufacturing process. These resins include: PE63, PE80, PE100, of which PE100 is the highest grade of resin currently available. The material properties of the PE100 resin can be found in table 2.2.

Density	960 [kg/m^3]
E-modulus at t = 0	1050 [MPa]
E-modulus at t= 50 yrs	200 [MPa]
Tensile Strength	23 [MPa]
Poisson's Ratio	0.45 [-]
Thermal Expansion Coefficient	$0.2 \cdot 10^{-3}$ [°C^{-1}]
Elongation at Break	> 400%

Table 2.2: Material Properties PE100 [42]

Multiple material characteristics make HDPE pipelines convenient to use in the marine environment in comparison to other traditional materials, such as steel or concrete. These characteristics are [43] [44] [10]:

- Smooth: Due to a low internal roughness, low frictional flow losses occur during operation. As a result, a smaller diameter can be used as compared to a pipeline of a different material and a higher surface roughness, such as concrete. Furthermore, due to the external roughness being low as well, the drag coefficient will be lower for a HDPE pipeline, reducing the environmental loading on the pipeline.
- Non-Corrosive: As HDPE is a non-corrosive material, implying it will not corrode in the seawater. This reduces the lifetime costs of the pipeline as no cathodic protection or coatings are required, as is the case for steel pipelines.
- Weight: HDPE has a density that is lower than water, it will remain floating even when filled with water. The pipeline can thus be easily transported by towing it along the water surface.
- Long Lengths: The pipeline segments can be extruded in lengths of up to 500 [m]. This results in a limited amount of segments and joints that are required to obtain the desired total pipeline length.
- Welding: The pipeline segments are jointed using a method called 'butt fusion welding'. Heated ends of the segments are pushed against each other, creating an air tight butt fusion weld that has the same properties as the pipeline itself. A second benefit that results from the welding property is that pipeline sections with different wall thickness can be welded together.

- Flexibility: Due to the flexibility of HDPE, it is easier to install the pipeline as it is allowed to be bend up to a certain degree. Furthermore, the pipeline is able to adapt its shape to the seabed profile minimizing the need for potential seabed preparations.

2.3.1. High Density Polyethylene Viscoelastic Behaviour

HDPE is a viscoelastic material, it shows material properties of both elastic as well as viscous materials. For an elastic material, the magnitude of strain (ϵ), the ratio of deformation over its original length, is proportional to the applied stress (σ). The strain is instantaneous after application of stress. This proportionality is called the Elastic Modulus, and is conform Hooke's law: $E = \frac{\sigma}{\epsilon}$. When the stress is released, the strain is instantaneously and completely recovered.
For a viscous material, the strain is not proportional to the applied stress. Furthermore, the strain is delayed and not instantaneous. The strain is not reversible when the stress is released and depends on the duration and magnitude of the applied stress.
A viscoelastic material, such as HDPE, shows a small instantaneous elastic strain that is then followed by a time dependent strain when a stress is applied. The elastic strain is recovered upon stress release which is then followed by a time dependent strain recovery. The strain recovery might be almost total after time, but there is almost always some remaining permanent deformation [17]. Figure 2.1 shows the response to a constant load which is shown in 2.1 (a) .

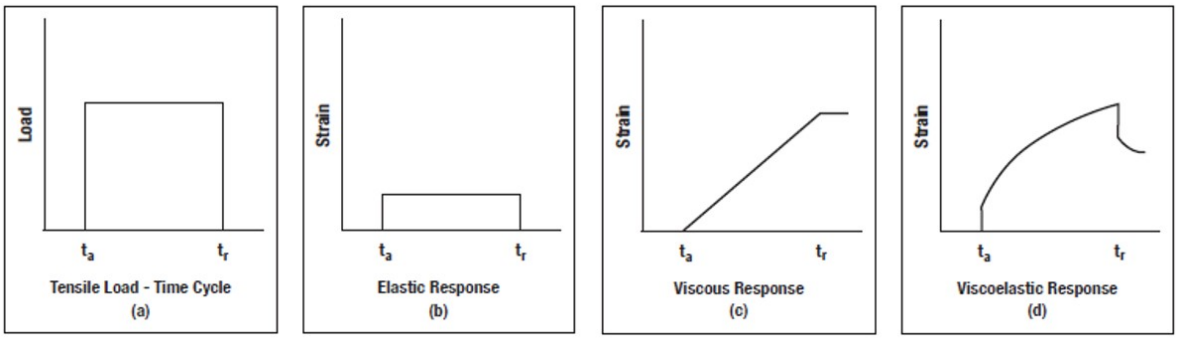

Figure 2.1: Load Response of Elastic, Viscoelastic and Viscous Material [44]

A method to quantify the viscoelastic behaviour is through stress relaxation. During stress relaxation, the strain is constant, while the stress that is needed to maintain this strain reduces over time due to molecular relaxation processes in the material. This time dependent elastic modulus is given by the relaxation modulus equation 2.1. Figure 2.2 shows the stress relaxation to the applied constant strain in Figure 2.2 (a)

$$E_r(t) = \frac{\sigma(t)}{\epsilon_0} \tag{2.1}$$

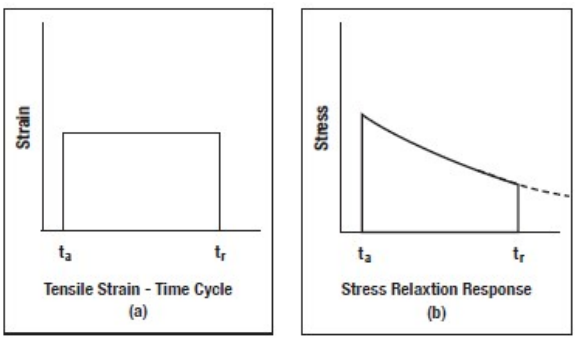

Figure 2.2: Stress Relaxation to a Load [44]

Like many polymeric materials, HDPE is susceptible to creep. Creep is the time dependent deformation when the applied stress is maintained constant. Creep can be divided in three stages. In primary creep, the strain rate decreases. In secondary creep, the strain rate is approximately constant. In tertiary creep, the strain rate increases. In the tertiary creep stage fracture or rupture will eventually occur when the strain rate is high. The time dependent creep modulus can be defined similar to the relaxation modulus and is given by equation 2.2.

$$E_c(t) = \frac{\sigma_0}{\epsilon(t)} \tag{2.2}$$

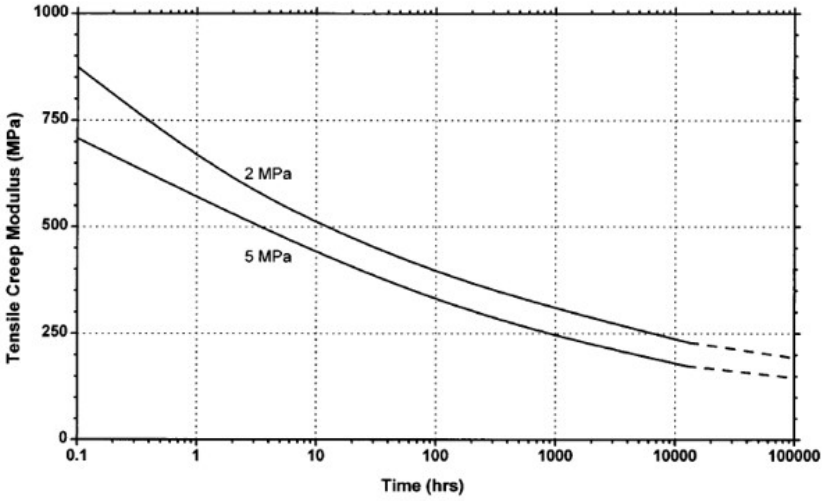

Figure 2.3: HDPE Creep Modulus Over Time [34]

The concept of the creep modulus and the relaxation modulus allows for the usage of the conventional equations that are based on the assumption of elastic behavior [44].

2.3.2. Temperature Effect on HDPE

The internal forces that bond the polymeric molecules decrease with increasing temperature. This results in the softening and eventually melting of the material. For decreasing temperature, these internal forces increase which results in the solid state of HDPE [44]. Table 2.3 shows how the temperature influences the E-modulus of HDPE. At a temperature of the HDPE pipeline higher than 20 °C, the reduction factor is multiplied with the E-modulus.

Temperature	5 °C	20 °C	25 °C	30 °C	35 °C	40°C
Reduction Factor	1.25	1	0.93	0.87	0.80	0.74

Table 2.3: Temperature Dependent Reduction Factor HDPE [43]

2.4. Installation Methods

Due to the large size of large diameter HDPE pipelines, installation methods that are normally used for oil and gas pipelines are not suitable. Currently, the largest pipeline laying vessel in the world, The Pioneering Spirit of Allseas, can lay pipes up to 1.6 [m] in diameter. Therefore, an installation method called the float and sink method was developed for the installation of HDPE marine pipelines. Due to the natural buoyancy of the material, a pipeline made out of HDPE remains floating on the water surface. Additional downward force is required to install a HDPE pipeline below the water surface. Usually, concrete ballast weights are attached to the pipeline to provide the required downwards force.

2.4.1. Float and Sink

The first step is to join the pipeline segments together, after which the ballast blocks are attached. This can either be done onshore or offshore, depending on the local circumstances, like for example the available

space on site. Next the pipeline is towed to the desired installation location. The pipeline is filled with air during the towing to prevent the pipeline from sinking. Additional buoyancy modules can be attached when the air filled section does not provide sufficient buoyancy.
At the installation site, water is injected from the shore end of the pipeline, which results in the pipeline starting to sink at the shore end of the pipeline. From the offshore end of the pipeline, the internal air pressure is regulated. The air pressure is used to control the amount of water that is entering the pipeline and thus the installation velocity. The air fill ratio is the amount of air that is required to balance the submerged section of the pipeline and is calculated via equation 2.3. With w_{ps} being the submerged weight of the concrete ballast, w_{cs} the submerged weight of the pipeline and γ_w the specific gravity of seawater.

$$a_a = \frac{w_{cs} + w_{ps}}{\pi \frac{D_i^2}{4} \gamma_w} \tag{2.3}$$

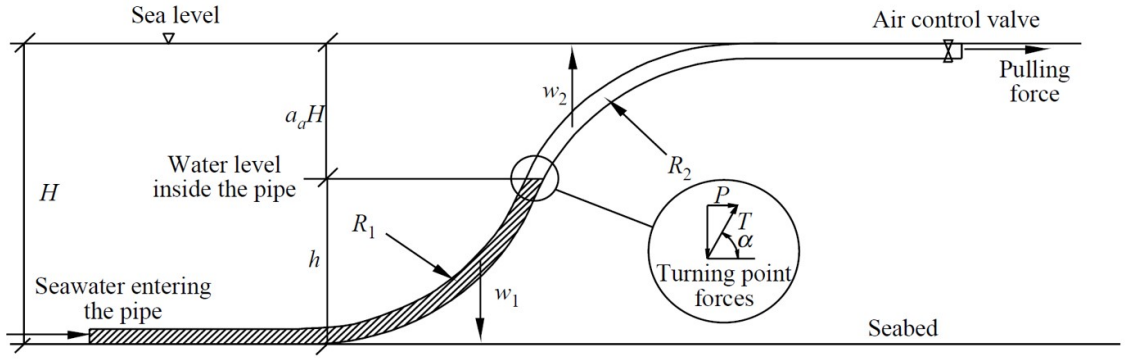

Figure 2.4: Float and Sink Installation Configuration [45]

Figure 2.4 gives an overview of the float and sink installation procedure and shows that an S-shape will form during the float and sink installation. The S-shape has two critical regions, the curvature at the seabed and the curvature at the sea surface (indicated by R_1 and R_2). The curvature radius must be larger than a minimum bending radius to prevent the pipeline from buckling. The minimum bending radius is a function of the outer diameter, D_o, and the specific dimension ratio and is given by equation 2.5 [45]. The specific dimension ratio (SDR) is the ratio of the outer diameter over the wall thickness and is given by equation 2.4. The curvatures can be controlled by applying a pull force, usually via a tug boat, on the offshore end of the pipe. In the case of $a_a \geq 0.5$, the curvature at the seabed is critical, the required pull force can be computed via equation 2.6, where w_1 is the net weight of the water filled section. In the case of $a_a < 0.5$ the curvature at the sea surface is critical, the required pull force can be computed via equation 2.7, where w_2 is the net buoyancy of the air filled section.[45]

$$SDR = \frac{D_o}{t} \tag{2.4}$$

$$R_{min} = 1.34 D_O (SDR - 1) \tag{2.5}$$

$$P_1 = w_1 R_1 \tag{2.6}$$

$$P_2 = w_2 R_2 \tag{2.7}$$

As the installation proceeds into deeper waters, the S-shape will slowly transform into a J-shape, illustrated in Figure 2.5. The pull force has to be increased accordingly to maintain the minimum bending radius. The 1.4 [m] outer diameter pipeline in Hawaii was installed using a similar installation method as the float and sink installation method [32]. For the Bonaire cold water pipeline, the required pull force to maintain the minimum bending radius in deep waters will result in an axial stress that exceeds the allowable limits of the material. Therefore, the float and sink installation method can not be used to install the total cold water pipeline.

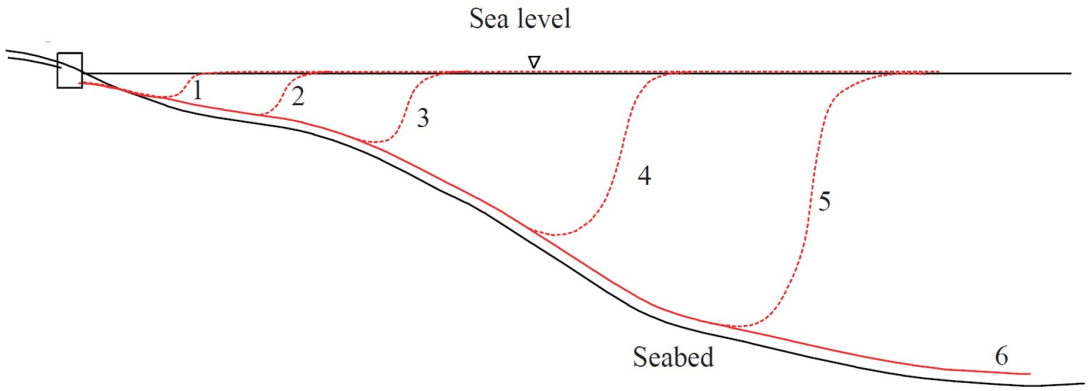

Figure 2.5: Installation Sequence Float and Sink [45]

2.4.2. Reversed Catenary By Ballast Weight

The installation method that was used for the installation of the 1 [m] cold water pipeline in Hawaii and the cold water pipeline in India is illustrated by Figure 2.6. The installation method consists of two phases. The first one is the installation of the near shore ballasted pipeline section via the float and sink installation method 2.4.1. The second phase consists of applying a ballast weight at the offshore end of the pipeline and gradually letting it sink to the seabed via a crane vessel. The pipeline section that is installed in the second phase remains unballasted except for the weight at the offshore end of the pipeline. The unballasted pipeline section remains in a reversed catenary shape during its operational life resulting from the upwards buoyancy force of the unballasted pipeline section. The pipeline is kept in place via the ballast weight at the offshore end of the pipeline. The required weight of the ballast has to be larger than the buoyancy force of the pipeline during the installation and has to withstand the increase in environmental loading during the operational life. The dimensions of the Bonaire cold water pipeline are more than double the dimensions of the cold water pipelines in Hawaii and in India that are installed via this method. The corresponding environmental loading makes this installation method not suitable for a controlled sinking of the Bonaire cold water pipeline.

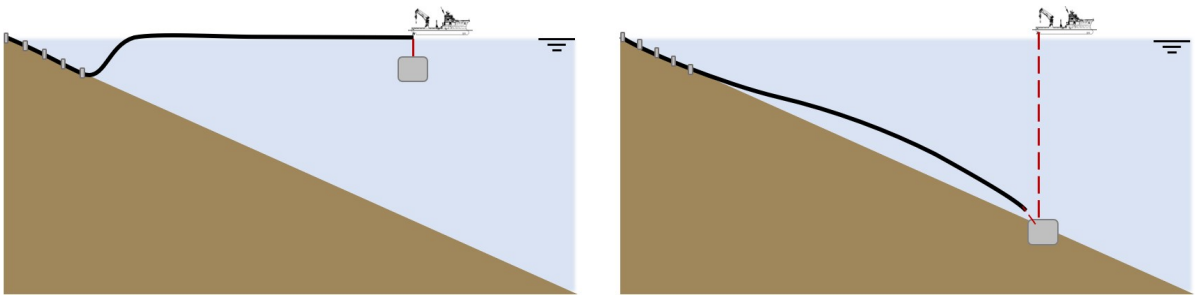

Figure 2.6: Reversed Catenary by Ballast Weight Installation Method

2.4.3. Hold and Sink

The hold and sink installation method was proposed by van Nauta Lemke as an alternative to the float and sink installation method and is the first installation method considered in this thesis. The cold water pipeline is ballasted with concrete weights and filled with air to make it float. The pipeline is then towed to the installation location where it will be filled with water. Filling the pipeline with water reduces the buoyancy. Due to the ballast weights, the pipeline will sink. Multiple hold points are attached along the length of the pipeline to control the sinking velocity. A pull force is applied by a vessel at the offshore end of the pipeline. The pull force allows for control of the trajectory of the pipeline and a reduction in bending stress that results from the hold points. A schematic of the installation procedure is shown in Figure 2.7

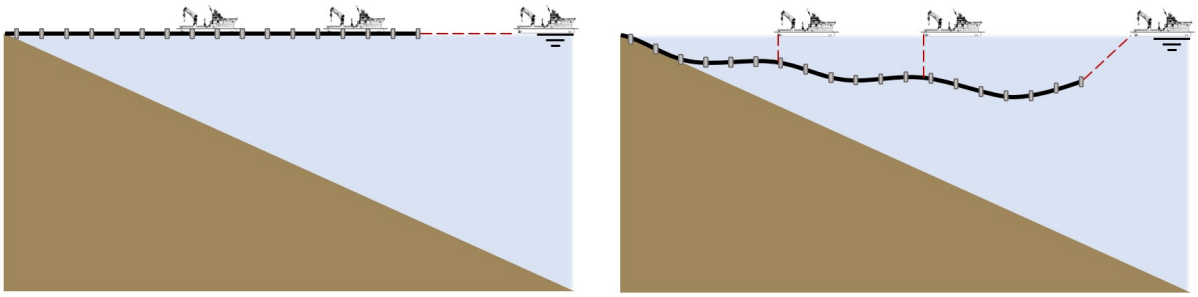

Figure 2.7: Hold and Sink Installation Method

2.4.4. Pull Down

The second installation method considered is the pull down installation method. The pull down installation method resembles the reversed catenary by ballast weight 2.4.2, with the main difference being that a pull force is used to pull the pipeline down instead of a ballast weight. Similarly, the pull down installation method consists of two installation phases. The first section of the pipeline, at the shore end, is ballasted and installed via the float and sink method. The second section of the pipeline is not ballasted and remains floating due to the buoyancy of the pipeline. An anchorbox, which is a large ballast weight, is installed at the seabed that will keep the pipeline at the position after the installation. A chain is attached to the offshore end of the pipeline to which the pull cable is attached. The pull cable goes through the anchorbox to the vessel. The pipeline is then pulled down after which the chain is secured in the anchorbox. The pipeline will assume a reversed catenary shape after installation, resulting in the unballasted section not touching the seabed during the operational life.

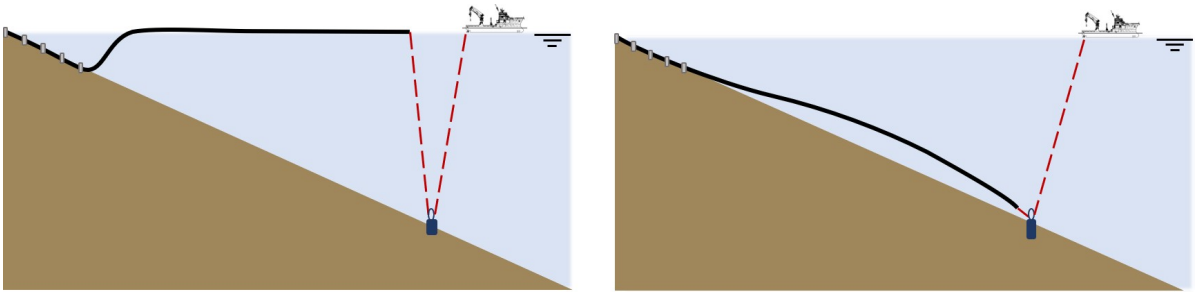

Figure 2.8: Pull Down Installation method

2.5. Stress in the Pipeline

During the installation of the cold water pipeline, stress occurs in three principal directions in the pipeline 2.9:

- Hoop stress, σ_H, along the circumference of the pipeline.
- Radial stress, σ_R, in radial direction.
- Longitudinal stress, σ_L, along the axis of the pipeline.

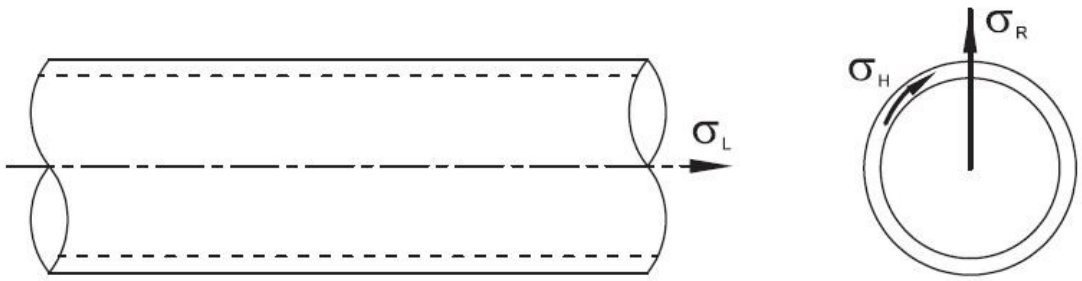

Figure 2.9: Principal Pipeline Stresses [12]

The hoop stress and the radial stress result from the internal and external pressure and can be computed with Lamé's equations 2.8 and 2.9. The hoop stress results from the internal pressure pushing the internal pipeline surface outwards and the external pressure pushing the external pipeline surface inwards. The radial stress results from the internal and external pressure compressing the pipeline radially [51]. The stress distribution resulting from the hoop stress and radial stress is illustrated in Figure 2.10.

$$\sigma_H = \frac{p_i D_i^2 - p_e D_e^2}{D_e^2 - D_i^2} + \frac{(p_i - p_e) D_i^2 D_e^2}{(D_e^2 - D_i^2) D^2} \tag{2.8}$$

$$\sigma_R = \frac{p_i D_i^2 - p_e D_e^2}{D_e^2 - D_i^2} - \frac{(p_i - p_e) D_i^2 D_e^2}{(D_e^2 - D_i^2) D^2} \tag{2.9}$$

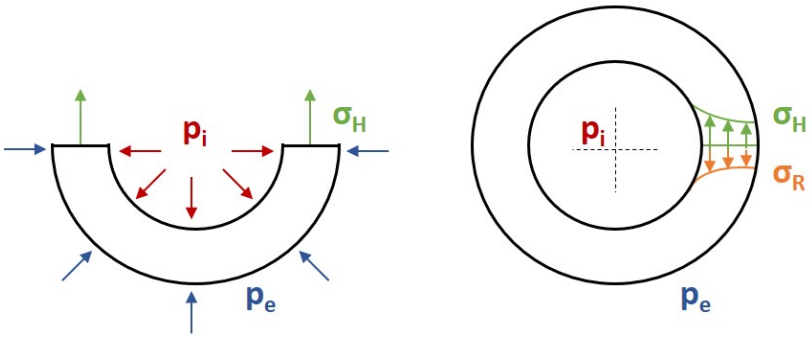

Figure 2.10: Hoop and Radial Stress in the Pipeline

The stress in longitudinal direction due to axial strain in the pipeline is given by equation 2.10.

$$\sigma_L = E\epsilon \tag{2.10}$$

During the installation of the pipeline, the following components contribute to the longitudinal stress:
Longitudinal stress due to tension or compression in the pipeline wall. Where a positive value indicates tension and a negative value indicates compression, given by equation 2.11. With T the pipeline wall tension and A the surface area of the pipeline.

$$\sigma_x = \frac{T}{A_p} \tag{2.11}$$

A component due to the pipeline bending given by equation 2.12, in which M is the applied bending moment, D_o is the outer diameter and I is the second moment of area. When a bending moment is applied, the pipeline will curve resulting in the inner surface experiencing a compressive load and the external curvature a tensile load, illustrated in Figure 2.11.

$$\sigma_b = \frac{M_b D_o}{2I} \tag{2.12}$$

The bending moment is given by equation 2.13, where κ is the curvature of the pipeline.

$$M_b = \kappa EI \tag{2.13}$$

Excessive bending can furthermore lead to ovality of the pipelines' surface area which can lead to local buckling of the pipeline. Local buckling of the pipeline is prevented by maintaining a minimum bending radius, given by equation 2.5

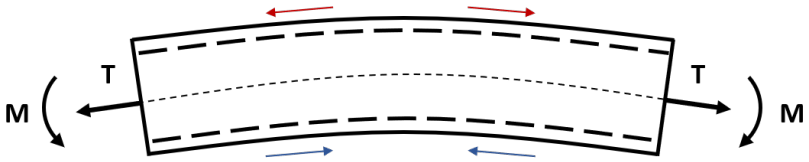

Figure 2.11: Pipeline Bending

For a combination of the three principal stresses, the Von Mises stress criterion is used. The Von Mises stress is the equivalent stress of the three principal stresses and is given by .

$$\sigma_{VM} = \sqrt{\frac{1}{2} * [(\sigma_H - \sigma_L)^2 + (\sigma_L - \sigma_R)^2 + (\sigma_H - \sigma_R)^2]} \tag{2.14}$$

To maintain the structural integrity of the pipeline, the Von Mises stress should remain below the design stress. The design stress for a HDPE pipeline can be obtained from Figure 2.12. As can be seen, the design stress reduces over time due to the viscoelastic behaviour of the pipeline.
The design stress is given by equation 2.15, where C is a safety factor and σ_t is the burst stress at a given time. Common safety factors are 1.25 or 1.6 [42].

$$\sigma_d = \frac{\sigma_t}{C} \tag{2.15}$$

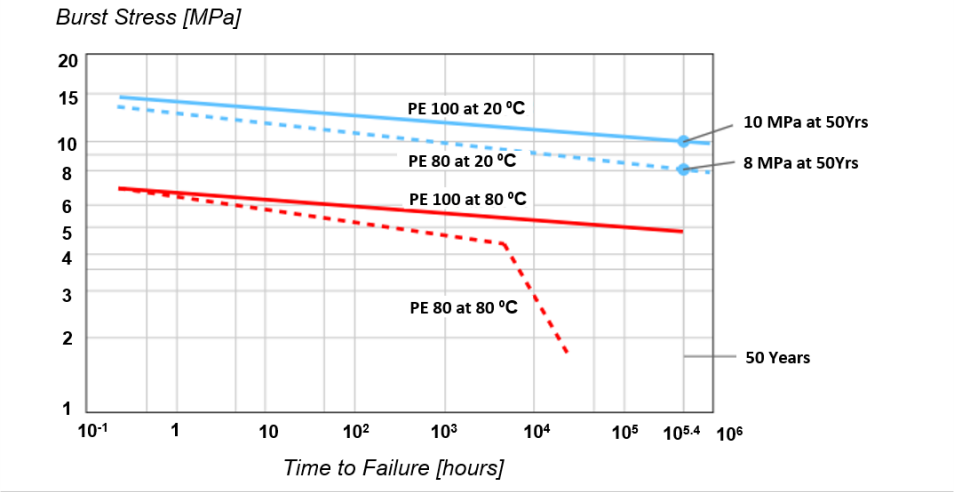

Figure 2.12: Stress Time Line HDPE [33]

A second method to check the structural integrity of the pipeline is via a global buckling analysis [19]. The pipeline is considered as a bar and in the case of the effective wall tension being compressive, the pipeline is susceptible to local buckling and failure. The effective wall tension is given by equation 2.16 and includes the pressure components acting on the pipeline. T is the true wall tension resulting from the loading in longitudinal direction in the pipeline wall given by 2.11.

$$S = T - p_i A_i + p_e A_e \tag{2.16}$$

The concept of the effective axial wall tension is illustrated in figure 2.13. The Figure shows an element of a submerged pipeline. Figure 2.13 (a) shows the forces all the forces acting on the element. The forces consist of the true axial wall tension, T, the internal pressure p_i and external pressure p_e. Three contributions can be used to describe the forces acting on the element. Figure 2.13 (b) illustrates the external pressure acting on the element with closed end, which includes external pressure loading on the end caps. Figure 2.13 (c) illustrates the internal pressure acting on the closed element. Figure 2.13 (d) illustrates the difference between (a) and (b+c), which includes end cap pressures to balance the non existing end cap pressures in (b) and (c). The effective axial wall tension is obtained by summing the components in axial direction.

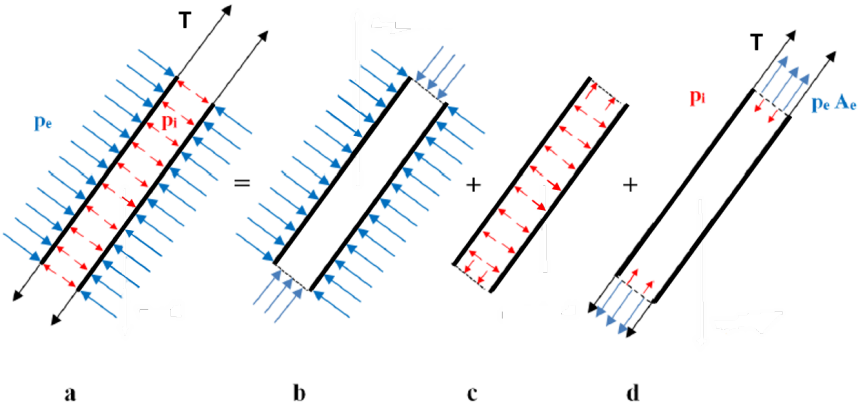

Figure 2.13: Concept of Effective Wall Tension [23]

3

Cold Water Pipeline Location Description

3.1. Bonaire

The location of the planned OTEC plant is on the North-West side of the island next to the Bonaire Petroleum Corporation terminal. From the open source website Copernicus Marine Service, metocean data is obtained of this area [2]. The exact locations of the plant and the location where the data is obtained can be seen in Figure 3.1.

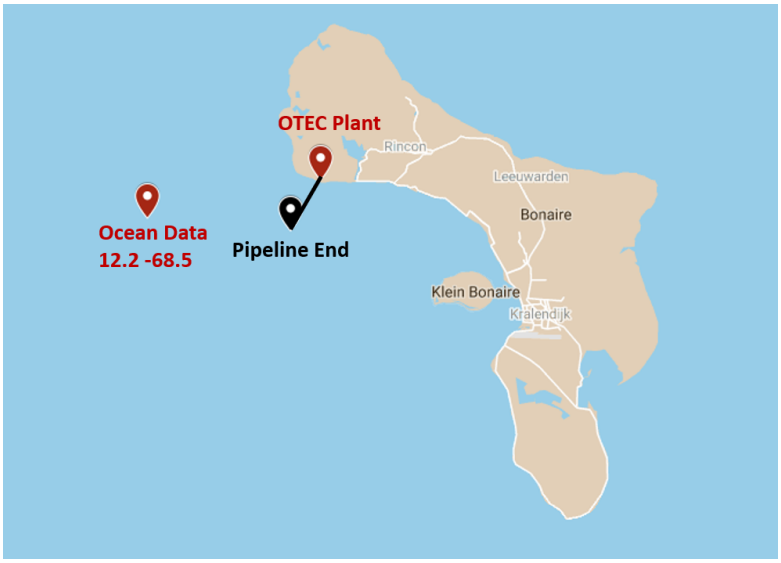

Figure 3.1: Location of OTEC Plant and Obtained Data

3.2. Environmental Loading

The hydrodynamic loading on a moving pipeline is given by the Morison equation 3.1 [27]. Where u_f represents the flow velocity, $\dot{u}_f$ the flow acceleration, v_p the pipeline velocity and $\dot{v}_p$ the pipeline acceleration.

$$F_H = \frac{\pi}{4}\rho_w D_o \dot{u}_f + \frac{\pi}{4}\rho_w C_a(\dot{u}_f - \dot{v}_p) + \frac{1}{2}\rho_w C_D D_o(u_f - v_p)|u_f - v_p| \tag{3.1}$$

Inertia Force

The first term in the Morison equation is the force that results from the pressure gradient that is present in the accelerating fluid. This force component is called the Froude-Krilov force and is equal to the displaced water by the pipeline multiplied with the acceleration of the fluid, given by equation 3.2.

$$F_{FK} = \frac{\pi}{4}\rho_w D_o \dot{u}_f \tag{3.2}$$

The second inertia term in the Morison equation is the disturbance force. As the pipeline is impermeable, the fluid flow cannot go through the pipeline and is directed around it. The disturbance force is also known as the added mass, given by equation 3.3.

$$F_{AM} = \frac{\pi}{4}\rho_w C_a(\dot{u}_f - \dot{v}_p) \tag{3.3}$$

Drag Force

The third term in the Morison equation is the drag force. The drag force is the resistance of the pipeline motion in the presence of a steady flow. The relative velocity is used in the case of a steady flow and a moving pipeline. The flow velocity is the superimposed velocity of the current velocity and the wave velocity, given by equation 4.2

$$F_D = \frac{1}{2}\rho_w C_D D_o(u_f - v_p)|u_f - v_p| \tag{3.4}$$

In the case of a non moving pipeline, the pipeline velocity and acceleration reduce to zero in the drag and added mass force. The drag coefficient and added mass coefficient are empirically determined and can be obtained from the diagrams that are given in Appendix A.

3.3. Environmental Data at Installation Location

3.3.1. Current

For the period January 2017 - December 2019, the surface current velocity (Figure 3.2) and the average current velocity over depth (Figure 3.3) are obtained. The current flows primarily from the Norht-East direction. The resulting absolute current velocity is illustrated as well in both figures. The average current over depth is approximated with the exponential function given by equation 3.5. This approximation is used to define the installation current velocity and the design current velocity that is used to compute the required amount of ballast weight.

$$u_c = 0.24 * exp(0.0095d) + 0.045 \tag{3.5}$$

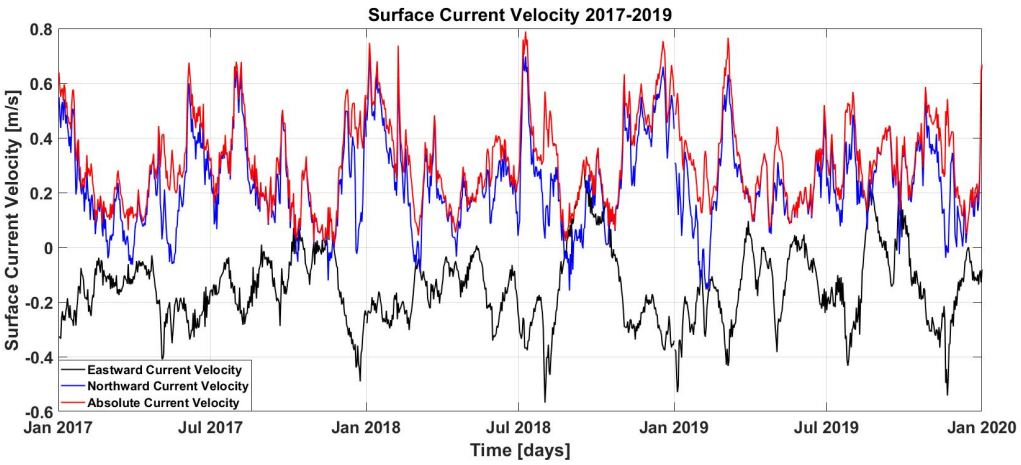

Figure 3.2: Surface Current Velocity 2017-2019

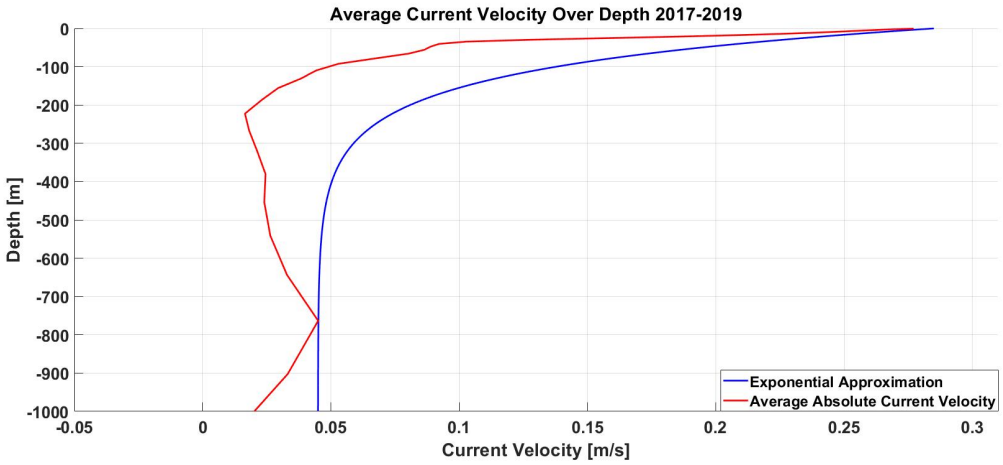

Figure 3.3: Average Absolute Current and Exponential Approximation 2017-2019

3.3.2. Waves

Time domain analysis is most frequently used for the design of subsea pipelines, where the waves are described via their wave heights and wave periods. The wave height that is used for the installation of pipelines is the significant wave height. The significant wave height is the mean of the highest one third of the waves, with a corresponding significant wave period [12]. The significant wave height in the period January 2017 - December 2019 is shown in Figure 3.4.

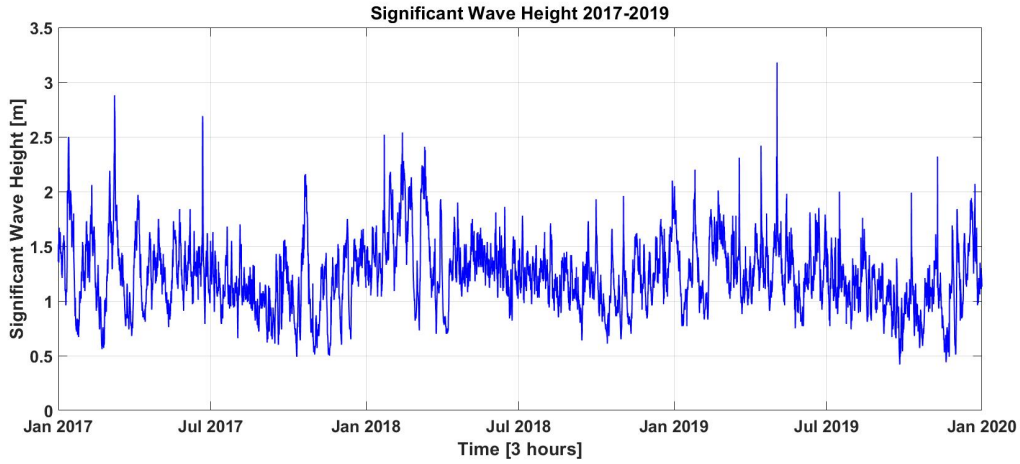

Figure 3.4: Significant Wave Height 2017 - 2019

L:	Wave Length [m]	t:	Time [s]
H:	Wave Height [m]	T:	Wave Period [s]
d:	Water Depth [m]	ω	Wave Frequency [rad/s] = $\frac{2\pi}{T}$
a:	Wave Amplitude [m] = $\frac{H}{2}$	k	Wave Number = $\frac{2\pi}{L}$

Table 3.1: Wave Parameters

Table 3.1 shows general wave parameters that are used when describing propagating waves. According to the potential theory, the relation between the wave period and wavelength is expressed via the dispersion relation:

$$\frac{\omega^2}{gk} = tanh(kd) \tag{3.6}$$

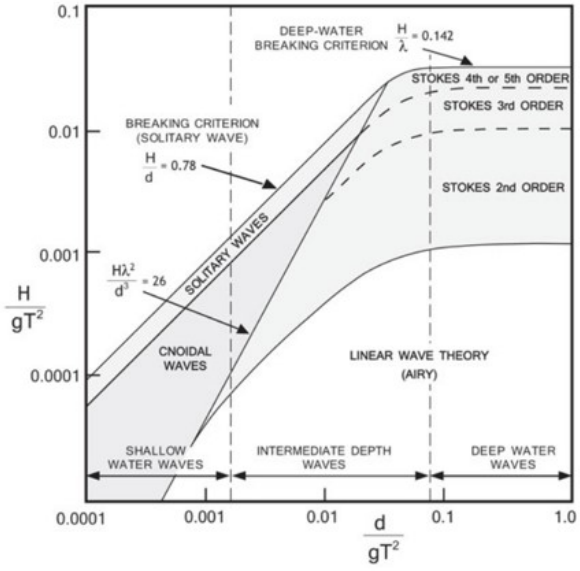

Figure 3.5: Wave Theory Applicability [5]

Multiple wave theories are defined that applicable for different wave conditions. The appropriate wave theory for given wave conditions depends on three parameters: the wave period, T, the wave height, H, and the water depth. The suitable wave theory for the given wave parameters can be obtained from Figure 3.5. The cold water pipeline is installed from very shallow water near shore to deep waters, therefore multiple wave theories apply along the length of the pipeline.

3.4. Installation Conditions and Parameters

The installation of the pipeline will happen in favourable weather conditions, where the combination of wave height and current velocity is at a minimum. Based on the obtained data, the best installation period with a combination of a low current velocity and minimum wave height, the best period is August – November. Table 3.2 shows the percentage significant wave heights lower than 1 [m] and the average absolute surface current velocity in this period [42].

Year	**Aug - Sept**		**Sept - Okt**		**Okt - Nov**	
	$H_s < 1$ [m]	$u_{surface}$ [m/s]	$H_s < 1$ [m]	$u_{surface}$ [m/s]	$H_s < 1$ [m]	$u_{surface}$ [m/s]
2017	51%	0.31	51%	0.21	45%	0.12
2018	18%	0.24	39%	0.21	31%	0.34
2019	59%	0.32	59%	0.35	56%	0.38
Total	43%	0.29	50%	0.26	41%	0.28

Table 3.2: Percentage $H_s < 1$ [m] and Average Surface Current Velocity

Listed below are assumptions made regarding the installation of the pipeline.

- Except for a short section of the pipeline in the near shore area, deep water conditions apply during the installation of the pipeline. In deep waters, the wave particles travel in orbital motions and quickly decay to zero [28]. It can therefore be assumed that the hydrodynamic loading is dominated by the current velocity [26]. The hydrodynamic loading resulting from the waves is therefore neglected during the installation of the pipeline.
- The surface current velocity is assumed to be 0.2 [m/s] during the installation and a velocity of 0.01 [m/s] at a depth of 1000 [m]. The resulting current velocity profile is based on the exponential approximation given by equation 3.5 and is illustrated in Figure B.4 in Appendix B.
- The pipeline is installed with the offshore end open, resulting in the internal pressure being equal to the external pressure, $p_i = p_e$.
- The E-modulus of the pipeline is assumed to be 800 MPa at the start of the installation. The E-modulus of 800 [MPa] value accounts for the warmer surface temperature and the loading that results from the transportation of the pipeline. During the installation, the E-modulus is assumed to remain constant.
- The seawater density increases slightly with increasing water depth. The density increase from 1025 [kg/m^3] at the surface to 1027.6 [kg/m^3] at 1000 [m] water depth. This density gradient is not taken into account. The average seawater density of the surface seawater and deep seawater is used [48].
- Three specific dimension ratios are considered for the cold water pipeline: SDR 21, SDR 26 and SDR 33. These are currently the largest standard dimension ratios in which HDPE pipelines are produced for a pipeline with an outer diameter of 2.25 [m].

Table 3.3 shows the general installation parameters that apply at the start of both installation methods. To take into account the viscoelastic behaviour, two design stresses are defined for the installation. A higher design stress of 9.5 [MPa] that can be applied for a short duration of 30 minutes and a lower design stress of 8 [MPa] that can be applied during the entire installation. The design stress follows from Figure 2.12. Furthermore, the minimum bending radius for the three specific dimension ratios is calculated via equation 2.5.

Pipeline Length	3300 [m]
Max. Allowed Von Mises Stress Short Term (t $\leq \frac{1}{2}$ hr)	9.5 [MPa]
Max. Allowed Von Mises Stress Long Term (t $> \frac{1}{2}$ hr)	8 [MPa]
Surface Current Velocity	0.2 [m/s]
Seabed Current Velocity	0.01 [m/s]
Average Seawater Density	1026.6 [kg/m^3]
E-modulus	800 [MPa]
Installation Depth Pipeline Offshore End	950 [m]
Minimum Bending Radius SDR 21	60 [m]
Minimum Bending Radius SDR 26	75 [m]
Minimum Bending Radius SDR 33	96 [m]

Table 3.3: Installation Parameters

4

Hold and Sink Installation Method

4.1. Introduction

The hold and sink installation method is the first installation method considered. The 3300 [m] cold water pipeline is made up of smaller pipeline segments of approximately 500 [m] in length that are joined together. Due to limited space onshore, the ballast weights are attached while the pipeline is floating on the sea surface. The pipeline is filled with air while the ballast weights are being attached, to prevent the pipeline from sinking. After the attachment of all the ballast weights, the pipeline is towed to the installation location. At the installation location, the hold points are connected and the pipeline is filled with water from the shore end of the pipeline. As the pipeline is filled with water, it starts to sink. The sinking process is controlled by the hold points and a pull force at the offshore end of the pipeline. This pull force acts as an additional vertical hold component as the pipeline sinks, it can be used to control the installation trajectory of the pipeline and it reduces the bending stress in the pipeline. And overview of the external loads on the pipeline during the installation is illustrated in Figure 4.1.

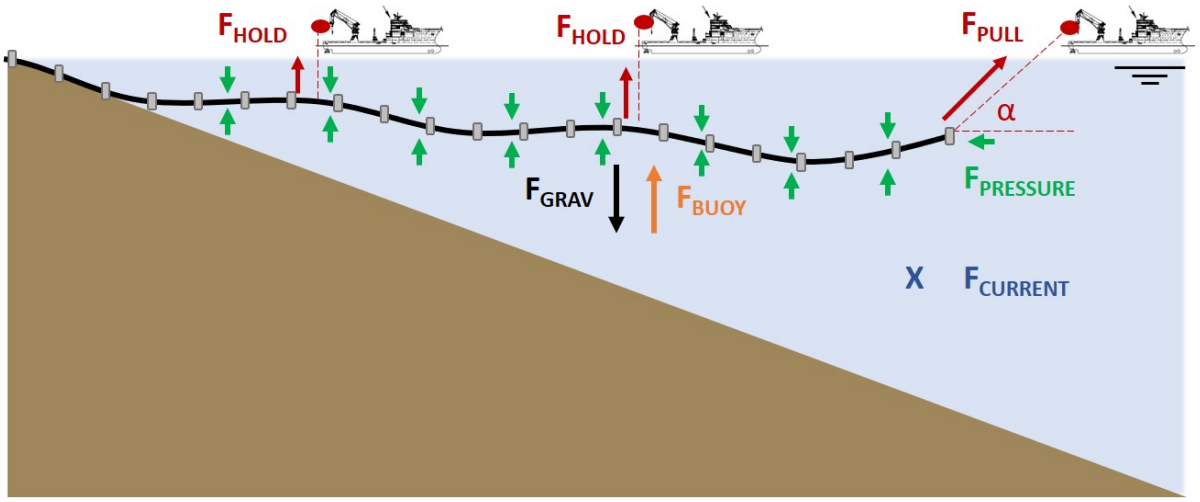

Figure 4.1: Overview of Hold and Sink Installation Method

4.2. Concrete Ballast Weights

The concrete ballast weights serve two purposes. The first one is to reduce the buoyancy of the pipeline to make the pipeline sink. The second is to provide stability on the seabed during the operational life of the pipeline. The required amount of concrete to satisfy the seabed stability criterion is used as the design concrete ballast weight, as it is significantly larger than the amount of concrete required to make the pipeline sink.

The seabed stability criterion is given by equation 4.1 [25]. F_D is the drag force given by equation 4.2, F_I is the inertia force given by equation 4.4, F_L is the lift force given equation by 4.3, μ is a friction coefficient, γ is a safety factor and W_{sub} is the submerged weight of the pipeline. The environmental loading is calculated based on the design conditions, which are taken as a 100-year wave height and a 10-year surface current velocity [20].

$$\gamma * (F_D + F_I) \leq \mu(W_{sub} - F_L) \tag{4.1}$$

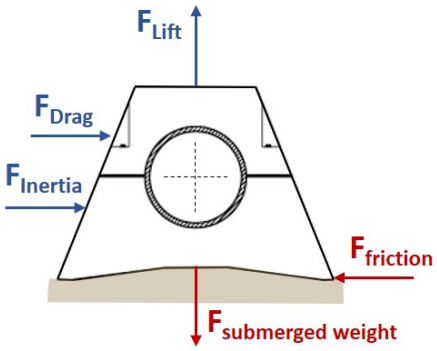

Figure 4.2: Loading on Concrete Ballast Weight

$$F_D = \frac{1}{2} C_D D_p \rho_w u_f^2 \tag{4.2}$$

$$F_L = \frac{1}{2} C_L D_p \rho_w u_f^2 \tag{4.3}$$

$$F_I = \frac{\pi}{4} \rho_w D_p^2 C_I \dot{u}_f \tag{4.4}$$

The amount of available data is limited to three years, which is discussed in Chapter 3. Therefore, the Weibull distribution is used to determine the design conditions[20]. The Weibull distribution is given by equation 4.5. The scale parameter a and the shape parameter b are obtained via the environmental data. The Weibull parameters are given in table 4.1. The design values used for the stability criterion are given in the tables 4.2, 4.3 and 4.4. More details about the design conditions are given in Appendix B.

$$F_{WB}(x) = \frac{b}{a}(\frac{x}{a})^{b-1} exp(-(\frac{x}{a})^b) \tag{4.5}$$

	a	b
Waves	1.36	4.01
Current	0.35	2.0836

Table 4.1: Weibull Parameters

	2017-2019	100-Year
H_{sig}	1.23 [m]	2.55 [m]
T_p	5.89 [s]	8.46 [s]

Table 4.2: Average Wave Parameters

	100-Year Storm
H_{max}	4.7 [m]
T_p	10 [s]

Table 4.3: 100-Year Storm Wave Parameters

	2017-2019	10-Year	Install
$u_{surface}$	0.31 [m/s]	1.13 [m/s]	0.2 [m/s]

Table 4.4: Surface Current Velocity

The submerged weight of the pipeline in equation 4.1 consists of: the weight of the pipeline, W_p, the weight of the concrete ballast, W_c, the buoyancy of the pipeline, $F_{B,p}$ and the buoyancy of the ballast, $F_{B,c}$. The submerged weight is given by equation 4.6. By combining equation 4.1 and 4.6 the required, amount of concrete ballast per meter is calculated.

$$W_{sub} = W_p - F_{B,p} + W_c - F_{B,c} \tag{4.6}$$

Once the required submerged weight is known, the specific gravity is calculated via equation 4.7 [26]. The specific gravity is the ratio of the density of the pipeline over the density of the seawater.

It indicates whether the pipeline sinks, $SG > 1$ or floats $SG \leq 1$. The specific gravity is used to model the weight of the pipeline in the numerical model [47].

$$SG = \frac{W_{sub} + F_B}{F_B} \tag{4.7}$$

The value of the specific gravity varies along the length of the pipe. It is highest in the coastal area, where the current velocity and wave height is highest and decreases with water depth. Using the specific gravity of the coastal zone for the entire pipeline, the deeper water pipeline would be overballasted. This results in unnecessary ballast for the deeper water regions and an increase in the required hold capacity as the submerged weight of the pipeline is higher. This is avoided by applying a constant specific gravity that is determined for a water depth beyond the coastal zone. Post ballasting is then be applied for the zones where higher specific gravity is required.
The specific gravity is calculated at a depth of 300 [m] where the design current assumes a nearly steady profile and the influence of the waves has reduced to zero, this is illustrated in Appendix B. As the submerged weight is determined via the stability criterion, the submerged weight for the three specific dimension ratios is equal. The difference in specific gravity follows from the amount of ballast that is required to obtain the submerged weight. A lower SDR value indicates a thicker walled pipeline which results in a larger buoyancy force. A lower SDR value thus requires more concrete ballast. The specific gravity values and the required amount of concrete per meter are given in table 4.5.

Pipeline Dimension	**Specific Gravity**	**Required Amount of Concrete [Kg/m]**
SDR 21	1.037	135
SDR 26	1.045	120
SDR 33	1.056	106

Table 4.5: SG Values For Different SDR at 300 [m] Water Depth

Figure 4.3: Ballasted HDPE Pipeline [49]

4.2.1. Post Ballasting Methods

Multiple methods of post ballasting are available. The most frequently used methods are listed below [9].

- Concrete mattresses. The concrete mattresses consist of interconnected concrete blocks. The flexibility that results form the connections between the concrete blocks allows for the concrete mattresses to be placed over the pipeline.
- Rock dumping. Rocks are dumped on top of the pipeline to provide the required additional ballast.
- Bags or nets filled with sand, grout or rocks. These bags or nets can be placed on top of the pipeline to provide the additional weight, similar to the concrete mattresses.

For the Bonaire cold water pipeline, either the concrete mattresses, bags or nets are preferred as they can be installed by a crane vessel that is already used for the installation of the cold water pipeline. Whereas for the rock dumping, a specialized rock dumping vessel is required.

4.3. Sensitivity Analysis

A sensitivity analysis is conducted to see how the pipeline reacts to different installation scenarios.

4.3.1. Pipeline Stress Sensitivity

To determine the influence of the dimension ratio in combination with the pull force on the pipeline stresses, the following scenario is created. The pipeline is held at the sea surface at five hold points and does not sink, illustrated by Figure 4.4. The specific gravity values of table 4.5 are used, resulting in an equal submerged weight for the three SDR pipelines. Lastly, three different pull loads are applied on the pipeline,
50 [mT], 100 [mT] and 150 [mT]. The resulting stresses are calculated via the equations given in section 2.5 and the results are given in table 4.6.

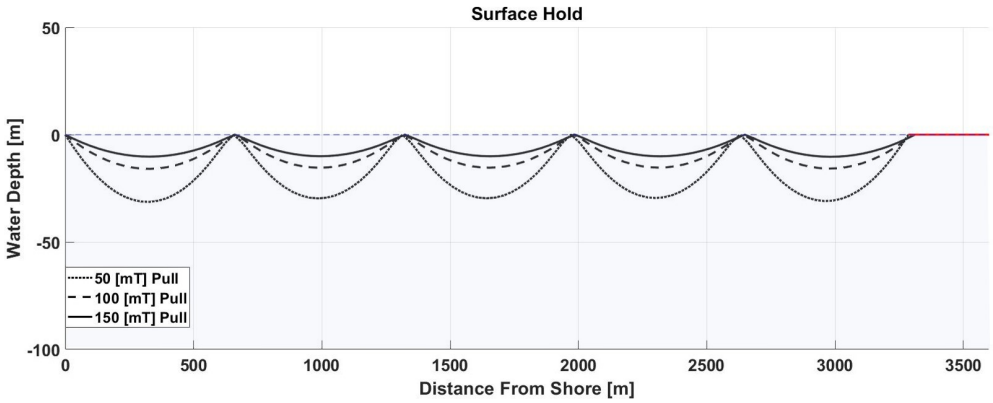

Figure 4.4: Sea Surface Hold With 5 Points

Both the bending stiffness and axial stiffness of the pipeline depend on the wall thickness. The axial stiffness is given by EA, with E the E-modulus and A the surface area calculated via equation 4.8.

$$A = \frac{\pi}{4}(D_o^2 - D_i^2) \tag{4.8}$$

The surface area increases with increasing wall thickness. An increase in the surface area results in an increase in axial stiffness and a decrease in axial stress. The corresponding axial stress that results from the axial strain is calculated via equation 2.10 and is given in table 4.6. Figure 4.5 shows the axial stress distribution in the pipeline. The maximum axial stress can be found in the hold points and the minimum axial stress in between two hold points. The axial stress results primarily from the applied pull force at the offshore end of the pipeline. The difference between the maximum axial stress and minimum axial stress is not significant with a maximum difference of 0.16 [MPa]. The axial stress will increase when the applied load is increased, following the relation given by 2.11. The highest axial stress occurs for the smallest wall thickness in combination with the highest applied load.

Similarly, the lowest axial stress occurs for the largest wall thickness, SDR 21, and the lowest applied load.

The bending stiffness of the pipeline is given by EI, where I is the second moment of area given by equation 4.9.

$$I = \frac{\pi}{64}(D_o^4 - D_i^4) \tag{4.9}$$

Similarly to the axial stiffness, the bending stiffness increases with increases wall thickness. This results in the highest bending stiffness for the pipeline with the largest wall thickness, SDR 21. The effect of the pull force is also clearly visible. A large pull force on the offshore end of the pipeline results in the straightening of the pipeline, which in turn reduces the sag and therefore the bending of the pipeline in between two hold points. Figure 4.6 illustrates the bending stress distribution in the pipeline which is calculated via equation 2.12. The highest bending stress occurs in the hold points and is significantly higher than the bending stress in between two hold points, where the bending radius is larger.

The Von Mises stress is calculated via equation 2.5. The longitudinal stress component is the combination of the component resulting from the axial strain, and the component resulting from the pipeline bending. The resulting Von Mises stress profile is given by Figure 4.7.

It can be concluded from this stress sensitivity analysis that both axial stress and bending stress increase for decreasing wall thickness. The bending stress can be decreased by applying a larger pull force which in return leads to an increase in axial stress as well.

Pull Force [mT]	Pipeline Dimension	Axial Stress [MPa]	Bending Stress [MPa]	Von Mises Stress [MPa]	Wall Thickness [m]
50	SDR 21	0.7	5.1	5.8	0.107
	SDR 26	0.9	5.5	6.3	0.087
	SDR 33	1.1	6.0	7.0	0.068
100	SDR 21	1.4	3.3	4.7	0.107
	SDR 26	1.7	3.6	5.2	0.087
	SDR 33	2.1	3.7	5.8	0.068
150	SDR 21	2.1	2.5	4.5	0.107
	SDR 26	2.5	2.6	5.1	0.087
	SDR 33	3.2	2.6	5.8	0.068

Table 4.6: Pipeline Stresses 5 Point Surface Hold

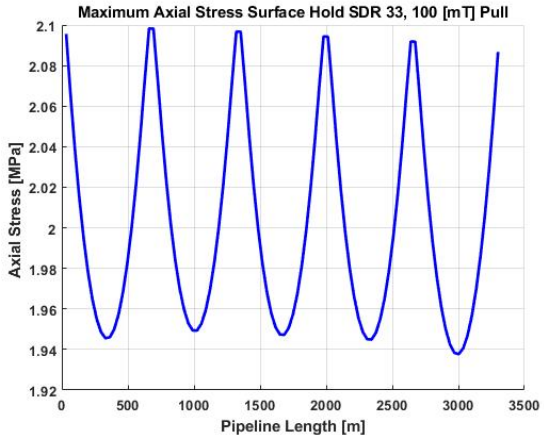

Figure 4.5: Maximum Axial Wall Stress Surface Hold SDR 33, 100 [mT] Pull Force

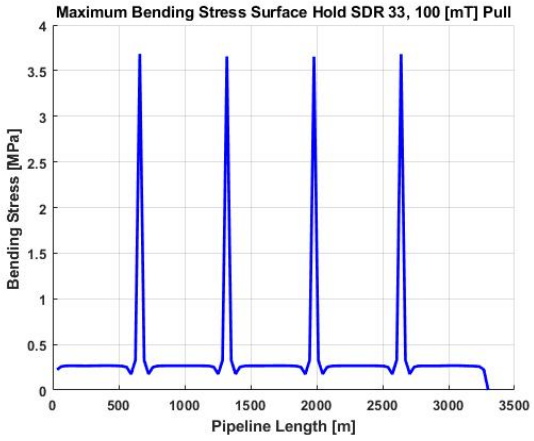

Figure 4.6: Maximum Bending Stress Surface Hold SDR 33, 100 [mT] Pull Force

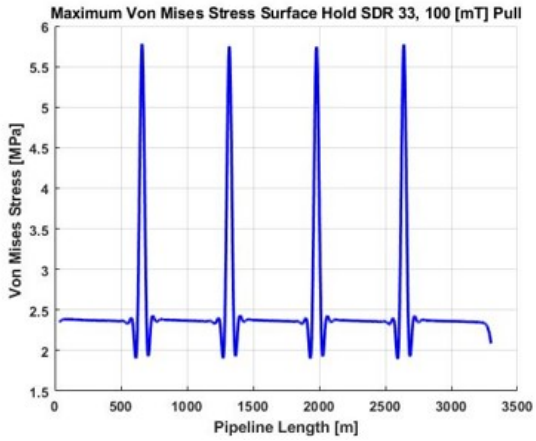

Figure 4.7: Maximum Von Mises Stress Surface Hold SDR 33, 100 [mT] Pull Force

4.3.2. Vertical Hold Capacity

The minimum required vertical Hold capacity that is required to install the pipeline with a maximum allowed installation Von Mises Stress of 8 [MPa] is given in table 4.7. The sinking velocity is limited to 0.2 [m/s], which corresponds to the average sinking velocity for the float and sink installation method and is used as a reference for this installation method [14]. The vertical hold capacity is limited to 150 [kN], which corresponds to a small crane vessel [6]. The additional buoyancy modules are attached to the pipeline in between two hold points. The amount of additional buoyancy available within Allseas is 15 [mT], which is not exceeded. The total submerged weight of the pipeline is 96 [mT] with the specific gravity values given in table 4.5. Part of the vertical hold capacity results from the pull force. As the pipeline sinks, the angle (α) between the pipeline and the pull force increases, resulting in an increase in the vertical component of the pull force, illustrated in Figure 4.8. The results show that the required hold force is equal for the three SDR pipelines, which is a result of the equal submerged weight. For the 50 [mT] pull force, an additional hold point is required as the vertical capacity of 150 [kN] was exceeded.

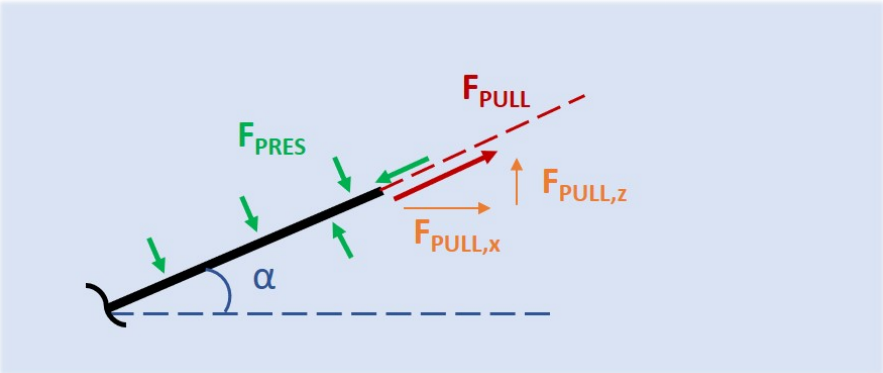

Figure 4.8: Forces Acting on the Offshore End of the Pipeline

Pipeline Dimension	Pull Force Vessel [mT]	Hold Vessels	Minimum Vertical Hold Force [kN]	Additional Buoyancy [mT]
SDR 21	50	5	130	15
	100	4	150	15
	150	4	150	15
SDR 26	50	5	130	15
	100	4	115	15
	150	4	115	15
SDR 33	50	5	130	15
	100	4	150	15
	150	4	150	15

Table 4.7: Minimum Required Vertical Hold Capacity

4.3.3. Lateral Deflection of the Pipeline

The drag force that results from the current flow is expected to have a significant influence on the lateral position of the pipeline due to the large diameter and long length of the pipeline. The drag force that results from the current is calculated with equation 4.2. The lateral position of the pipeline at the sea surface including the installation surface current velocity of 0.2 [m/s] is illustrated in Figure 4.9. The figure illustrates a scenario where no additional lateral forces are applied and a scenario where 4 additional lateral forces are applied to the pipeline. The figure illustrates that a larger pull force provides more resistance against lateral deflection. To keep the pipeline at the intended installation position, the hold vessels can apply a lateral push or pull force to the pipeline at the sea surface. The lateral deflection at the sea surface has been reduced to a maximum of 11 [m] after application of 4 [mT] lateral force per vessel.

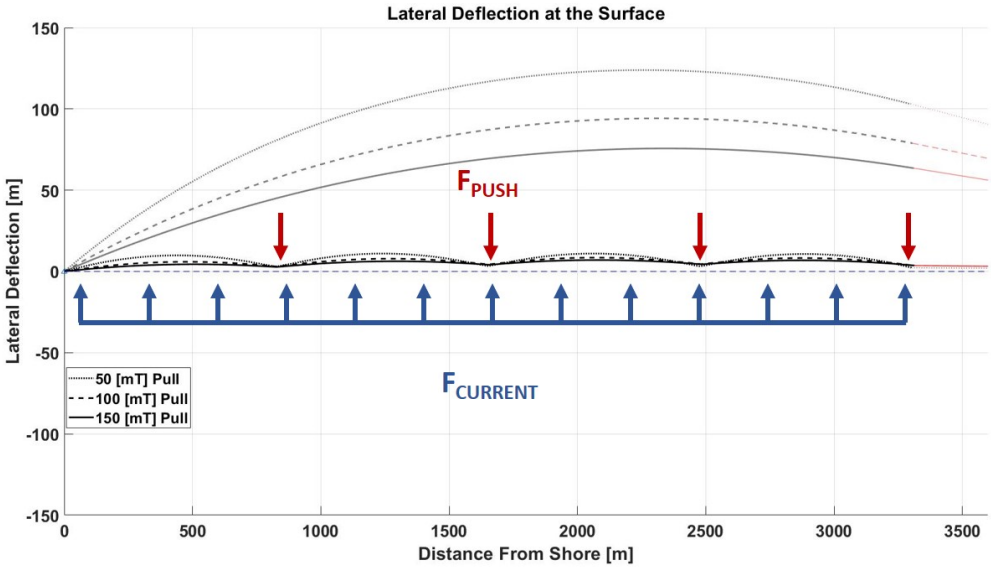

Figure 4.9: Lateral Deflection of Pipeline at Sea Surface with 0.2 [m/s] Surface Current Velocity

The maximum lateral deflection of the pipeline after the installation is given in table 4.8. The 100 [mT] and the 150 [mT] yield similar results, the lateral deflection for the 50 [mT] is approximately three times larger than the 100 and 150 [mT] pull force. A second scenario is checked where the current velocity is increased. The current velocity is increased to 0.25 [m/s] at the sea surface and 0.045 [m/s] at the seabed at 1000 [m] water depth. The current profile is illustrated in Appendix B Figure B.4. An increase in the current significantly increases the lateral deflection of the pipeline, as can be seen in table 4.8.

It is not taken into account that the hold vessels can provide lateral resistance during the installation. It is assumed that only a vertical force is applied.

Current Velocity Profile	50 [mT] Pull Deflection [m]	100 [mT] Pull Deflection [m]	150 [mT] Pull Deflection[m]
Installation Velocity Profile	36	10.6	8.3
Increased Velocity Profile	93.8	36.5	34.5

Table 4.8: Maximum Lateral Pipeline Deflection After Installation

4.3.4. Cost Estimation

A cost estimation for the installation method is based on the material cost price and the day rate of the required vessels. This allows for a comparison between the two installation methods as the same criteria are used. Additional costs, such as the transportation of the materials, is not taken into account in this estimation. The price of a HDPE pipeline is calculated based on a price indication of €2.7 per kilogram HDPE pipeline. The weight for the concrete ballast weights is calculated based on a quotation from Pipeshield [8]. The costs for the materials are given in table 4.9. The costs of the ballast are for the S.G values in table 4.5. A second ballast price is given for the amount of additional ballast that is required for post ballasting. The costs of the required vessels are estimated to be €20.000 per day [22].

SDR	HDPE [1000 €]	Concrete Ballast [1000 €]	Additional Ballast [1000 €]
21	6200	120	120
26	5000	100	120
33	4000	90	110

Table 4.9: Material Costs Hold and Sink Installation Method

4.4. Hold and Sink Installation Method Results

From the conducted sensitivity analysis, it is concluded that larger pull forces, 100 [mT] and 150 [mT], are beneficial during the installation. Under the assumptions made, the pipeline has less lateral deflection after the installation and less vertical hold vessels are required compared to the 50 [mT] pull force. Therefore, the 50 [mT] pull force installation is not considered for the hold and sink installation. The maximum Von Mises stresses for the three SDR pipelines are all lower than the design stress and the minimum required vertical hold capacity is equal for the 100 [mT] and 150 [mT] pull force. Based on the cost price of the HDPE pipeline, the SDR 33 pipeline is considered for the hold and sink installation method. The installation procedure for the hold and sink installation over time is illustrated in Figure 4.10. The modelling time of the simulation is 7200 [s]. Four hold points are attached to the pipeline which are illustrated by the dashed red lines. Four sets of buoyancy modules are attached in between two hold points, illustrated by the blue dots. The red line illustrates the pull cable that is attached to the end of the pipeline and the pull vessel, with an initial pull force of 100 [mT] at the start of the installation.

As the pipeline sinks, the angle between the pipeline end and the pull force will increase. Subsequently, the pull force gradually becomes more vertical, illustrated in Figure 4.8. In the case that the submerged weight and the total vertical hold capacity become equal during the installation, an equilibrium will be reached and the pipeline will not sink further. Therefore, both the hold forces and pull force are reduced over time. Both the hold forces and buoyancy modulus are released when their designated depth is reached.

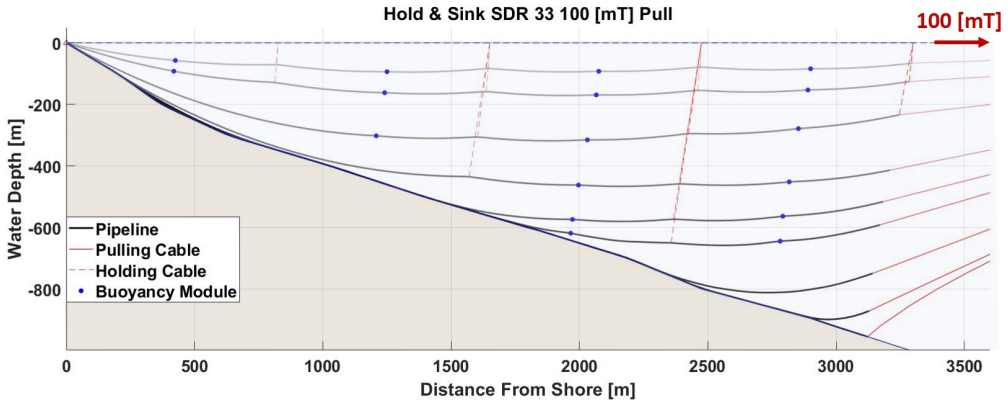

Figure 4.10: Hold & Sink Installation For 100 [mT] Pull as Modelled

The bending stress that occurs in the pipeline during the installation over time is illustrated by Figure 4.11. The bending stress in the pipeline wall is given by equation 2.12. The highest bending stress occurs at the hold points, where the bending radius is the smallest. The bending stress at the hold points decreases over time with the decreasing vertical hold force. Furthermore, the bending stress is removed at the hold point when the hold point is released. Towards the end of the installation, the offshore end of the pipeline curls upwards as the downward force is equal to the upward force. The occurring bending radius results in a bending stress which can be observed in Figure 4.11. As the pull force decreases further with time, the pipeline will gradually sink to the bottom. The remaining bending stress peaks that can be observed in the figure after approximately 5000 [s] result from the pipeline bending over the seabed slope.

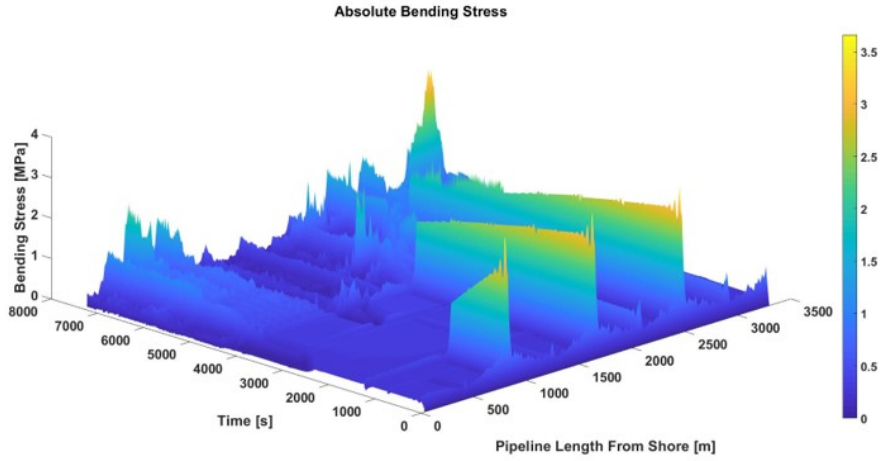

Figure 4.11: SDR 33 100 [mT] Pull Force, Bending Stress

The axial stress in the pipeline wall is illustrated in Figure 4.12. The axial stress is given by equation 2.11. The maximum value of the axial stress occurs at the start of the installation, where the applied pull force is at a maximum. During the installation, the pull force decreases, resulting in a decrease in axial stress. Furthermore, the hydrostatic pressure, given by equation 4.10, increases with water depth (z). The hydrostatic pressure results in an increase in compressive axial stress with increasing water depth.

$$F_p = \rho_w g z \tag{4.10}$$

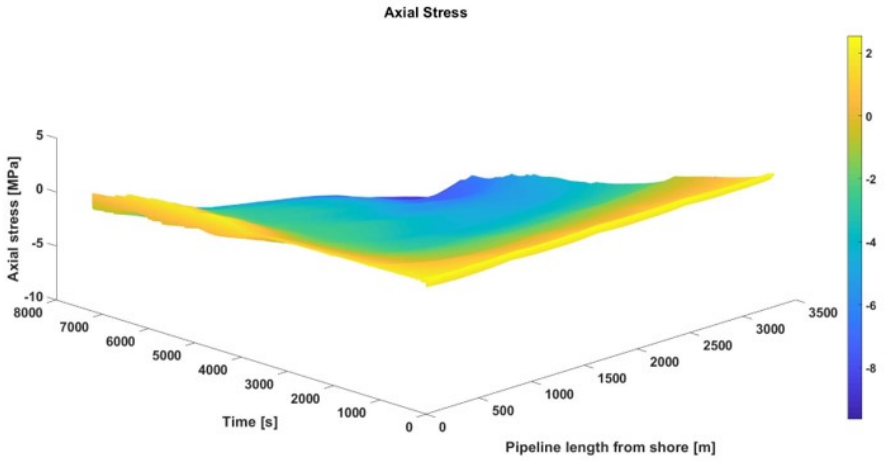

Figure 4.12: SDR 33 100 [mT] Pull Force, Axial Wall Stress

The resulting maximum Von Mises stress is illustrated in Figure 4.13. The Von Mises stress is the equivalent stress of the combined longitudinal stress, the hoop stress and the radial stress. The longitudinal stress is the summation of axial stress component in the pipeline wall and the bending stress component. Both the hoop stress and radial stress depend on the hydrostatic pressure. As the internal pressure is equal to the external pressure, the hoop and radial stress are equal, which follows from equation 2.8 and equation 2.9. As the outer surface area is larger than the inner surface area, both the hoop and radial stress are compressive. The hoop stress and radial stress in the pipeline with water depth are illustrated in Figure 4.14 and Figure 4.15. The pressure related stress components cancel out in the Von Mises stress. The main contribution to the Von Mises stress results from the bending stress component.

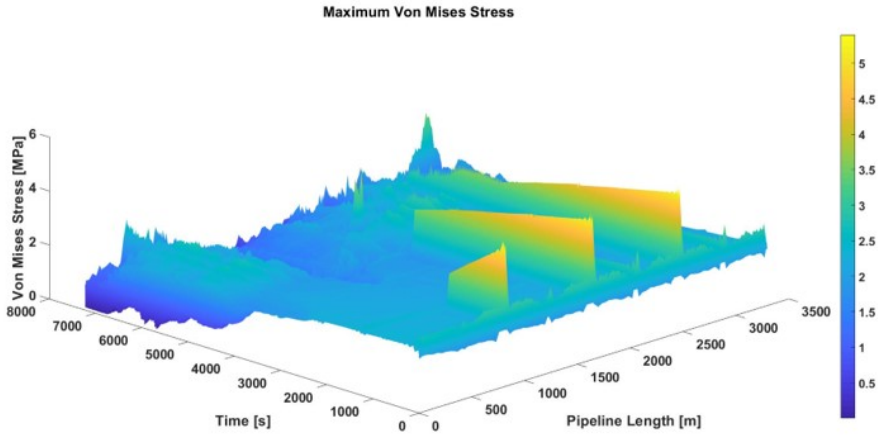

Figure 4.13: SDR 33 100 [mT] Pull Force, Maximum Von Mises Stress

Figure 4.14: Hoop Stress in the Pipeline

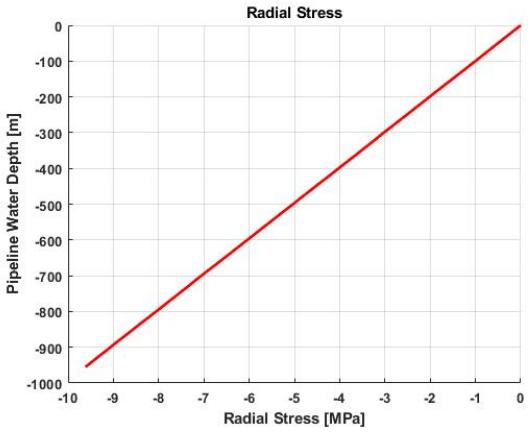

Figure 4.15: Radial Stress in the Pipeline

The effective wall tension during the installation is illustrated in Figure 4.16. The effective wall tension has a positive value during the entire installation procedure. It can be concluded that the global buckling analysis is satisfied, which indicates that it is not likely that local buckling occurs during the installation. Furthermore, a decrease in effective wall tension can be observed over time. This results from the decrease in pull force at the offshore end of the pipeline over time.

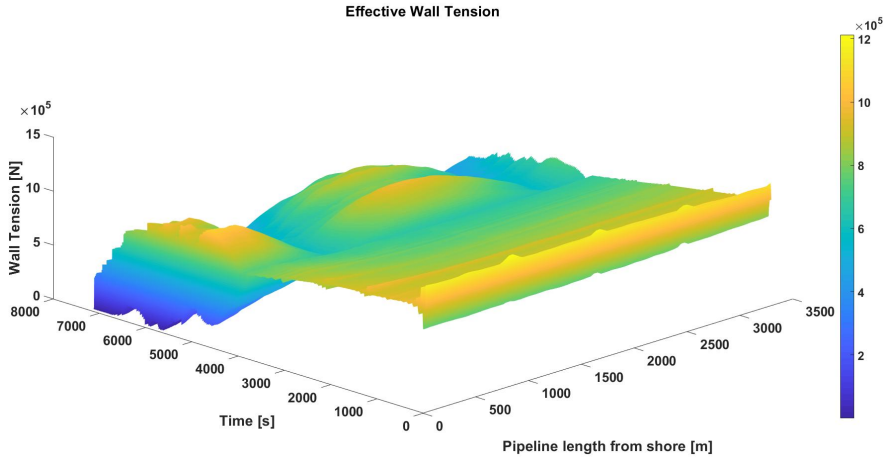

Figure 4.16: SDR 33 100 [mT] Pull Force, Effective Wall Tension

Table 4.10 gives an overview of the occurring stresses in the pipeline for the hold and sink installation. The stresses for both the installations with 100 [mT] and 150 [mT] remain below the design stress. The last column shows the minimum bending radius that occurs during the installation, which satisfies the minimum bending radius criterion for a SDR 33 pipeline given in section 3.4.

Pull Force [mT]	**Max. Axial Stress [MPa]**	**Min. Axial Stress [MPa]**	**Max. Bending Stress [MPa]**	**Max. Von Mises Stress [MPa]**	**Min. Bending Radius [m]**
100	2.5	-9.6	3.7	5.4	245
150	3.4	-9.6	2.4	5.7	259

Table 4.10: Overview of Occurring Installation Values

4.4.1. Effect of Varying E-modulus

In Chapter 2, the varying elastic modulus of HDPE is discussed. The E-modulus varies due to loading time and temperature variations. The influence of the varying modulus is checked by running the same installation configuration with different E-moduli. Based on a constant applied stress of 4 [MPa], the corresponding E-modulus is obtained according to the data provided by Pipelife [43]. An E-modulus of 510 corresponds to a constant loading of 2 hours, 425 corresponds to a constant loading of 10 hours and 1050 corresponds to the E-modulus at time = 0.

The results are given in table 4.11. A decrease in the E-modulus results in a decrease in bending stiffness. The pipeline will bend more with decreasing bending stiffness, which is illustrated by the decrease in minimum bending radius. The bending moment is given by equation 2.13. The reduction in the E-modulus reduces the stress due to bending given by equation 2.12. The opposite holds for an increase in E-modulus.

The axial stress is given by equation 2.11. With a decreasing E-modulus, the axial stiffness decreases as well. As the axial stiffness decreases, the strain in the pipeline will increase. Following the relation between the axial stress and strain given by equation 2.10, the change in E-modulus results in minimal change in axial stress. It is concluded that for the hold and sink method, the variation in E-modulus does not result in exceedance of the design stress. Furthermore, the minimum bending radius is maintained for all installation scenarios.

E-modulus MPa	Max. Axial Stress [MPa]	Min. Axial Stress [MPa]	Bending Stress [MPa]	Von Mises Stress [MPa]	Min. Bending Radius [m]
1050	2.6	-9.6	4.5	6.2	266
510	2.5	-9.6	2.6	4.4	219
425	2.4	-9.6	2.3	4.1	205

Table 4.11: Occuring Stresses due to Variation in E-modulus

4.5. Final Configuration

The final configuration is illustrated in Figure 4.17. As the maximum Von Mises stress for the three SDR pipelines remain below the design stress, the SDR 33 pipeline is selected based on the cost price of HDPE. A pull force of 100 [mT] or 150 [mT] is considered most efficient, as the lateral deflection for the 50 [mT] installation is significantly larger without any additional lateral force during the installation. Furthermore, the installation with a 50 [mT] pull vessel requires an additional hold vessel. The differences in stress and lateral deflection between the 100 [mT] and 150 [mT] pull force installation are negligible and the occurring maximum Von Mises stress is well below the design stress for both pull forces. For the final installation configuration, a pull force of 100 [mT] is chosen, as it is expected that a 150 [mT] vessel is more expensive. During the analysis, it is assumed that post ballasting is applied after installation. The required amount of additional ballast in the coastal area is given in Appendix B. Applying post ballast leads to reduction in required hold capacity and concrete costs, it does lead however to an increase in installation costs. Lastly, the maximum vertical hold capacity of the vessels is assumed to be 150 [kN]. The relatively low maximum Von Mises stress indicates that the installation could be possible with less hold points. In Appendix D an extension to the sensitivity analysis of this chapter can be found, where a higher SG is considered and an installation scenario with less vertical hold points.

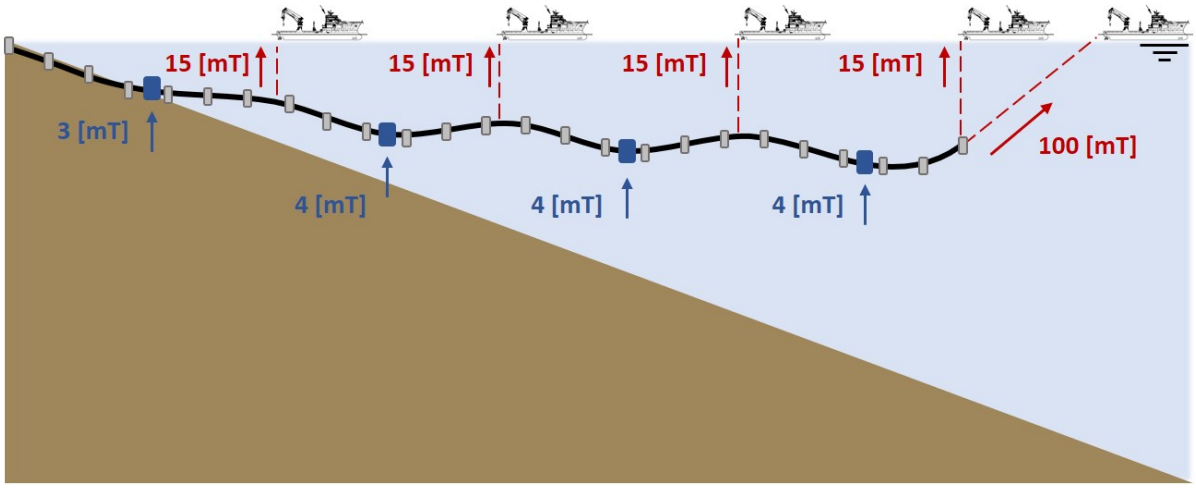

Figure 4.17: Final Configuration Hold and Sink Installation Method

5

Pull Down Installation Method

5.1. Introduction Pull Down Installation Method

The second installation method considered is the pull down installation method, which consists of two installation phases. The pipeline is divided into two sections; a ballasted section and an unballasted section. The first 450 [m] of the pipeline is ballasted with a specific gravity of 1.66 (Appendix B) and reaches a depth of 200 [m]. The ballasted section is installed using the float and sink installation method, while the unballasted section of the pipeline remains floating.

The required air fill ratio during the float and sink installation method is calculated via equation 2.3. During the float and sink installation, the air fill ratio is 19%, which reduces to 0 when the last section of ballasted pipeline is installed and the pipeline is filled with water. The pull force required during the float and sink installation follows from equation 2.6. A minimum pull force of 60 [mT] is required. After completion of the float and sink installation method, the pipeline remains in the equilibrium position illustrated in Figure 5.1.

An anchorbox is installed prior to the second installation phase. The anchorbox is a ballast weight of 150 [mT]. A chain is connected to the offshore end of the pipeline and attached to the pull cable on the other end. The chain is secured in the anchorbox when the target depth is reached. The pull cable runs through the anchorbox and the other end of the cable is attached to a winch on the crane vessel. The pull down installation phase consists of pulling the pipeline down until the chain is secured at the anchorbox.

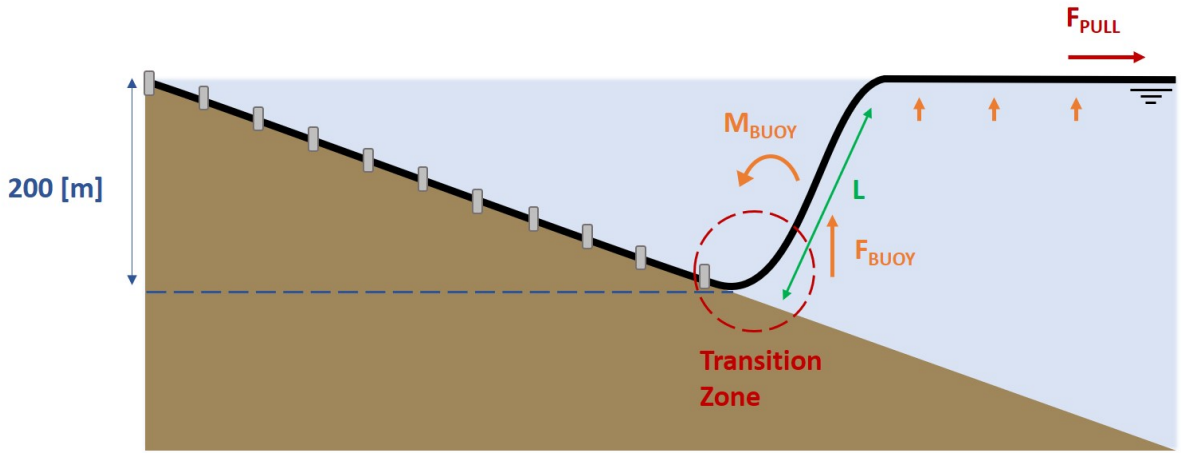

Figure 5.1: Pipeline Configuration After Float and Sink Installation

5.2. Sensitivity Analysis

Similar to the hold and sink installation method, a sensitivity analysis is conducted to see how the pipeline reacts to different installation scenarios for the pull down installation method.

5.2.1. Transition Zone Bending

The transition zone is found to result in critical bending values for the three SDR considered, illustrated by the values in table 5.1. The high bending stresses result from the bending moment that is generated by the upward buoyancy force of the free hanging pipeline inbetween the seabed and the sea surface. The distributed buoyancy force of the pipeline is equal to 300 [N/m] and for the free hanging section the total upward buoyancy force is equal to 300 * L. The resulting bending stresses for the three SDR are almost equal. Based on the cost price of the HDPE pipeline, discussed in section 4.9, the SDR 33 pipeline is considered for the pull down installation method.

SDR	Bending Stress [MPa]
21	13.2
26	13.4
33	13.5

Table 5.1: Bending Stress Before Bend Stiffening

The bending stress can be decreased by increasing the bending stiffness of the pipeline in the transition zone. The bending stiffness of the pipeline is given by EI and can be increased by increasing second moment of area, I or by increasing the E-modulus, illustrated by Figure 5.2

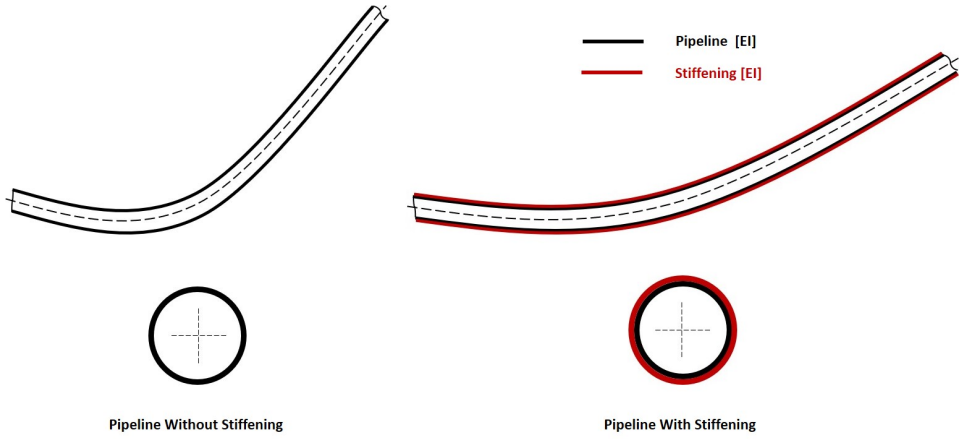

Figure 5.2: Bend Stiffening Working Principle

The second moment of area is increased by increasing the outer diameter of the pipeline. The outer diameter is increased by sliding an additional, or multiple, HDPE pipeline over the main pipeline, as a sleeve. SDR 21 is the largest pipeline wall thickness that can be extruded for a pipeline with an outer diameter of 2.25 [m]. Extruding a pipeline with the required thickness corresponding to the required bending stiffness is therefore not possible. As the same material is used, the E-modulus remains constant and the new bending stiffness is given by equation 5.1.

$$(EI)_{new} = E_1(I_1 + I_2) \tag{5.1}$$

The second method to increase the bending stiffness is achieved by adding a second stiffer material layer with a higher E-modulus. A beam consisting of multiple layers of different materials is called a composite beam. The resulting bending stiffness can be obtained via the transformed section method [24]. Using the transformed section method, the different materials that make up the composite beam are transformed into one material. Transforming the material is done via the modular ratio given by equation 5.2, which is the ratio of the E-moduli of the different materials.

$$n = \frac{E_2}{E_1} \tag{5.2}$$

Hereafter, the equivalent bending stiffness of the composite beam can be calculated via equation 5.3. The resulting bending stress is calculated via equation 2.12. For the transformed material, the bending stress is multiplied with the modular ratio.

$$(EI)_{new} = E_1(I_1 + nI_2) \tag{5.3}$$

Via the numerical model it is found that the bending stress can be decreased to 6.7 [MPa], which allows for a safety margin of 1.3 [MPa], by increasing the bending stiffness by a factor 10 of the original bending stiffness of the pipeline. By increasing the bending stiffness via the application of an additional HDPE sleeve, the required outer diameter would be 3 [m]. The inner diameter remains equal to the initial value. Increasing the pipeline diameter to 3 [m] requires three additional SDR 21 HDPE pipeline segments to be attached to the pipeline.

If steel is used as a stiffer material, this would require a steel pipeline with a wall thickness of 5 [mm]. As the bending stress in the steel pipeline results in the Von Mises stress exceeding the allowed stress for the steel pipeline, smaller steel segments can be used as a replacement of a single steel pipeline. This allows for the bending of the pipeline while at the same time increasing the bending stiffness in the transition zone section [13].

At the start of the pull down phase, the pull force is primarily in a downward vertical direction. To maintain a constant bending moment in the transition zone, an additional horizontal pull force of 5 [mT] is applied to the pipeline at the point where the pipeline reaches the sea surface after the transition zone.
Figure 5.3 shows the bending stress for the SDR 33 pipeline before and after the application of bending stiffening. A second bending stress peak can be observed after the maximum bending stress peak. This is peak is located where the stiffening section ends.

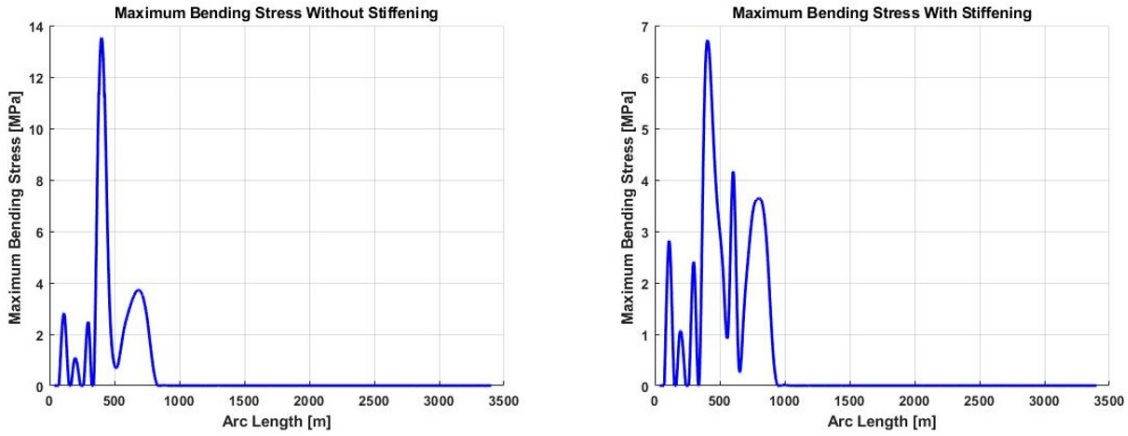

Figure 5.3: Maximum Bending Stress Before and After Stiffening for SDR 33 Pipeline

5.2.2. Pull Down Force

The pull down force is limited to the weight of the anchorbox, which is 150 [mT]. The unballasted pipeline section has a total upwards buoyancy force of 90 [mT] which has to be pulled down. During the pull down phase, the angle (β) between the anchorbox and the pipeline decreases, resulting in an increase in the horizontal component of the pull force, illustrated in Figure 5.4. At the end of the installation, the angle attains a value of approximately 23°. This results in a pull force required to pull the pipeline in position of 230 [mT], which is beyond the capabilities of the anchorbox.

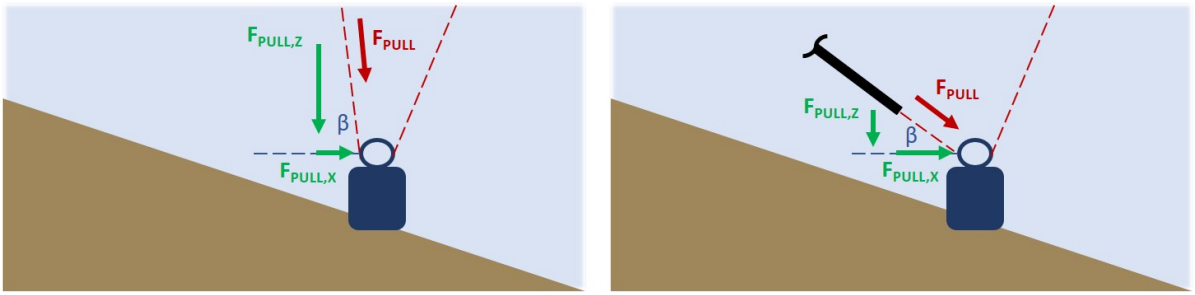

Figure 5.4: Anchor Box Pull Force First Installation Stage and Last Installation Stage

The following approach is used to reduce the pull force. Additional ballast of 50 [mT] is applied to floating free span to reduced the upwards buoyancy force. Three ballast distributions are considered along the free span of the pipeline, 5 * 10 [mT], 10 * 5 [mT] and 20 * 2.5 [mT] ballast weights.
The ballast distribution with 5 * 10 [mT] ballast weights results in high local stress and is therefore not taken into consideration, illustrated in Figure 5.5. Both the 5 [mT] ballast distribution and the 2.5 [mT] ballast distribution are considered. The local maximum Von Mises stress figures of the 20 * 2.5 [mT] and the 10 * 5 [mT] ballast distribution are given in Appendix E.
The pipeline is elongated by 100 [m] compared to the hold and sink pipeline, and the anchorbox is placed an additional 100 [m] from shore, which is therefore installed deeper as well. The angle, β, at the end of the installation is increased by 4°, which increases the vertical component of the pull force resulting in a reduction of required pull force.
The required pull force to install the pipeline is reduced to 105 [mT].

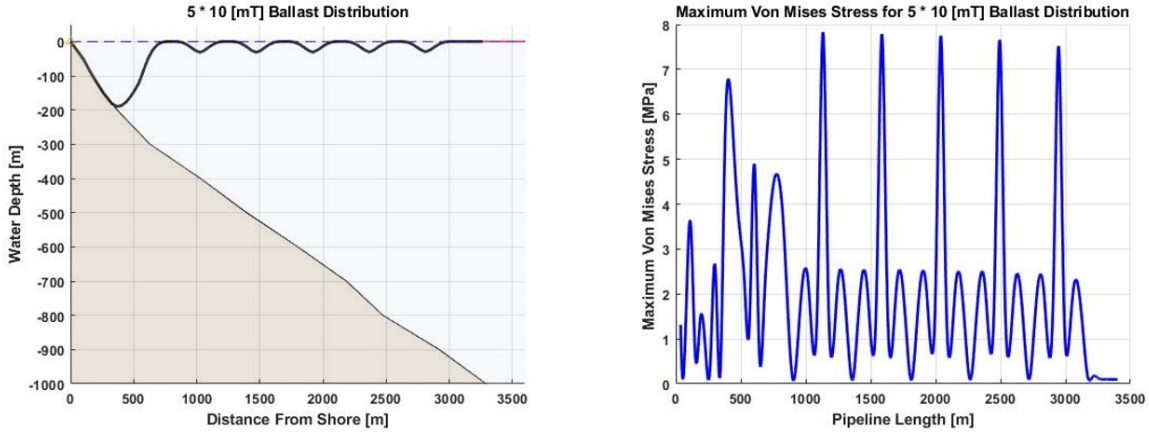

Figure 5.5: Maximum Von Mises Stress for 5 * 10 [mT] Ballast Distribution

5.2.3. Lateral Deflection

Similar to the hold and sink installation method, the lateral position of the pipeline is significantly affected by the current as well. The pipeline consists of three sections after the initial float and sink installation phase. The section on the seabed that was installed via the float and sink installation method that is kept in position by the ballast weights. The section that spans from the transition zone at the seabed to the sea surface. The third section is the pipeline section that remains floating on the sea surface. The drag force due to the current velocity results in an additional bending moment in the lateral direction at the transition point, illustrated in Figure 5.6. Without lateral resistance the bending moment will result in the ballasted section being lifted and moved from the installation position when the lateral resistance capacity of the ballast weights is exceeded, or the pipeline can fail due to excessive bending in the lateral direction. Figure 5.6 illustrates the lateral deflection of the pipeline after the float and sink installation phase. A pull force of 5 [mT] is still applied at the offshore end of the pipeline.
Similar to the hold and sink installation method, the lateral deflection can be reduced by applying lateral forces to the pipeline in opposite direction. In Figure 5.6 the situation is illustrated where four vessels each apply a 2.5 [mT] lateral resistance force to the pipeline.
As the unballasted section takes on the reversed catenary shape after the installation and does not touch the seabed, the lateral deflection of the pipeline is taken as the deflection of the offshore end compared to the lateral position of the anchorbox. The position is checked for the installation current velocity and the increased current velocity. For both current profiles, the pipeline end is pulled into its intended position and the lateral deflection is 0 [m] after the installation. This results from the increase in pull force over time to 105 [mT] and the decrease in current velocity over water depth.

Current Profile	Lateral Deflection [m]
Installation Current	0
Increased Current	0

Table 5.2: Lateral Deflection of Offshore Pipeline End After Installation

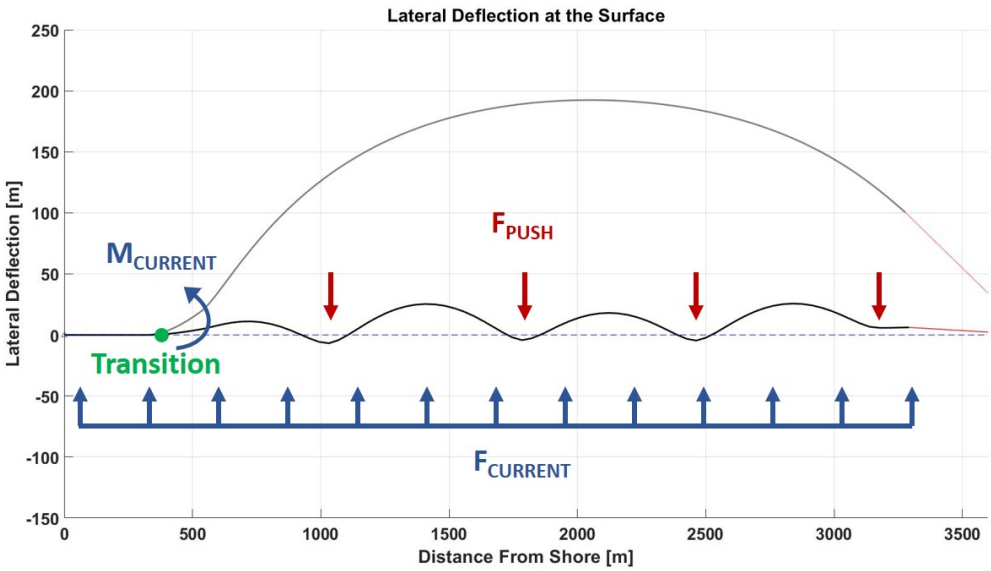

Figure 5.6: Lateral Deflection at Surface Without and Without Lateral Resistance

5.2.4. Cost Estimation

For the pull down installation method, only a SDR 33 pipeline is considered. This results from all three SDR's requiring additional bending stiffness in the transition zone and the cost price of HDPE. Due to the 100 [m] elongation of the pipeline, the cost for the pipeline is slightly higher than that of the hold and sink installation method. The anchorbox itself will be engineered by Allseas, no clear cost estimation can be given as of now. As an indication, the cost price of a ballast weight that was used for the ballast price in section 4.3.4 is scaled up to a ballast weight 150 [mT]. The day rate for the required crane vessel is €40.000 per day [3]. The day rate of the vessel is estimated to be higher than the required vessels for the hold and sink installation method, as a larger crane is required to install the anchorbox. The price for the vessels that provide the lateral resistance force is not included, as local vessels can be used which results in negligible costs as compared to the other costs that are made.

SDR	HDPE [1000 €]	Concrete Ballast [1000 €]	Anchorbox [1000 €]
33	4100	120	40

Table 5.3: Material Costs Pull Down Installation

5.3. Pull Down Installation Method Results

The pull down method installation sequence over time for the 20 * 2.5 [mT] ballast configuration is illustrated in Figure 5.7. The pull cable is illustrated by the red line and the anchorbox is located at the seabed at 3350 [m] offshore. The simulation time is 7200 [s]. The chain that connects the offshore end of the pipeline with the pull cable is not modelled, only the cable itself is modelled.

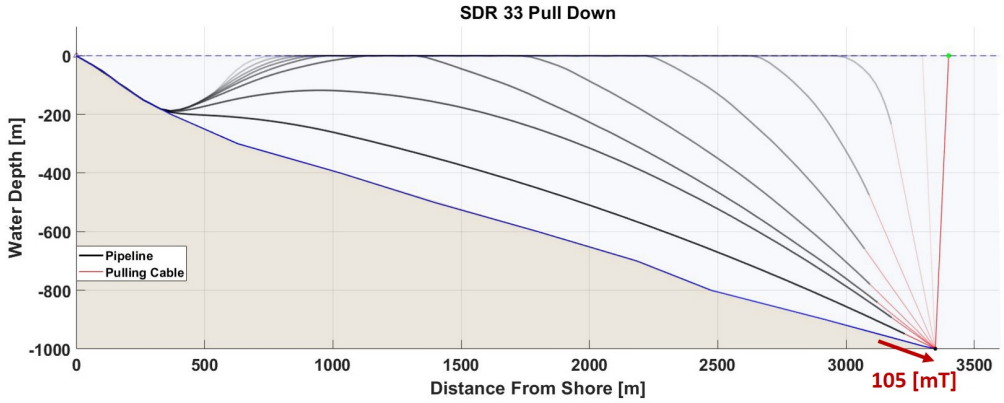

Figure 5.7: Pull Down Installation SDR 33 With 20 * 2.5 [mT] Ballast

Figure 5.8 illustrates the bending stress in the pipeline during the pull down installation phase. The bending stress in the transition zone remains high during the installation as the bending moment in the transition zone is maintained until the entire pipeline is pulled below the sea surface. The transition zone bending decreases when the complete pipeline is submerged. The figure also shows high bending stress at the offshore end where the pipeline is pulled down, with the highest stress occurring at the start of the pull down. This results from the fact that the pipeline is initially pulled down nearly vertically resulting in a small bending radius and therefore a high bending stress. This bending stress decreases as the the angle between the pull cable and anchorbox decreases, resulting in an increase in the bending radius at the sea surface.

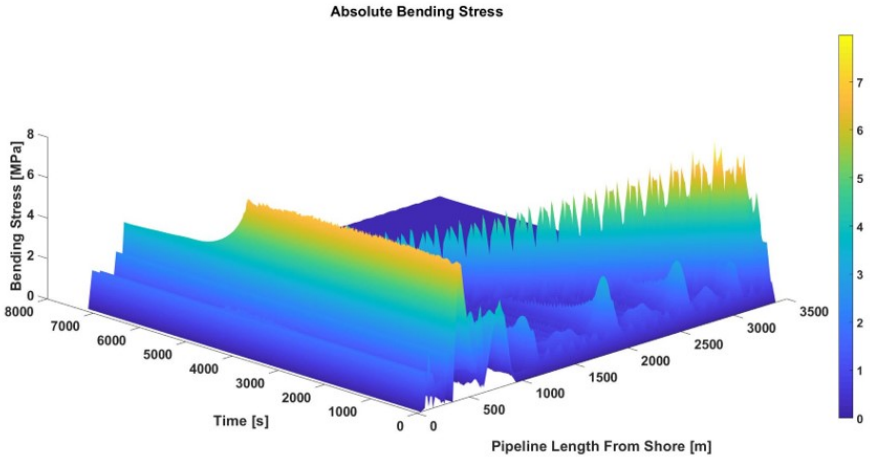

Figure 5.8: SDR 33 20 * 2.5 [mT] Ballast Distribution, Bending Stress

Figure 5.13 illustrates the axial stress in the pipeline wall. For the pipeline section that remains floating at the sea surface, the axial stress increases with the increase in the pull force. The maximum axial stress occurs prior to the moment that last floating pipeline section is submerged. Similar as to the hold and sink installation method, the increase in hydrostatic pressure with water depth results in an increase of compressive stress in the pipeline wall. The maximum value of compressive stress for the pull down installation method is lower than that of the hold and sink method, as the pull force acts as a tensile stress component in the opposite direction of the compressive hydrostatic pressure.

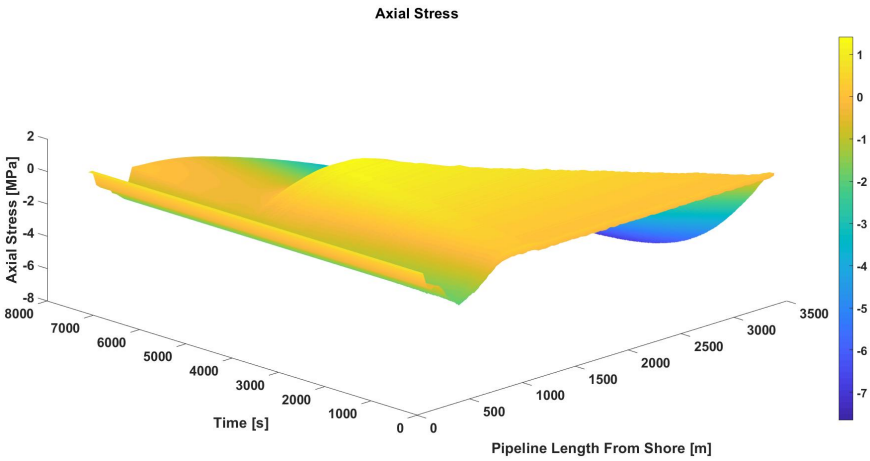

Figure 5.9: SDR 33 20 * 2.5 [mT] Ballast Distribution, Axial Wall Stress

The resulting Von Mises stress is shown in Figure 5.10. As is explained in section 4.4, the Von Mises stress is highest where the bending stress is highest. The hydrostatic pressure stress components cancel out in the Von Mises stress.

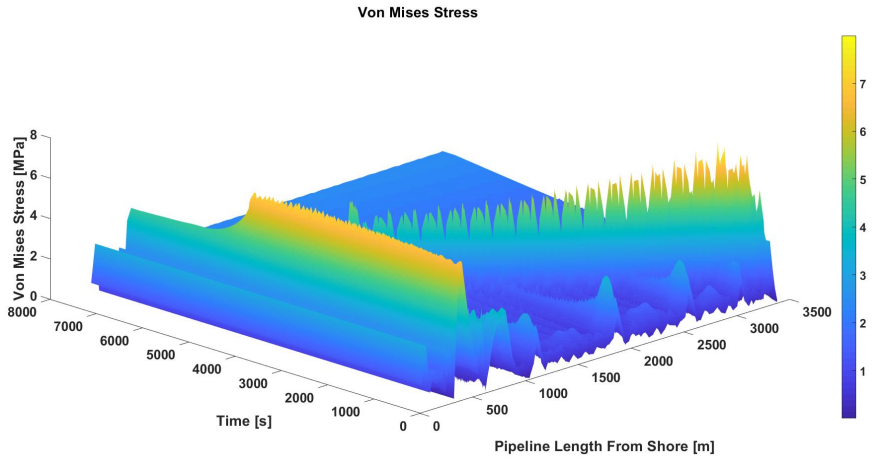

Figure 5.10: SDR 33 20 * 2.5 [mT] Ballast Distribution, Maximum Von Mises Stress

The effective wall tension is illustrated in Figure 5.11. The effective wall tension has a positive value during the installation. It can be concluded that the global buckling analysis is satisfied, which indicates that it is not likely that local buckling occurs during the installation. Furthermore, an increase in the effective wall tension in the free span of the pipeline can be observed. The increase in effective wall tension corresponds to the increase in pull force over time. After the installation of the pipeline, this effective wall tension is maintained in the pipeline.

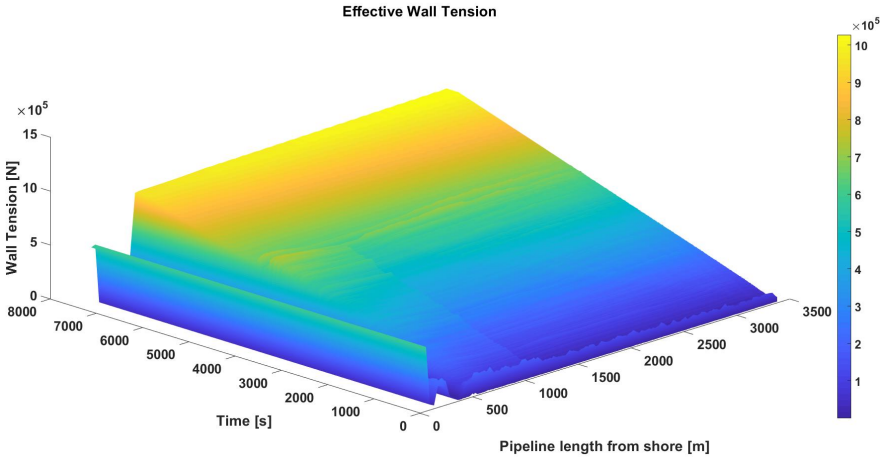

Figure 5.11: SDR 33 20 * 2.5 [mT] Ballast Distribution, Effective Wall Tension

The maximum occurring stresses for the pull down installation for the 20 * 2.5 [mT] and the 10 * 5[mT] ballast distribution are given in table 5.4. The bending stress for the 10 * 5 [mT] ballast distribution is 23% higher than for the 20 * 2.5 [mT] ballast distribution. The pipeline submerges when the downward force is greater than the upward buoyancy force. The downward force results from the pull force and the additional ballast weights. As the pull force increases, larger sections of pipeline are being pulled below the sea surface. In the case of a more distributed ballast configuration, the buoyancy force is reduced at shorter intervals along length of the pipeline. This leads to a more gradually increasing and larger bending radius. Whereas for the less distributed configuration, the buoyancy is reduced at longer intervals along the length of the pipeline. The longer unballasted segments lead to a less gradual increasing and smaller bending radius and therefore a higher bending stress. Figure 5.12 illustrates the bending radius during the initial pull down stages for both ballast distributions at the same time step and with the same pull force. A larger bending radius can be observed for the 20 * 2.5 [mT] ballast distribution.
The bending stress figure and the Von Mises stress figure of the 10 * 5 [mT] ballast distribution are illustrated in Appendix E. Furthermore, the shape of the bending stress figure is discussed in Appendix E

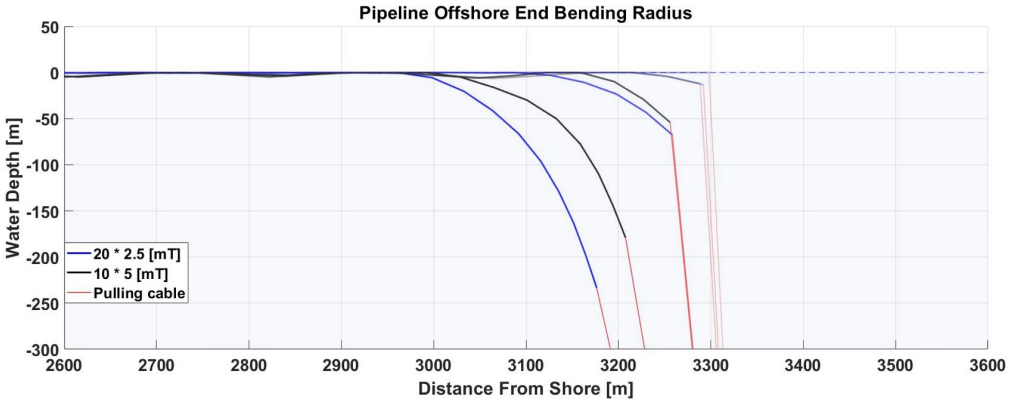

Figure 5.12: Bending Radius at the Offshore End of the Pipeline

Ballast Configuration	Max. Axial Stress [MPa]	Min. Axial Stress [MPa]	Max. Bending Stress [MPa]	Max. Von Mises Stress [MPa]	Minimum Bending Radius [m]
10 * 5 [mT]	1.6	-7.7	9.3	9.4	108
20 * 2.5 [mT]	1.6	-7.7	7.6	7.7	126

Table 5.4: Maximum and Minimum Occurring Values During Installation

5.3.1. Effect of Varying E-modulus

Similarly to the hold and sink installation method, the effect of a varying E-modulus is checked. The 20 * 2.5 [mT] ballast distribution is used with E-moduli of 425, 510 and 1050. The results are given in table 5.5. The behaviour of the bending stress and axial stress under varying E-modulus is similar to the hold and sink installation, explained in section 4.4.1. Whereas the stresses stay below the design stress in the case of the hold and sink installation method, this is not the case for the pull down method. For the 1050 [MPa] E-modulus, the bending stress and therefore the Von Mises stress exceed the long term installation design stress of 8 [MPa] in the transition zone. An additional mitigation to prevent exceedance of the design stress would be to increase the bending stiffness further. The transition section remains under loading during the installation which leads to a decrease in E-modulus, so it is not expected that the E-modulus will increase in this section.

E-Modulus MPa	Max. Axial Stress [MPa]	Min. Axial Stress [MPa]	Bending Stress [MPa]	Von Mises Stress [MPa]	Minimum Bending Radius [m]
1050	1.6	-7.6	9.1	9.2	142
510	1.4	-7.6	5.8	5.9	107
425	1.3	-7.7	5.2	5.3	100

Table 5.5: Comparison Between Stresses Resulting from

5.4. Final Configuration

The final configuration for the pull down method consists of a SDR 33 pipeline. The transition zone is stiffened to reduce the bending stress to an allowable level below the long term design stress. The anchorbox is limited to 150 [mT]. Without any additional measures the pull force required to pull the pipeline into position is 230 [mT]. The following approach is used to reduced the pull force. The pipeline is elongated by 100 [m] to compensate for the free span and reduce the required pull force and additional ballast is applied on the free span of the pipeline. Based on the resulting stresses for the three different ballast scenarios that were considered, the 20 * 2.5 [mT] is preferred based on the occurring pipeline stresses. Application of both measures results in a force reduction of 125 [mT] with a final required pull force of 105 [mT]. The anchorbox is placed at a depth of 1000 [m] and located at a distance of 3350 [m] from the shore.

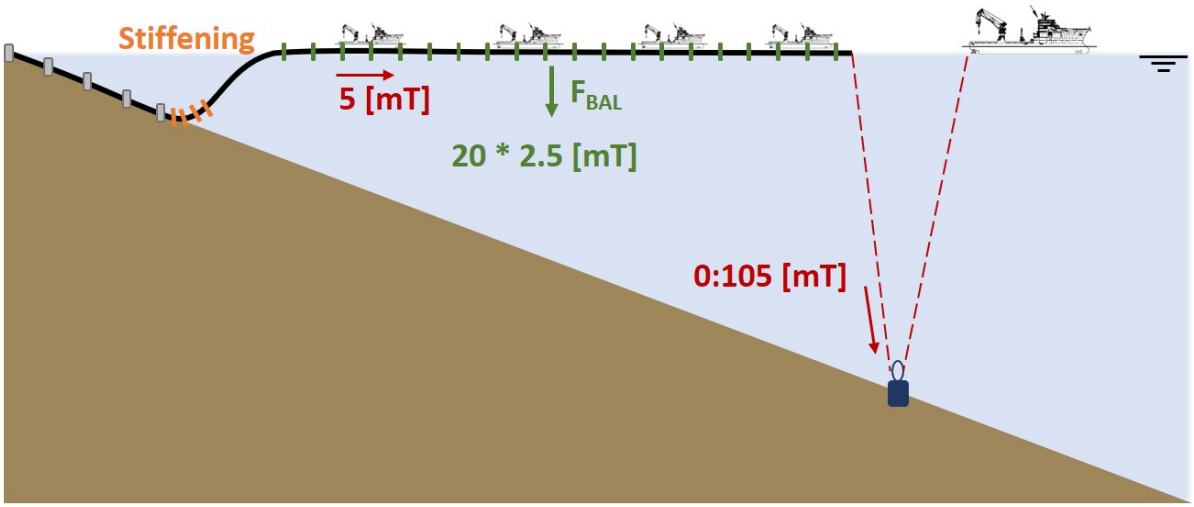

Figure 5.13: Final Pull Down Installation Configuration

6

Comparison of Installation Methods

A preliminary multi-criteria analysis is used as an initial comparison between both installation methods. The preliminary multi-criteria analysis is discussed in this chapter.

6.1. Preliminary Multi-Criteria Analysis

In consultation with the OTEC project department within Allseas, five installation criteria are defined and listed below. The installation criteria include several considerations that are found to influence the installation of the pipeline, during the analysis of both installation methods.

- *Structural integrity.* To maintain the structural integrity of the pipeline during installation, the Von Mises stress in the pipeline is not allowed to exceed the design stress. A second consideration is the viscoelastic behaviour of the material. HDPE has an E-modulus that varies with loading duration and temperature. Therefore, the effect of a varying elastic modulus on the structural integrity is taken into account.

- *Installation.* The installation criterion is divided into four considerations. The first consideration is the complexity of the installation method, which includes how many different installation steps are executed during the installation. The second consideration is the risk of pipeline failure during the installation. The third consideration is to what extend the installation can be paused or reversed. The last consideration is the controllability of the pipeline during the installation.

- *Costs.* For the costs of the installation methods, three considerations are taken into account. The costs for the materials are taken into consideration, such as the pipeline material and ballast weights. Secondly, the costs for all the additional equipment that is required is taken into account, such as the required vessels. The third consideration is the duration of the installation process. The longer the duration of pipeline installation, the larger the expenses become.

- *Environmental.* The first consideration of the environmental criterion is the effect of the environmental loads on the pipeline. The second consideration is the effect of the pipeline on the environment itself. The third consideration is the sensitivity of the installation method to the seabed bathymetry.

- *Operational Life.* The last criterion considered is the structural integrity of the pipeline during its operational life after the pipeline has been installed.

Different weight factors are assigned to all criteria, where the value of the weight factor is determined based on the importance of that criterion. The sum of the weight factors equals 1. The considerations taken into account are given a weight factor as well, adding up to 1 for each criterion. For both installation methods, the considerations are given a value between 1 and 5, where 5 is the best score possible. The final value of the criterion is given as: the assigned value, Val, multiplied by the weight factor of the consideration, w_{cons}, and multiplied by the weight factor of the criteria, w_{crit}, given by equation 6.1.

$$R = w_{crit}(w_{cons}Val) \tag{6.1}$$

By combining the considerations and criteria both installation methods are compared. The analysis has been filled in independently by engineers of the pipeline engineering department and the OTEC department of Allseas and van Kooten, the results are given in table 6.1.

Criteria	Weight	Consideration	Weight	Hold and Sink	Pull Down
Structural Integrity	0.25	Von Mises	0.7	4.5	3.5
		E-modulus	0.3	4	3
Installation	0.2	Complexity of Installation	0.4	3	2.7
		Risk of Failure	0.3	2.3	3.3
		Pause or Reverse	0.1	2	3.3
		Controlability During Installation	0.2	3.3	2.7
Costs	0.2	Material	0.2	2.7	3
		Additional Cost	0.4	2	3
		Duration	0.4	2	3.3
Environmental	0.2	Effect on Pipeline	0.4	2.3	3.7
		Effect on Environment	0.3	2.3	3.7
		Seabed Sensitivity	0.3	1.7	4
Operational Life	0.15	Structural Integrity	1	4	2.3
Result	1			3.1	3.15

Table 6.1: Preliminary Multi-Criteria Analysis Installation Methods

6.2. Preliminary Multi-Criteria Analysis Discussion

The results of the analysis are discussed in this section.

- *Structural Integrity:* For the hold and sink installation method, the maximum Von Mises stress remains below the design stress. During the pull down installation method, the transition zone results in a maximum Von Mises stress that exceeds the design stress, resulting from pipeline bending. Additional bending stiffness is added to reduce the Von Mises stress to below the design stress. An overview of the occurring installation stresses and minimum bending radius is given in table 6.2. The maximum Von Mises stress during the pull down installation method is 43% higher than the maximum Von Mises stress during the hold and sink installation method. Both installation methods show a reduction in bending stress when the E-modulus is decreased. For an increase in E-modulus, the maximum Von Mises stress remains below the design stress for the hold and sink installation method. However, for the pull down installation method, the increase in E-modulus results in a bending stress that leads to the maximum Von Mises stress exceeding the design stress in the transition zone.

Installation Method	Max. Axial Stress [MPa]	Min. Axial Stress [MPa]	Max. Bending Stress [MPa]	Max. Von Mises Stress [MPa]	Min. Bending Radius [m]
Hold and Sink	2.5	-9.6	3.7	5.4	245
Pull Down	1.6	-7.7	7.6	7.7	126

Table 6.2: Final Installation Configuration Stress Comparison

- *Installation:* The installation procedure for the hold and sink installation method is straightforward. The pipeline sinks due to the gravity; the sinking velocity is controlled by the hold points and the pull vessel. The pull down installation is more complex since two installation methods are used. Initially, the float and sink installation method is used to install the ballasted pipeline section. Thereafter, the remainder of the pipeline is pulled down. The float and sink installation method has to be correctly aligned with the anchorbox. Furthermore, additional measures are required in the transition zone to reduce the bending stress and measures are required to reduce the required pull force.
  The main risk of failure for both installation methods is the failure of the pull cables. In the case of the hold and sink method, this comprises of either the pull cable or a hold cable. In this scenario,

the pipeline will sink with an increased velocity to the seabed, which may lead to a pipeline failure on impact. The sinking velocity can be compensated for by the remaining hold vessels that can increase their hold force. Furthermore, the pull vessel can increase the applied pull force to compensate for the missing hold vessel. A secondary risk of the hold and sink installation occurs when the communication between the vessels fails and the applied forces are not reduced at an equal rate, resulting in the pipeline not sinking as intended. Since multiple hold vessels are used in the hold and sink installation method, the probability of a potential failure of a cable is higher than for the pull down installation method.
In the case of a failure of the pull down cable for the pull down installation method, the pipeline will float back up to the surface. The resulting bending moment in the transition zone can be significant enough to result in pipeline failure. The failure of the pull cable can not be compensated for by other vessels, therefore an option is to attach a second cable to the pipeline as a back-up. This secondary cable can either run through the anchorbox in a similar way as the main pull cable, to allow for the continuation of the installation, or the cable can be directly attached to the crane vessel. This allows for the crane vessel to apply a pull force, similar to the hold and sink installation method, in order to minimize the bending moment in the transition zone.
The pull down installation method can be easily paused or reversed by maintaining a constant pull load or decreasing the pull force. Pausing the installation can be done for the hold and sink installation method when the total vertical hold force is equal to the downward gravity force. Reversing the installation is however not easily done, as large vertical forces are required that lead to excessive bending.
Both ends of the pull down pipeline are fixed. The shore end is fixed via the ballast weights and the offshore end is fixed to the anchorbox. The only method of controlling the pull down installation method is by increasing or decreasing the applied pull force. The pipeline during the hold and sink installation method is fixed only at the shore end, the offshore end is free. This allows for changing the installation trajectory and final installation position during the installation itself by the pull vessel.

- *Costs:* The costs of the materials for both installation methods are expected to be higher for the hold and sink installation method. This primarily results from the amount of concrete ballast weights that are required for the pipeline. The additional costs for the the hold and sink installation method are higher as well. The final installation configuration uses four hold vessels and a pull vessel, whereas one crane vessel is required for the pull down installation method. The vessels that apply a lateral resistance force at the sea surface can be local vessels and are not expected to contribute significantly to the total costs.
  Lastly, the costs that result from the duration of the installation are taken into consideration. The main cost drivers for the duration of the hold and sink installation method are the attachment of the concrete ballast weights to the pipeline and the required post ballasting after the installation. The ballast weights are attached while the pipeline floats on the sea surface due to a lack of space onshore. Attaching the ballast weights while the pipeline floats is a time consuming process and therefore costly. Furthermore, significantly more ballast weights are required for the hold and sink pipeline than for the pull down pipeline, since the hold and sink pipeline is ballasted along its total length. Less ballast weights are required for the pull down pipeline and therefore the duration will be shorter compared to the hold and sink pipeline. The pull down installation method requires the installation of the anchorbox prior to the installation, but no post installation work is required.

- *Environmental:* For both installation methods, the current has a significant influence on the lateral position of the pipeline at the sea surface. Due to the large applied pull down force, the offshore end of the pull down pipeline is installed as intended, without lateral deflection after the installation. In the scenario where the current velocity is increased, the pull down pipeline is installed without lateral deflection as well. As the pull force for the hold and sink installation decreases over time, the lateral resistance against the current decreases as well. This results in the final position of the pipeline after the installation being laterally displaced from the intended position.
  The majority of the pull down pipeline remains in the reversed catenary shape and will therefore not disturb the seabed to a great extend. However, the hold and sink pipeline lies in its totality on the seabed and will therefore have a larger impact on the environment.
  Since the hold and sink pipeline lies on the seabed, the pipeline is also more dependent on the seabed bathymetry. Any unexpected changes in the bathymetry or unexpected objects may lead to failure or a displacement of the pipeline. The pull down pipeline is less affected by the seabed bathymetry, as

the pipeline floats above the seabed. For the pull down installation method, only the ballasted pipeline segment and the anchorbox depend on the seabed bathymmetry.

- *Operational life:* The amount of ballast on the hold and sink ballast is designed so that the pipeline remains in position during its operational life and does not move for the design conditions. After the pull down installation method, the pipeline is fixed via a chain to the anchorbox. The floating segment of the pipeline is free to move with the environmental loading, within the limits of the length of the chain. The movement of the pipeline leads to additional stress at the offshore end of the pipeline and in the transition zone. Furthermore, fatigue can occur in the transition zone due to the pipeline movement and creep can occur resulting from the tension at the anchorbox.

The combined scores of the criteria for both installation methods result in a slightly higher value for the pull down installation method. However, the difference between the two methods is so small that an obvious preferred installation method cannot be selected. The hold and sink installation method has a better structural performance, whereas the pull down installation method has a better performance regarding the environmental conditions. To be able to determine a preferred installation method, the analysis has to be extended. An extension to the preliminary multi-criteria analysis is discussed in the recommendations.

7

Conclusion and Recommendations

In this chapter, the results of the thesis research are discussed and recommendations for future works are given.

7.1. Conclusion

The objective of this thesis is to define the optimal installation configuration for the cold water pipeline of a 3MW onshore based OTEC plant. The material of the cold water pipeline is high density polyethylene (HDPE), the pipeline has an outer diameter of 2.25 [m] and a target water depth of 950 [m]. The density of HDPE is lower than that of sea water and remains floating at the surface. Therefore, an additional downward force is required.
Environmental data is obtained for the period January 2017 - December 2019, from the open source website: Copernicus Marine Services. During the installation of the pipeline, the environmental loading is required to be at a minimum. Based on this requirement, the preferred installation period is August - November, where the average current velocity and significant wave height are at their lowest.
The installation method that is normally used for the installation of marine HDPE pipelines is the float and sink method. The float and sink method is however not suitable to install the deep cold water pipeline as it is limited to a maximum water depth. Therefore, two promising other installation methods are considered: the hold and sink installation method and the pull down installation method. The Von Mises equivalent stress criterion is used to asses whether the structural integrity of the pipeline during the installation is maintained. Furthermore a global buckling analysis is performed to check whether the pipeline is susceptible to local buckling. A numerical non-linear Euler Bernoulli beam model is used to optimize these installation methods.

The first installation method considered is the hold and sink method, where the pipeline is ballasted with concrete weights to reduce the buoyancy. The sinking process is controlled by applying vertical hold forces and a horizontal pull force at the offshore end of the pipeline.
Using a Weibull distribution, the design wave height and absolute current velocity are obtained. The absolute seabed stability is used to determine the required amount of concrete ballast weights to keep the pipeline in place. The required amount of ballast decreases with water depth, as a result of the decrease in environmental loading with water depth. More vertical hold force is required for a heavier ballasted pipeline.
HDPE pipelines are extruded in specific dimension ratio's (SDR), which is the ratio of the diameter over the wall thickness. Three specific dimension ratios are considered: SDR 21, SDR 26 and SDR 33. SDR 21 has the largest wall thickness and SDR 33 has the smallest wall thickness. Furthermore, three pull forces are considered: 50 [mT], 100 [mT] and 150 [mT].
A larger wall thickness results in a higher bending stiffness and a higher axial stiffness. Therefore, the bending stress and axial stress of a pipeline with a larger wall thickness are lower than the stress of a smaller wall thickness. The main contribution to the Von Mises stress results from the bending stress in the pipeline. An increase in pull force reduces the bending stress in the pipeline, but increases the axial stress. Furthermore, the pull force acts as an additional vertical component as the pipeline sinks. For an installation with 100 [mT] or 150 [mT] applied force, less vertical hold components are required than for a 50 [mT] pull installation. During the installation of the pipeline, the lateral position of the pipeline is influenced by the current veloc-

ity. At the sea surface, the hold vessels can provide a lateral resistance force to keep the pipeline in position. For the installation current velocity profile, the 100 [mT] and 150 [mT] pull forces yield a maximum lateral deflection of 10 [m] and 8 [m] of the pipeline after the installation. The maximum lateral deflection of a 50 [mT] pull force is 36 [m].
HDPE is a viscoelastic material, therefore the E-modulus varies with loading time and temperature. A reduction in E-modulus results in a decrease in bending stress, whereas an increase in E-modulus results in an increase in bending stress. The axial stress is not significantly affected by a variation in E-modulus. For both an increase and decrease in E-modulus, the Von Mises stress remains below the design stress.
Concluding, the final hold and sink installation method configuration consists of a 3300 [m] HDPE pipeline. The attached ballast is designed for a water depth of 300 [m] to reduce the required vertical hold vessels. Post ballasting is therefore required for the pipeline section prior to 300 [m] water depth. The applied pull force is 100 [mT]. Four vertical hold vessels are required providing a vertical force of 150 [kN]. Furthermore, 15 [mT] of additional buoyancy, which is available within Allseas, is attached to the pipeline. Both the Von Mises stress criterion and the global buckling analysis are satisfied.

The second installation method considered is the pull down installation method. The HDPE pipeline is divided into two sections: a ballasted section of 450 [m] and the remainder of the pipeline that is not ballasted. A ballast weight of 150 [mT], called the anchorbox, is installed at the designated installation position of the offshore end of the pipeline.
The ballasted pipeline section is installed via the float and sink installation method. The ballasted section is installed to a depth of 200 [m], where the transition between the ballasted pipeline section and the floating pipeline section is located. The bending stress in the transition zone results in the Von Mises stress exceeding the design stress for the three SDR considered. By applying additional bending stiffness the bending stress is reduced to 6.7 [MPa]. The decrease in bending stress results in a Von Mises stress below the design stress. The required amount of additional bending stiffness is 10 times the bending stiffness of the pipeline.
After the float and sink installation method, the pipeline is pulled down and secured in the anchorbox. The maximum pull force is limited to the weight of the anchorbox. When the pull force exceeds the weight of the anchorbox, it will be lifted from the seabed. The required pull force to pull the pipeline in position is 230 [mT], which is significantly higher than the weight of the anchorbox. This high required pull force results from the decrease in the angle between the pull cable and the anchorbox. The required pull force is reduced by applying 50 [mT] of distributed additional ballast along the pipeline free span. A more distributed ballast weight configuration along the length of the free span, results in more gradual increase in bending radius and lower bending stress. Furthermore, the pipeline is elongated by 100 [m] and the anchorbox is placed 100 [m] further from shore, to account for the free spanning section of the pipeline. The required pull force is reduced to 105 [mT].
At the sea surface lateral resistance force is applied to minimize the bending moment in lateral direction in the transition zone. The final lateral position of the pipeline is not affected by the installation current. This results from the large pull force that is applied and pulls the offshore end of the pipeline in position.
Similar to the hold and sink installation method, the variation in E-modulus results in a decrease in bending stress for a decrease in E-modulus and an increase in bending stress for an increase in E-modulus. An increase in E-modulus results in an exceedance of the design stress in the transition zone.
Concluding, the final pull down installation configuration consists of a SDR 33 pipeline. The bending stiffness in the transition zone is increased by a factor 10 of the original pipeline bending stiffness by applying additional bending stiffness. The additional ballast of 50 [mT] is divided into 20 smaller ballast weights of 2.5 [mT] that are distributed along the free spanning section. This distribution results in a gradual increase in bending radius at the offshore end of the pipeline during the pull down stage. The pull down force increases over time to the maximum value of 105 [mT]. Both the Von Mises stress criterion and the global buckling analysis are satisfied.

A preliminary multi-criteria analysis is conducted as an initial comparison between the two installation methods. The hold and sink installation method has a better structural performance, whereas the pull down installation method has a better performance regarding the environmental conditions. As the final results are almost equal, no obvious preferred installation method can be selected. An extension to this analysis is required to conclude the preferred installation method.

7.2. Recommendations

Based on this thesis research, the following recommendations are made.

- An important aspect of the pipeline is the structural integrity during its operational life, which is not analysed in this thesis work. Especially the pull down pipeline is susceptible to environmental loading during its operational life, since the pipeline remains floating in a reversed catenary position. The movement of the pipeline can result in fatigue in the pipeline in the transition zone. The pipeline is under tension resulting from the chain at the anchorbox, this tension can lead to creep in the pipeline. Furthermore, the chain itself is under tension and moves with the pipeline, while the other end is fixed in the anchorbox. The chain is therefore also susceptible to fatigue failure. It is essential to include a detailed analysis of the structural integrity of the pull down installation pipeline in further research.

- During the pull down installation method, the pipeline is especially susceptible to bending stress. High bending stress occurs at the offshore end of the pipeline, during the pull down of the first 500 [m] of pipeline. A requirement can be to reduce this bending stress. A possible solution to decrease the bending stress could be to increase the bending stiffness of this pipeline section. This can be done by applying additional bending stiffness, or by replacing the pipeline segments in the high bending stress area by segments with a larger wall thickness, SDR 21. It was found that by applying additional ballast at shorter intervals, the bending stress decreases and the bending radius increases. Therefore, a different approach to reduce the bending stress could be to apply additional distributed ballast weights in the high bending stress area.

- During the installation of the pipeline, the wave loading is neglected. The waves are expected to be low during the installation and the wave loading will quickly decay to zero with water depth. The bending stress during the pull down of the first 500 [m] of pipeline is already significant. Wave loading can increase the bending stress at the offshore section of the pipeline. Therefore, the effect of the wave loading should be considered. Furthermore, the environmental data is obtained at one location. The pipeline is over 3000 [m] long, resulting in varying environmental conditions and pipeline response to these conditions along the length of the pipeline. This should be considered as well.

- The local bending stiffness effects of the concrete ballast weights are not taken into account in the numerical model. The ballast weights increase the bending stiffness of the pipeline locally. The hold and sink pipeline is ballasted along its entire length. Therefore, the global pipeline behaviour of the hold and sink method will be affected by the local bending stiffness effects. The local effect of the ballast weights on the global behaviour of the pipeline has to be taken into account in further design stages.

- It is found that the transition zone for the pull down installation method the bending stress can be decreased by applying additional bending stiffness. A more detailed design of the additional bending stiffness in the transition is required.

- An alternative method to decrease the bending stress in the transition zone is by installation a second anchorbox. A downward force is applied to the pipeline in the transition zone to increase the bending radius and decrease the bending stress. A preliminary sensitivity analysis is conducted for this configuration in Appendix F and shows promising results. An extension to this analysis is required to give a final conclusion on the second anchorbox configuration.

- A preliminary multi-criteria analysis is used as an initial comparison between the two installation methods. The result of the preliminary multi-criteria analysis is that there is no clear preferred installation method. To be able to give a final verdict on which installation method is preferred, an extension of the multi-criteria is required. This extension has to include a detailed cost estimation of both installation methods and a detailed analysis of the structural integrity during the operational life of both pipelines. Furthermore, the assigned weight factors, criteria and considerations can be re-evaluated.

Bibliography

[1] Alleas Engineering B.V. URL https://allseas.com.

[2] Copernicus Marine Service. URL https://resources.marine.copernicus.eu/?option=com_csw&task=results.

[3] Hornbeck Offshore Services. URL https://gcaptain.com/hornbeck-offshore-mpsv-gulf-of-mexico-market.

[4] Technical Report on Design and Execution of Desalination Plans in Minicoy and Agatti, UT Lakshadweep. URL https://www.niot.res.in/img/Island_Desalination_Technical_Report.pdf.

[5] Flow-3d. URL https://www.flow3d.com/modeling-capabilities/waves/.

[6] Harmony marine shipbrokers. URL https://www.hmsbroker.com.

[7] Matlab. URL https://uk.mathworks.com/?s_tid=gn_logo.

[8] Pipeshield. URL https://www.pipeshield.com.

[9] Marine Pipelines Lecture Notes, 2019.

[10] AGRU. *HDPE Manual.*

[11] Avery, W. H. and Wu, C. *Renewable Energy Form the Ocean: A Guide to OTEC.* 1994.

[12] Bai, Y. and Bai, Q. *Subsea Pipeline Design, Analysis and Installation.* 2014.

[13] Bjorklund, I. and Radeljic, I. Performance of Large Marine HDPE Pipes During the Submersion as Based on Laboratory Testing. *Proceedings of the* 19^{th} *Plastic Pipes Conference*, 2018.

[14] Bjorklund, I., Blomster, T., and Radeljic, I. Challenges in the Development of the Market for Large Diameter PE Pipes for Marine Installations. *Proceedings of the* 18^{th} *Plastic Pipes Conference*, 2016.

[15] Brewer, J. H., Minor, J., and Jacobs, R. *Feasibility Design Study Land-Based OTEC Plants.* 1979.

[16] Brown, M. G., Gauthier, M., and Meurville, J. George Claude's Cuban OTEC Experiment: A Lesson of Tenacity For Entrepreneurs. URL http://www.clubdesargonautes.org/otec/vol/vol13-4-2.htm.

[17] Callister, W. D. and Retwish, D. G. *Materials Science and Engineering.* 2014.

[18] Department Communities and Local Government. *Multi-Criteria Analysis: A Manual.* 2009.

[19] Det Norske Veritas AS. DNV-RP-F110 Global Buckling of Submarine Pipelines. 2007.

[20] Det Norske Veritas AS. DNV-RP-C205 Environmental Conditions and Environmental Loads. 2010.

[21] Dhanak, M. R. and Xiros, N. I. *Springer Handbook of Ocean Engineering.* 2016.

[22] Dismukes, D. E. *Fact Book: Offshore Oil and Gas Industry Support Sectors.* 2010.

[23] Fergestad, D. and Løtveit, S. *Handbook on Design and Operation of Flexible Pipes.* 2014.

[24] Gere, J. M. and Goodno, B. J. *Mechanics of Materials.* 2009.

[25] Guo, B., Song, S., Chacko, J., and Ghalambor, A. *Offshore Pipelines.* 2005.

[26] JEE. Marine Pipelines Lecture Notes, 2017.

[27] Jensen, G. A. *Offshore Pipelaying Dynamics.* 2010.

[28] Journée, J. M. J. and Massie, W. W. *Offshore Hydromechanics*. 2008.

[29] Keesmaat, K. *Installation Limits of Large Diameter Cold Water Pipes in Deep Water for Land-Based OTEC Plants*. 2015.

[30] Keijdener, C. Computational Dynamics Lecture Notes, 2019.

[31] Krah Group. Large Diameter HDPE Helical Structured Pipes for Sea Outfalls.

[32] Makai Ocean Engineering. URL `https://www.makai.com/pipelines/pipelines_extended/#40`.

[33] Marley Pipesystems. HDPE Physical Properties. 2009.

[34] McKeen, L. W. *The Effect of Creep and Other Time Related Factors on Plastics and Elastomers*. 2009.

[35] Moran, M. J., Shapiro, H. N., Boettner, D. D., and Bailey, M. B. *Principles of Engineering Thermodynamics*. 2012.

[36] Natural Energy Laboratory of Hawaii Authority. *Annual Report*. 2017.

[37] Neto, A., de Mattos Pimenta, P., and de Arrude Martins, C. Hydrostatic Pressure Load in Ppes Modeled using Beam Finite Elements: Theoretical Discussions and Applications. 2017.

[38] Nihous, G. A Preliminary Assesment of Ocean Thermal Energy Conversion Resources. 2007.

[39] Papusha, A. N. *Beam Theory for Subsea Pipelines*. 2015.

[40] Pelc, R. and Fujita, R. Renewable energy from the ocean. 2002.

[41] Pipelife Norge AS. Advantages and Experiences of the Use of Long Length PE Pipes for Marine Pipeline Construction Installation Techniques for flexible PE pipes.

[42] Pipelife Norge AS. Technical catalogue for submarine installations of polyethylene pipes. 2002.

[43] Pipelife Norge AS. Long Length Large Diameter Polyethylene (LLLD HDPE) System. 2016.

[44] Plastic Pipe Institute. *Handbook of Polyethylene (PE) Pipe*. 2008.

[45] Roberts, P. J. W., Reiff, F. M., Labbe, A., Salas, H. J., Libhaber, M., and Thomson, J. C. *Marine Wastewater Outfalls and Treatment Systems*. 2010.

[46] U.S Energy Information Administration. *International Energy Outlook 2019 with projections to 2050*. 2019.

[47] van der Veer, M. *Numerical Modelling of a Large Diameter Cold Water Pipe Installation for Land Based OTEC and SWAC*. 2018.

[48] van Nauta Lemke, M. *Installation Method Analysis for a Large Diameter Cold Water Pipe for Land - Based OTEC Plants*. 2017.

[49] Vardakosta Marine Construction. URL `https://www.vardakosta.com/en/index.html`.

[50] Vega, L. A. Ocean Thermal Energy Conversion (OTEC). 1999.

[51] Vullo, V. *Circular Cylinders and Pressure Vessels*. 2014.

A

Loading Coefficients

In this appendix, the coefficients used for the computation of the drag force, lift force and added mass are given.
The drag coefficient as a function of the surface roughness and the Reynolds number is in given Figure A.1. The Reynolds number indicates whether the flow is laminar or turbulent and is given by equation A.1, with ν the kinematic viscosity and u_f the flow velocity. The drag coefficient is equal to 1 for the hold and sink installation method, to account for the concrete ballast weights [47]. For the pull down installation method, the drag force is equal to 0.7.

$$Re = \frac{u_f D_o}{\nu} \tag{A.1}$$

The added mass coefficient as a function of the Keulegan-Carpenter number is given in Figure A.2. The Keulegan-Carpenter number provides information about the flow separation around the pipeline and is given by equation A.2, with U_m the flow velocity amplitude and T the oscillating flow period. The added mass coefficient is 1 for both installation methods. The inertia coefficient is defined as $C_a + 1$.

$$KC = \frac{U_m T}{D_o} \tag{A.2}$$

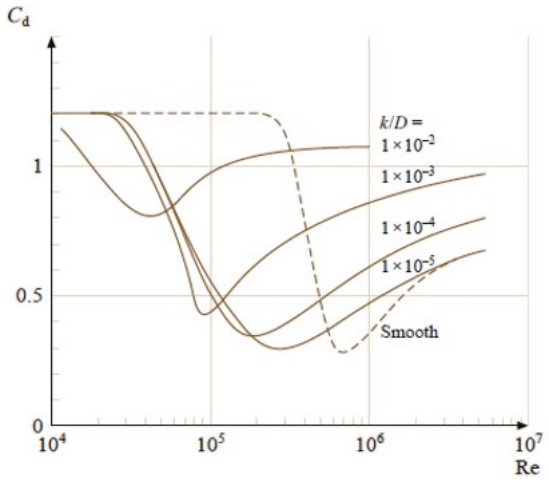

Figure A.1: Drag Coefficient [21]

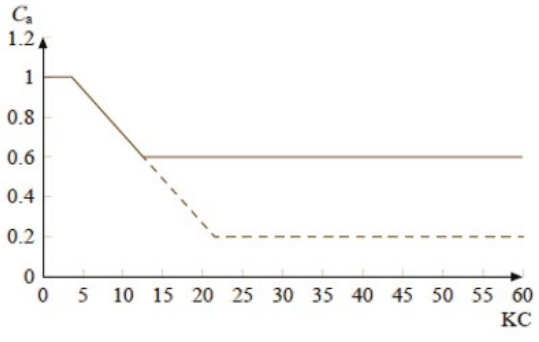

Figure A.2: Added Mass Coefficient [21]

The lift coefficient is obtained from Figure A.3 and is equal to 0.85.

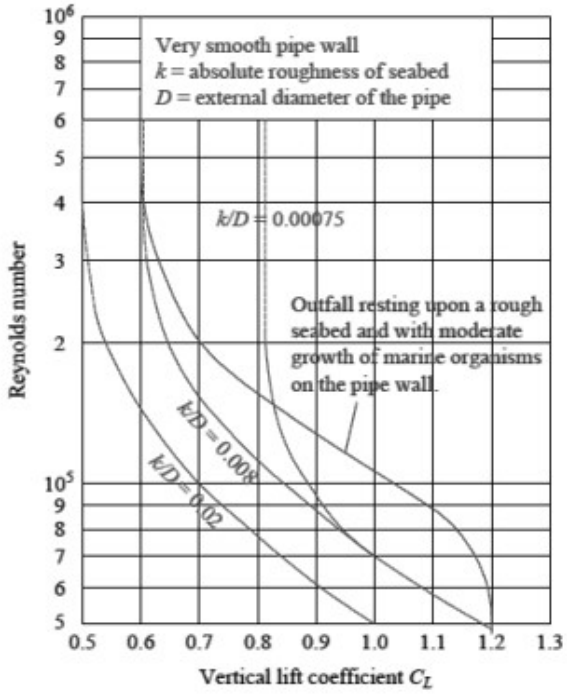

Figure A.3: Lift Coefficient [45]

B

Ballast and Design Conditions

As discussed in the main report, the design wave and current conditions are computed via the Weibull distribution. The Weibull distribution is given by equation 4.5. Figure B.1 illustrates the corresponding Weibull distribution for the significant wave height and Figure B.2 illustrates the Weibull distribution for the absolute surface current velocity.

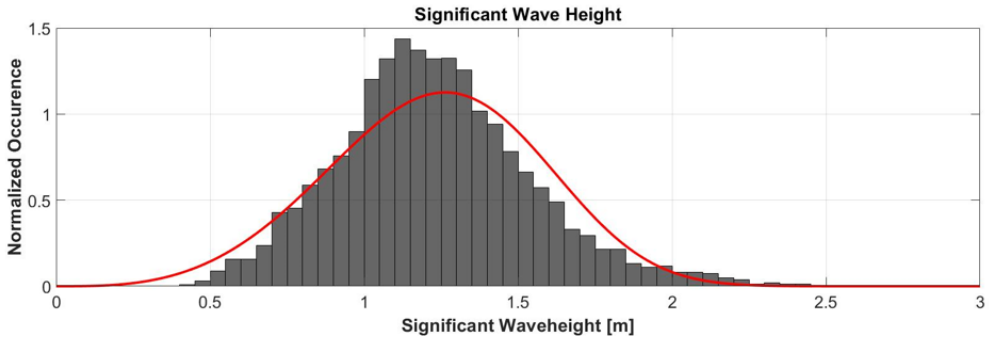

Figure B.1: Significant Wave height Weibull Distribution

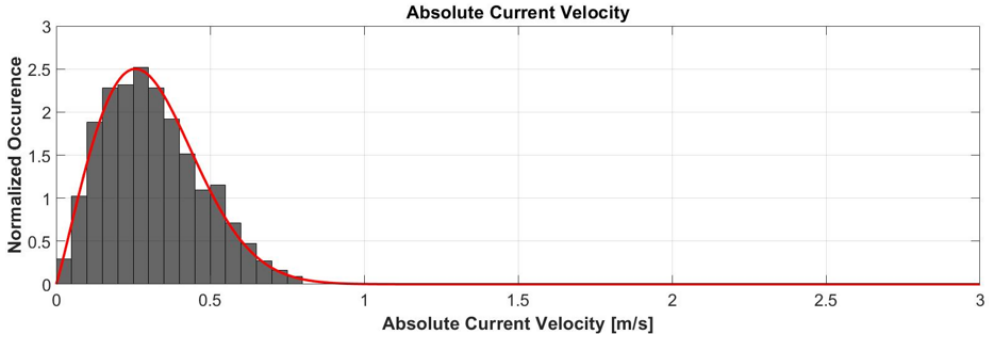

Figure B.2: Absolute Current Velocity Weibull Distribution

The velocity and acceleration over depth of the design wave are illustrated in Figure B.3. The acceleration and velocity of a significant wave height of 1 [m] is included in the figure, which illustrates the rapid decrease in velocity and acceleration of a wave during installation in deep water. Figure B.4 illustrates all the current velocity profiles that were used in this thesis.

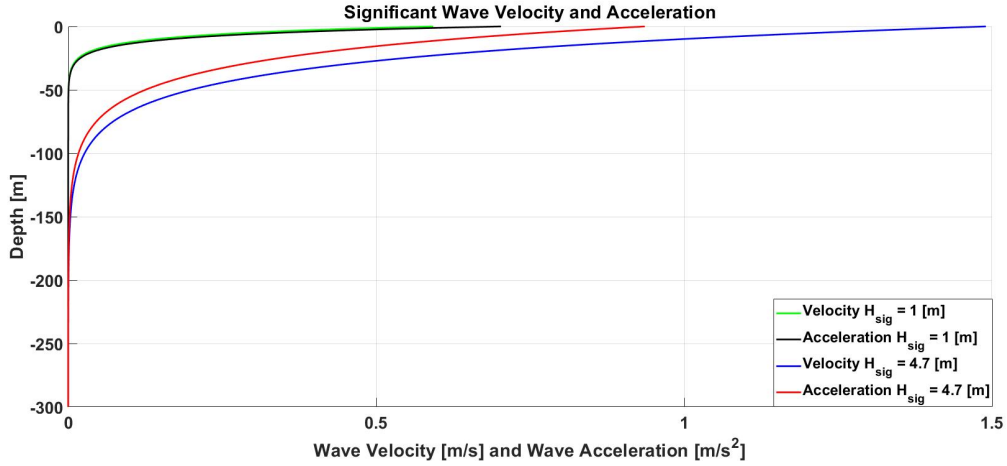

Figure B.3: Wave Particle Velocity and Acceleration Over Depth

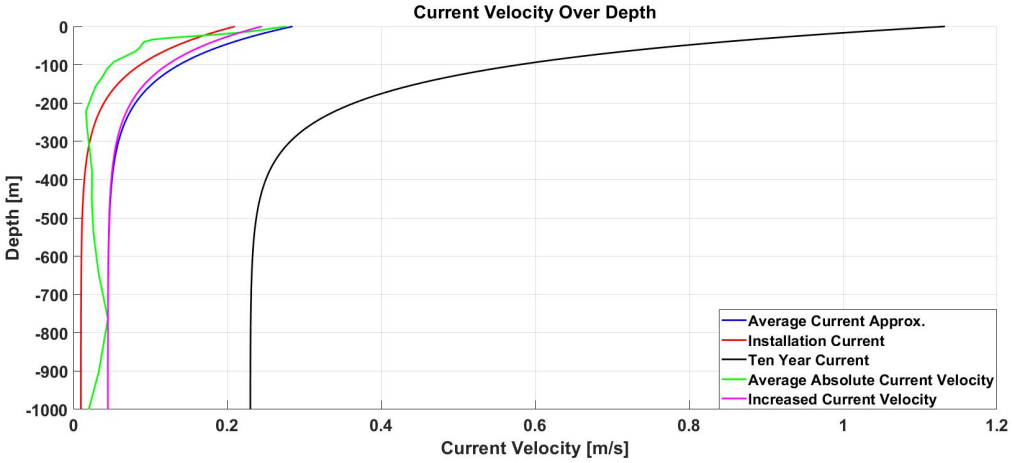

Figure B.4: All Current Velocities Over Depth Used in Thesis

The friction coefficient of the concrete ballast weight is a function of its shape. In this thesis, a trapezoidal shape is assumed, illustrated in Figure 4.2, as it provides the highest frictional resistance. A secondary benefit of the trapezoidal ballast shape is that rotation of the pipeline is minimized due to a heavier bottom section and a lighter top section. The friction coefficient, μ, is equal to 0.5 [45]. The safety factor in the seabed stability, γ, is equal to 1.1 [20]. In table B.1, the required SG values and corresponding amount of ballast for a SDR 33 pipeline are given.

Depth [m]	**SG**	**Required Amount of Ballast [Kg/m]**
0 - 100	1.66	1193
100 - 200	1.29	374
200 - 300	1.09	144
300 - 1000	1.056	106

Table B.1: SG Values For SDR 33 Including Coastal Zone

C

Numerical Model

In this appendix, the numerical model that is used is summarized. A more elaborate description and verification of the numerical model can be found in the report of M. van der Veer [47].

The pipeline is discretized into n elements [30]. The pipeline elements are represented by the model as massless linear springs with nodes at the end of the springs. Each element is connected to two nodes, for element $n-1$ these are: node $n-1$ and node n. The mass properties and external loads that act on the pipeline are applied in the nodes. Node n represents the loads that act on the second half of element $n-1$ and the first half of element n. In order to capture the bending in the pipeline, rotational springs are applied in the nodes. An overview of the numerical model representation is given by Figure C.1. The axial stiffness is given by equation C.1 and the bending stiffness is given by equation C.2

$$K_{axial} = \frac{EA}{L} \tag{C.1}$$

$$K_r = \frac{EI}{L} \tag{C.2}$$

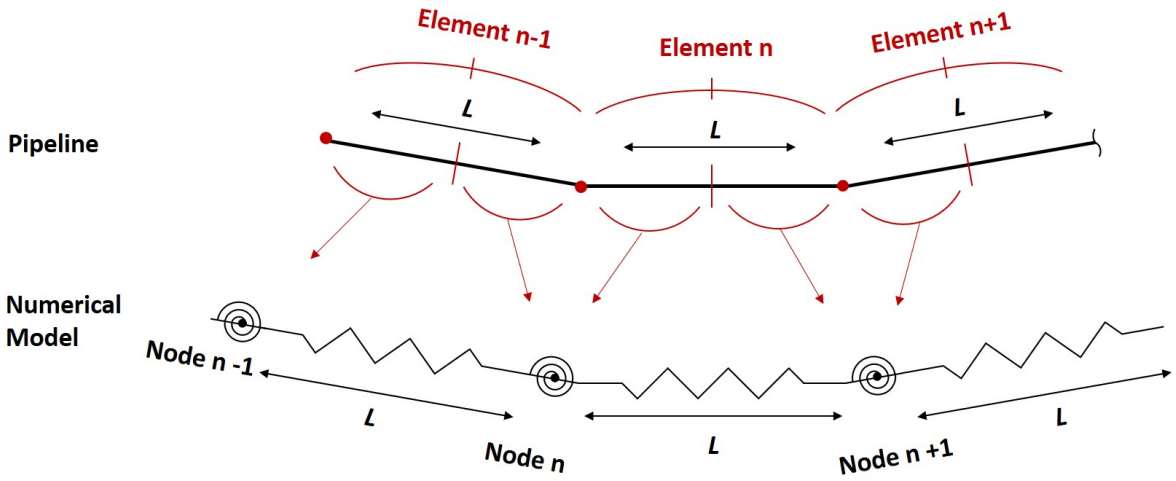

Figure C.1: Pipeline Representation by the Numerical Model

C.1. Equation of Motion for Pipeline Strain

The equation of motions of the nodes are obtained via the Lagrangian approach, given by equation C.3.

$$L_a = P - K \tag{C.3}$$

The potential energy P of a pipeline element is given by equation C.4.

$$P = \frac{EA}{2L}(\sqrt{(z_n - z_{n-1})^2 + (y_n - y_{n-1})^2 + (x_n - x_{n-1})^2} - L)^2 \tag{C.4}$$

The kinetic energy of a pipeline element is given by equation C.5.

$$K = \frac{1}{8}\rho AL(\dot{z}_n^2 + 2\dot{z}_n\dot{z}_{n-1} + \dot{z}_{n-1}^2 + \dot{y}_n^2 + 2\dot{y}_n\dot{y}_{n-1} + \dot{y}_{n-1}^2 + \dot{x}_n^2 + 2\dot{x}_n\dot{x}_{n-1} + \dot{x}_{n-1}^2) \tag{C.5}$$

The corresponding equations of motions for the element with nodes $n-1$ and n are obtained by solving the Lagrangian for the degrees of freedom per node and for node n these xresult in equation C.6.

$$\begin{aligned}
\frac{\rho AL}{4}(\ddot{x}_n + \ddot{x}_{n-1}) - \frac{\Delta xEA(L_c - L)}{L \cdot L_c} &= F_{x_{n-1}} \\
\frac{\rho AL}{4}(\ddot{x}_n + \ddot{x}_{n-1}) + \frac{\Delta xEA(L_c - L)}{L \cdot L_c} &= F_{x_n} \\
\frac{\rho AL}{4}(\ddot{y}_n + \ddot{y}_{n-1}) - \frac{\Delta yEA(L_c - L)}{L \cdot L_c} &= F_{y_{n-1}} \\
\frac{\rho AL}{4}(\ddot{y}_n + \ddot{y}_{n-1}) + \frac{\Delta yEA(L_c - L)}{L \cdot L_c} &= F_{y_n} \\
\frac{\rho AL}{4}(\ddot{z}_n + \ddot{z}_{n-1}) - \frac{\Delta zEA(L_c - L)}{L \cdot L_c} &= F_{z_{n-1}} \\
\frac{\rho AL}{4}(\ddot{z}_n + \ddot{z}_{n-1}) + \frac{\Delta zEA(L_c - L)}{L \cdot L_c} &= F_{z_n}
\end{aligned} \tag{C.6}$$

For the equation of motion in the x direction, Δx is given by equation C.7, similarly this is done for the y and z direction.

$$\Delta x = x_n - x_{n-1} \tag{C.7}$$

L_c is the length of the element between two consecutive nodes and is given by equation C.8.

$$L_c = \sqrt{(z_n - z_{n-1})^2 + (y_n - y_{n-1})^2 + (x_n - x_{n-1})^2} \tag{C.8}$$

C.2. Pipeline Bending

To account for the bending in the pipeline, the bending moment in the rotational spring is decomposed in bending forces and added on the right hand side of the equations of motions. The bending moment is given by equation C.9, where $\frac{EI}{L}$ is the bending stiffness per unit length.

$$M_b = \frac{EI}{L}\kappa \tag{C.9}$$

The bending moment is decomposed in forces perpendicular to the nodes, illustrated in Figure C.2 and given by equation C.10.

$$\begin{aligned}
2M_b &= F_{n-1}L + F_{n+1}L \\
M_b &= F_B L
\end{aligned} \tag{C.10}$$

The resulting bending force is then given equation C.11:

$$F_B = \frac{EI}{L^2}\kappa \tag{C.11}$$

Where the curvature κ is the summation of the angles β and α between two consecutive nodes given by equation C.12.

$$\begin{aligned}\beta &= tan^{-1}(-\frac{\Delta z_{n-1}}{\Delta x_{n-1}})\\ \alpha &= tan^{-1}(\frac{\Delta z_{n+1}}{\Delta x_{n+1}})\end{aligned} \tag{C.12}$$

The loads resulting from the bending moment in node $n-1$, n and $n+1$ are given by equation C.13.

$$\begin{aligned}F_{x_{n-1}} &= F_B sin(\alpha)\\ F_{z_{n-1}} &= -F_B cos(\alpha)\\ F_{x_{n+1}} &= F_B sin\beta\\ F_{z_{n+1}} &= -F_B cos(\beta)\\ F_{x_n} &= -F_B sin(\beta) - F_B sin(\alpha)\\ F_{z_n} &= F_B cos(\beta) + F_B cos(\alpha)\end{aligned} \tag{C.13}$$

Vector projection is used to transform the two dimensional bending loads to a three dimensional system [47].

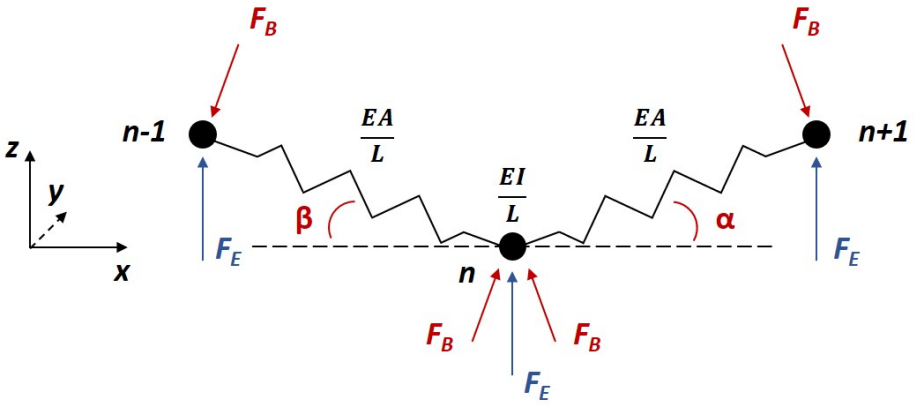

Figure C.2: Axial and Bending Loads

C.3. Complete Equation of Motion for an Element

The complete equation of motion for element $n-1$ is given by equation C.14, which includes all external loadings on the pipeline.

$$\begin{aligned}
&(\frac{\rho AL}{4} + M_{a_x})(\ddot{x}_n + \ddot{x}_{n-1}) - \frac{\Delta x EA(L_c - L)}{L \cdot L_c} + F_{Bx_{n-1}} = F_{Dx_{n-1}} + F_{px_{n-1}} + F_{x_{n-1}}\\
&(\frac{\rho AL}{4} + M_{a_x})(\ddot{x}_n + \ddot{x}_{n-1}) + \frac{\Delta x EA(L_c - L)}{L \cdot L_c} + F_{Bx_n} = F_{Dx_n} + F_{px_n} + F_{x_n}\\
&(\frac{\rho AL}{4} + M_{a_y})(\ddot{y}_n + \ddot{y}_{n-1}) - \frac{\Delta y EA(L_c - L)}{L \cdot L_c} + F_{By_{n-1}} = F_{Dy_{n-1}} + F_{py_{n-1}} + F_{y_{n-1}}\\
&(\frac{\rho AL}{4} + M_{a_y})(\ddot{y}_n + \ddot{y}_{n-1}) + \frac{\Delta y EA(L_c - L)}{L \cdot L_c} + F_{By_n} = F_{Dy_n} + F_{py_n} + F_{y_n}\\
&(\frac{\rho AL}{4} + M_{a_z})(\ddot{z}_n + \ddot{z}_{n-1}) - \frac{\Delta z EA(L_c - L)}{L \cdot L_c} + F_{Bz_{n-1}} = F_{Dz_{n-1}} + F_{pz_{n-1}} + F_{gz_{n-1}} + F_{z_{n-1}}\\
&(\frac{\rho AL}{4} + M_{a_z})(\ddot{z}_n + \ddot{z}_{n-1}) + \frac{\Delta z EA(L_c - L)}{L \cdot L_c} + F_{Bz_n} = F_{Dz_n} + F_{pz_n} + F_{gz_n} + F_{z_n}
\end{aligned} \tag{C.14}$$

The first term in the equations of motions represents the mass and added mass of the pipeline elements. The second term captures the axial strain in the pipeline elements, followed by the bending force. On the right hand side, the first term represents the drag force, the second term is the hydrostatic pressure. In the z direction, the third term represents the gravity force, which does not apply in x and y direction. The last force term represents all additional external loads.

C.4. Hydrostatic Pressure

An equivalent load per unit length is used to incorporate the hydrostatic pressure in the numerical model [37]. The equivalent pressure loading is given by equation C.15 and applied to the nodes of the numerical model. Figure C.3 illustrates the mechanical equivalence of internal and external pressure acting on a curved pipeline element.

$$\mathbf{f}(\mathbf{s}) = (\rho_i \pi R_i^2 - \rho_e \pi R_e^2)\mathbf{g} - (\rho_i \pi R_i^2 - \rho_e \pi R_e^2)\mathbf{g} \cdot \mathbf{t}(\mathbf{s})\mathbf{t}(\mathbf{s}) + [\pi R_e^2 p_e - \pi R_i^2 p_i]\kappa(s)\mathbf{n}(\mathbf{s}) \tag{C.15}$$

Three components can be distinguished in the equivalent loading. The first term represents the internal fluid weight and buoyancy per unit length. The first term is always directed vertically. The second term is a correction to the first term and subtracts gravity loading in the tangential direction ($\mathbf{t}(\mathbf{s})$) from the weight of the pipeline. The third term accounts for a curvature in the pipeline. It represents a loading in direction $\mathbf{n}(\mathbf{s})$. The loading is directed towards the center of curvature or away from it. The direction depends on the internal and external pressure and the inner and outer radius of the pipeline. In the case that the pipeline is straight and no bending occurs, this term is equal to zero.
Furthermore, a force acts on the offshore end of the pipeline. This force is equal to the hydrostatic pressure integrated over the surface area of the pipeline. This force acts in the axial direction of the pipeline.

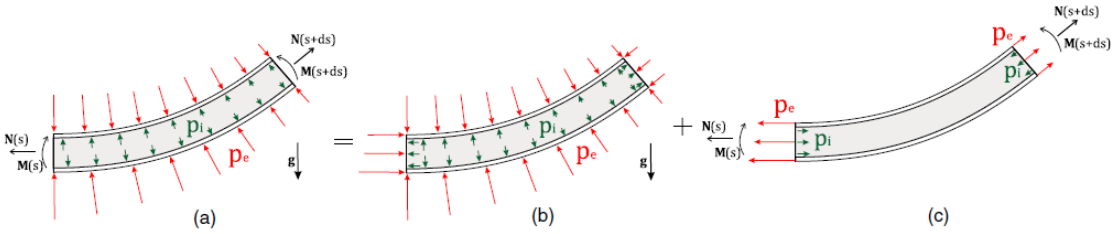

Figure C.3: Mechanical Equivalence of Pressure Acting on Curved Pipeline Element

D

Additional Hold and Sink Installation Method Results

In this appendix, the sensitivity analysis of Chapter 5 is extended for a SDR 33 pipeline. The relatively low Von Mises stress gives the impression that using fewer holding points is possible without exceeding the design stress. In table D.1, the maximum Von Mises stress is given for an installation with 3 hold points. The maximum vertical hold force is increased to 250 [kN] and the additional buoyancy of 15 [mT] is applied. The sinking velocity is limited to 0.2 [m/s] and the allowed installation design stress is 8 [MPa], similar to the scenario in the main report. The maximum Von Mises stress remains below the design stress, from which it can be concluded the the pipeline can be installed with 3 hold vessels.

Pull Force [mT]	**Vertical Hold Force [kN]**	**Maximum Von Mises Stress [MPa]**
100	250	7
150	250	6.7

Table D.1: Hold and Sink With 3 Hold Points

The specific gravity used in the main report is determined at a water depth 300 [m], where there is no influence of waves and the current velocity assumes a steady profile. This results in less vertical hold points required during the installation and less post ballasting is required. The impact of an increase in the SG of the pipeline on the installation is checked by increasing the SG value to 1.09, which corresponds to the design conditions at 200 [m] water depth. The submerged weight of a SDR 33 pipeline with SG 1.09 is equal to 169 [mT]. In table D.2, the required amount of hold points and corresponding vertical forces are given. The maximum Von Mises stress stays below the design stress for all scenarios. It is concluded that by increasing the SG, the required amount of vertical hold points significantly increases and even doubles if a maximum vertical force of 150 [kN] is assumed. The requirement for more hold vessels results in an increase in installation costs. Furthermore, the risk of a failure increases with increasing vessels.

Pull Force [mT]	**Hold Points**	**Vertical Hold Force [kN]**	**Maximum Von Mises [MPa]**
100	8	150	5.1
100	6	220	6.3
150	8	150	5.5
150	5	250	6.6

Table D.2: Verical Hold Capacity SG 1.09

E

Additional Pull Down Installation Method Results

Figure E.1 illustrates the local maximum Von Mises stress resulting from the 20 * 2.5 [mT] ballast distribution at the sea surface.

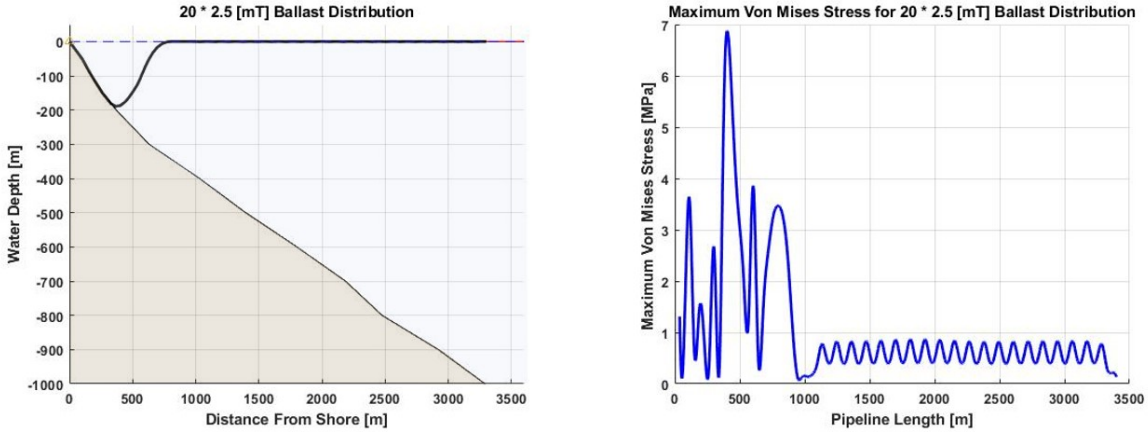

Figure E.1: SDR 33 20 * 2.5 [mT] Ballast Distribution, Local Maximum Von Mises Stress

Figure E.2 illustrates the local maximum Von Mises stress resulting from the 10 * 5 [mT] ballast distribution at the sea surface.

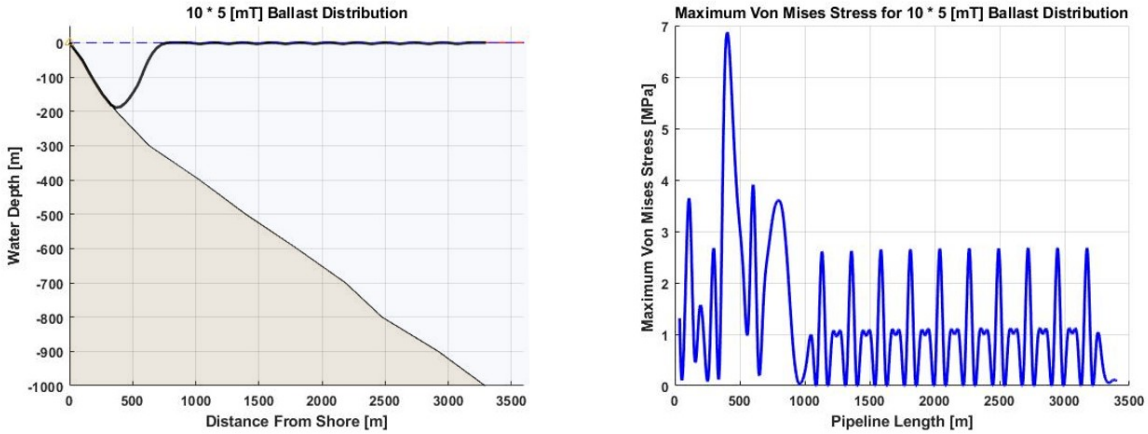

Figure E.2: SDR 33 10 * 5 [mT] Ballast Distribution, Local Maximum Von Mises Stress

An increase in the maximum local maximum Von Mises stress can be observed when comparing the 20 * 2.5 [mT] and 10 * 5 [mT] ballast distribution. This results from an increase in local bending due to the heavier ballast weights. In both scenarios, the local maximum Von Mises stress remains below the design stress.

Figure E.3 illustrates the bending stress for a pull down installation with a 10 * 5 [mT] ballast distribution. The simulation time is 7200 [s]. During the pull down of the first 500 [m], the occurring bending stress is significantly (23 %) higher than for the 20 * 2.5 [mT] ballast distribution, which is discussed in section 5.3.

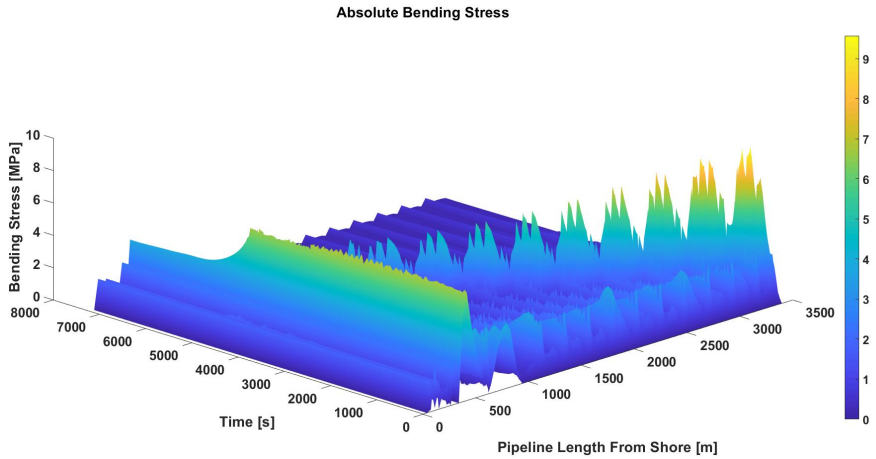

Figure E.3: SDR 33 10 * 5 [mT] Ballast Distribution, Bending Stress

The maximum Von Mises stress of the 10 * 5 [mT] ballast distribution is illustrated in Figure E.4.

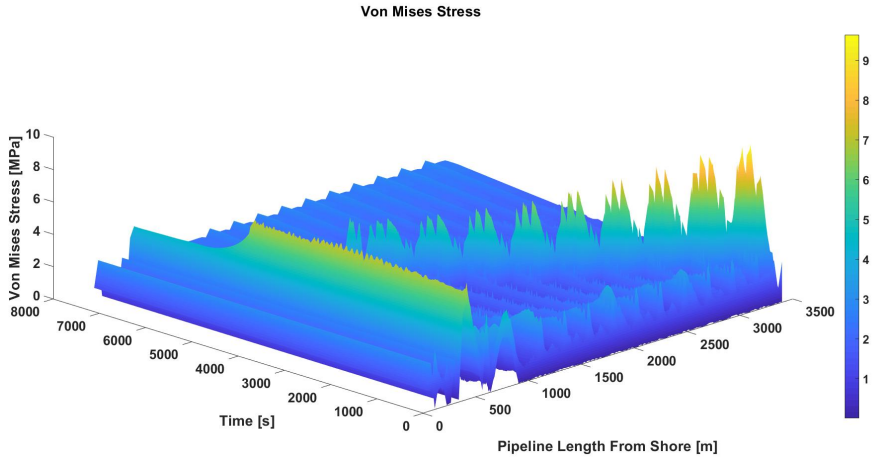

Figure E.4: SDR 33 10 * 5 [mT] Ballast Distribution, Maximum Von Mises Stress

.

E.0.1. Offshore End Bending Stress Discussion

The bending stress figures, therefore the Von Mises stress figures as well, show a distinct pattern over time. High stress peaks occur during the initial pull down stages where the bending radius is small. The stress peaks then decrease over time with increasing surface bending radius. Furthermore, small individual peaks can be observed in these high stress peaks. These smaller individual peaks correspond to the individual nodes that are used in the numerical model, Appendix C. The pipeline is discretized into smaller pipeline elements of which the mass and external loading are applied in the nodes. Each node has an upward force resulting from the buoyancy and a downward force resulting from the weight of the pipeline. As the buoyancy force is larger than the downward force, the pipeline remains floating on the surface. This results in a node being submerged only when the downward, provided by the pull cable, force exceeds the upward force. A bending stress then occurs between a node that is pulled down and a node that remains floating on the sea surface.

For the 20 * 2.5 [mT] ballast distribution, the local upwards buoyancy force is reduced on more locations along the pipeline by the ballast weights, which results in a more gradual bending profile as compared to the 10 * 5 [mT] ballast distribution. For the 10 * 5 [mT] ballast distribution the upwards buoyancy force is reduced on less locations along the pipeline, which results in a less gradual surface bending profile.

Figure E.5 illustrates the bending stress of a pull down installation with a 20 * 2.5 [mT] ballast distribution, where half of the amount of nodes is used as compared to the installation method discussed in the main report. Less individual stress peaks can be observed when comparing the two stress figures. Furthermore, the surface bending profile is less gradual. If more nodes are used, more individual peaks can be observed, leading to a more gradual profile. This will however lead to a significant increase in computational time as well.

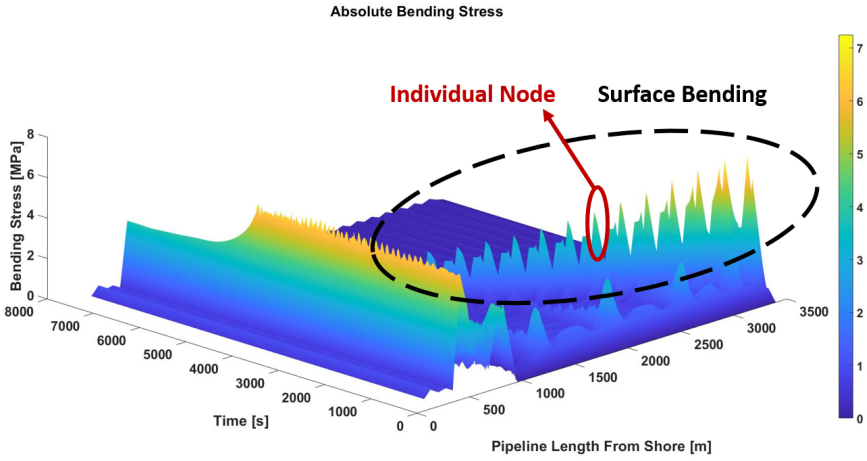

Figure E.5: SDR 33 20 * 2.5 [mT] Bending Stress Half of the Nodes Used

F

Second Anchorbox Configuration

In section 5.2.1 the bending in the transition zone is discussed, which results in exceedance of the allowed design stress. In order to decrease the bending stress in the transition zone, the bending stiffness is increased by a factor 10. In this appendix, the implementation of a second anchorbox as a method to decrease the bending stress in the transition zone is discussed. An overview of the transition zone, including a second anchorbox, is illustrated in Figure F.1. The anchorbox is installed prior to the float and sink installation phase. Tension is applied to the chain at the anchorbox while the other end is connected to the pipeline. The required tension should result in a downward bending moment that is greater than the moment resulting from buoyancy force.

Three chain configurations are considered combined with three loading configurations. A one chain configuration where total load is applied on that one chain, a two chain configuration where the load is distributed equally between the two chains and a three chain configuration where the total load is equally distributed among the three chains. The distance between two consecutive chain connection points on the pipeline is 30 [m], where the first chain is connected 30 [m] from the anchorbox. Table F.1 gives the resulting bending stresses for the different scenario's. The bending stress is decreased as compared to the bending stress without additional measures, but still results in the Von Mises stress exceeding the design stress for most scenarios. The single chain 18 [mT] tension configuration, results in a higher bending stress than the other configurations. This results from the high pull tension that is applied at one location, resulting in a downwards bending moment at one point just after the anchorbox that is too large. Whereas for three hold points, the downward bending moment is distributed over a longer pipeline segment. It can be concluded that the optimum configuration of pull tension and number of chains depends on the position and magnitude of the resulting downward bending moment.

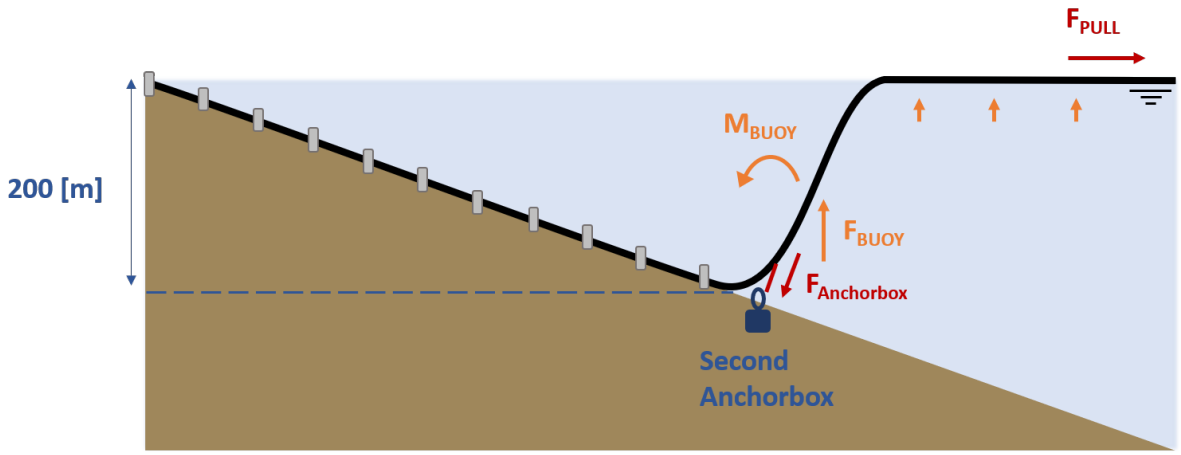

Figure F.1: Second Anchorbox in the Transition Zone

Total Tension	**12 [mT]**			**15 [mT]**			**18 [mT]**		
Number of Chains	1	2	3	1	2	3	1	2	3
Bending Stress [MPa]	8.8	7.8	8.1	10.2	8.6	7.6	11.7	10.1	8

Table F.1: Bending Stress In Transition Zone With Second Anchorbox

To further reduce the bending stress, the bending stiffness is increased by applying an additional layer of HDPE. By applying the additional layer, the stiffness is increased with a factor 3. The results are given in table F.2. Except for the 18 [mT] one chain configuration, the bending stress is reduced to under the design stress. It can be concluded that the bending stress can be reduced to an acceptable value in the transition zone, by installing a second anchorbox and increasing the bending stiffness by a factor 3. The optimal configuration depends on the magnitude and location of the applied downwards bending moment. Furthermore, the preferred amount of attached chains can be influenced by requirements for the operational lifetime of the pipeline in the transition zone.

Total Tension	**12 [mT]**			**15 [mT]**			**18 [mT]**		
Number of Chains	1	2	3	1	2	3	1	2	3
Bending Stress [MPa]	6.9	7	7.3	6.8	6.4	6.5	8.3	7.1	6.5

Table F.2: Bending Stress in Transition Zone Without Additional Stiffness

Figure F.2 illustrates the bending stress for a second anchorbox configuration where a 15 [mT] tension is applied. Figure F.3 illustrates the same configuration including the additional bending stiffness.

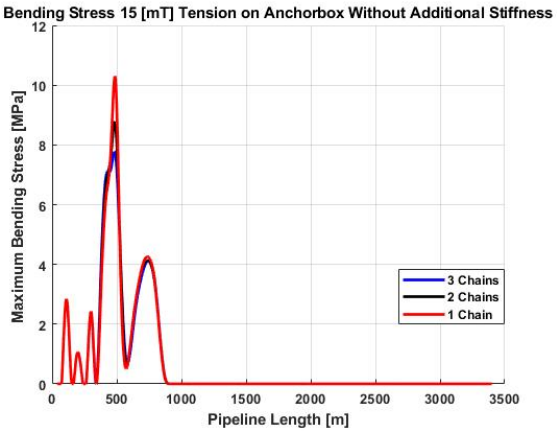

Figure F.2: Bending Stress in Transition Zone Without Additional Stiffness

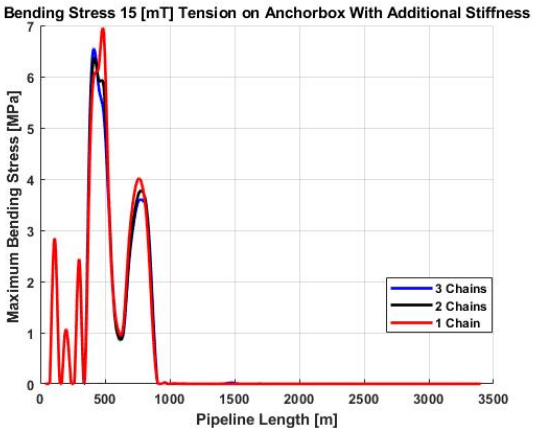

Figure F.3: Bending Stress in Transition Zone With Additional Stiffness